Hydraulic and Environmental Modelling of Density Stratified Shallow Waters(Dissertation_全文)

AUTHOR(S):

Hiramatsu, Ken

Hydraulic and Environmental Modelling of Density Stratified Shallow Waters

1999

Ken HIRAMATSU

Contents

Notations

The following symbols are the major symbols used in this thesis.

$\bar{a}$,$\bar{b}$,$\bar{c}$,$\bar{d}$ = empirical constants
C_a = coefficient of wind stress
c_a = specific heat of air (=0.24[cal/g/k]$\simeq$1.005[J $K^{-1}g^{-1}$])
c_w = specific heat of water (=4.17$\sim$4.21[J $K^{-1}g^{-1}$])
E_x = horizontal eddy viscosity [m^2/s]
E_z = vertical eddy viscosity [m^2/s]
e_a = vapor pressure of air (hPa)
e_w = saturated vapor pressure (hPa) for θ at z=0
g = gravitational acceleration (=9.79707[m/s^2])
I_{max} = maximum intensity of light (=783 [$cal/cm^2/day$])
I_{opt} = saturating intensity of light (=200 [$cal/cm^2/day$])
K_C= carbonaceous oxidation rate (=0.23[day^{-1}])
K_D = removal rate by sedimentation and absorption (=0.23[day^{-1}])
K_N = nitrification rate (=0.1[day^{-1}])
K_x = horizontal eddy diffusivity [m^2/s]
K_{xy} = horizontal eddy diffusivity [m^2/s]
K_z = vertical eddy diffusivitiy [m^2/s]
k = von Karman constant ($\simeq$0.4)
k_b = bottom resistance coefficient under the assumption of linear inadhesive condition

($\simeq$0.0025[m/s]

k_c= heat transfer coefficient (=1.1×10^{-3})

k_N= half-saturation constant for nutrient uptake (=3.1 [$\mu gP/\ell$])

N_{zx},N_{zy} = vertical eddy viscosities [m^2/s]

n_c = amount of cloud ($\simeq$0.1)

$\boldsymbol{n}$ = outward unit vector normal to the boundary surface

n_x,n_y = components of the outward unit vector normal to the 2-D boundary surface

P_c = baroclinic pressure [m]

P_t = barotropic pressure [m]

p = hydrostatic pressure [m]

p_0 = atmospheric pressure on the surface [m]

Q = net heat flux [J m^{-2} s^{-1}]([W m^{-2}],[cal/cm^2/day])

Q^* = heat flux of internally absorbed radiation [W m^{-2}]

Q_a = long wave radiation [W m−2]

Q_{br} = released long wave radiation [W m^{-2}]

Q_c = sensible heat [W m^{-2}]

Q_e = latent heat [W m^{-2}]

Q_s = short wave radiation [W m^{-2}]

Q^*_{sur} = heat flux absorbed and released at the water surface. [W m^{-2}]

Q_{s0} = amount of short wave radiation on a clear day

($\simeq$783[cal m^{-2} day^{-1}] ([4.1868 J/m^2·s])

R_{max} = maximum grazing rate of zooplankton (=0.05 [hr^{-1}])

t = time [s]

V_{max} = maximum uptake rate of phytoplankton (= 0.02 [hr^{-1}])

W = wind speed (m/s)

α_N = rate of oxygen uptake per unit of ammonia oxidation (=4.57[mg O/mg N])

α_{OC} = oxygen uptake rate of phytoplankton(=1000[kg O /kg chl.a])

α_{OP} = oxygen production rate of phytoplankton (=1000[kg O/kg chl.a])

α_T = volumetric expansion coefficient(=0.00021[K^{-1}])

α_s = albedo (reflectivity) ($\simeq$0.05)

α_a = albedo (reflectivity) for long wave radiation($\simeq$0.03)

β = fraction of incident light absorbed by the water surface ($\simeq$0.4)

β_T = temperature coefficient (=0.06931)

γ = unassimilated grazing fraction (= 0.3 [ℓ/μgP])

γ_r = respiration rate of phytoplankton (=0.1[m^{-1}])

Δt = time increment [s]

δ_v = mortality of phytoplankton (= 0.064[hr^{-1}])

δ_z = zooplankton death rate (= 0.032 [hr^{-1}])

η = vertical displacement of the free surface from mean water level [m]

Θ = absolute temperatures of water (K)

Θ_a = absolute temperatures of air(K)

θ = water temperature (°C)

θ_a = temperature (°C)

θ_0 = reference temperature (= 4°C)

λ_I= Ivlev constant (=0.080645 [ℓ/μg])

μ= phytoplankton growth rate (=2.0[day^{-1}])

ν = extinction coefficient of light [m^{-1}]

ρ = water density [kg/m^3] or [psu]

ρ_a = atmospheric density [kg/m^3]

ρ_0 = water density at reference temperature ($\simeq$1000[kg/m^3])

σ = salt and/or heat flux

σ_S = Stefan-Boltzman constant (=5.67×10^{-8}[W/m^2·K^4])

τ = components of shearing stress [N/m^2]

τ_s=share stresses on the surface [N/m^2]

τ_b=share stresses on the bottom [N/m^2]

ϕ_c= ratio of TOD/COD (=5.1)

Ω = Coriolis parameter [s^{-1}]

List of Tables

List of Figures

Acknowledgments

First of all, the author would like to express his sincere gratitude to Dr.Toshihiko KAWACHI, Professor of Water Resources Engineering, Division of Environmental Science and Technology, Graduate School of Agricultural Science, Kyoto University, for his proposition of environmental hydraulic problems and his invaluable guidance to completion of this research.

The author is also grateful to the remaining members of the Examination Committee, Professor Shigeyasu AOYAMA and Professor Tsuyoshi TAKAHASHI for their discussions and constructive suggestions in reviewing the manuscript.

Thanks are due to late Dr. Isao MINAMI, Emeritus Professor of Kyoto University, for his exhaustive educating and encouragements.

The author also extends his appreciation to Ms. Yukiko OHKI for her kind assistance and cooperation.

The author is truly thankful to his seniors, colleagues and friends including my family who supported him in every respect to complete this research.

This thesis is the result of the researches executed in these seven years at Graduate School of Agricultural Science, Kyoto University. A part of this thesis was financially supported by 1997-98 grant-in-aid for scientific research by the Ministry of Education, Science and Culture of Japan.

Chapter 1

INTRODUCTION

1.1 Water Resources and the Environment

Water is essential for our human activities and also for natural environment. However, it is not easy to identify the nature of water or to utilize it as we desire. This is because water is unequally distributed around the earth and its availability at any given place varies greatly with time. It is not an exaggeration to say that three major efforts are involved with building of our civilization. They are the planning, the managing, and the controlling of water as a resource and as our environment. Moreover, with the rapid growth in world population, the importance of the skilled planning and the careful management of water resources is increasing. People should realize that the water which is available to us could not be easily or economically reclaimed tomorrow. Moreover, it is also important to note that even the available water is polluted and so severely degraded that it is unfit for use in many of our daily activities.

When human activities are relatively few and beyond the ability of recovery that nature possesses, efforts in water resources and hydraulic engineering are mainly directed to the "quantity of water". However, the rapidly increasing population brings the degradation of resources to a serious level which necessitates scientists and engineers to address the issue of maintaining the "quality of water" or "water environment" as well as "quantum of water". Efforts must be made not only to maintain the amount of water available but also to preserve it in its original form.

Although it is not easy to make developments which are compatible with the conservation of nature, nonetheless, they are not essentially in antagonism to each other. For building a contemporary and comfortable society, the development of water resources is indispensable and the conservation of our water environment should not be neglected. It is logical, therefore, to say that there must be a mean to modulating the conflict between them.

How should the water environment be considered? Strictly speaking, the natural cycle, including the cycle of water environment, on the earth is not sustainable. All flows have self-purification and the resultant sedimentation will not be restored back to its original place. All other naturally and/or artificially occurring phenomena result in fundamentally irreversible processes. Even man-made reservoirs and natural lakes are not permanent bodies. They too will inevitably be changed or disabled over a long-term process. The only thing that can be done is to try to understand what is going on in the waters and then to treat them in order to maintain them at their maximum level.

1.2 Numerical Modelling in Environmental Hydraulics

Advances in hydrodynamics, mass transport and water quality modelling have reached the point where it is feasible to use models to make comparative risk assessment of alternative environmental management scenarios. (D.R.F. Harleman, 1992[21])

Understanding the phenomena occurring in bodies of the water is the first and most significant step, while forecasting the phenomena and developing appropriate proposals for the management of water resources and our natural environments is the second step.

There may be some good ways to approach this goal. Conventional hydraulic experiments are surely useful in understanding the phenomena, but they inevitably include errors in measurement and strain due to gravitational acceleration and they cost an enormous amount of money. Observation is undoubtedly the most important part to grasping the phenomena and is required for identifying the parameters of numerical model. However, observation does not provide solutions to future problems and can never tell how the water environment will change under various conditions. A numerical model, on

the other hand, can produce situations under various scenarios without destroying or polluting the actual water environment. Numerical models do not consume the same amount of time as the actual phenomena and even climatic conditions can be changed for the simulation. Therefore, it can be said that numerical modelling is one of the most advantageous approaches. While it is wiser to keep in touch with other approaches than to discard them, the relative importance of numerical models is sure to grow.

Here, the author emphasizes that it does not take a long time to reach a place where decisions can be made with enough information that is obtained by numerical simulations and without gambling as Harleman's comment showed at the beginning of the section.

1.3 Aim of this Study and Approach to the Solution

These days it has become quite common to hear that a red tide, a water bloom and other unusual phenomena are occurring in the waters close to us. Most of them are brought about by the influence of human activities. The transitions of our daily lives cause more and more wastewater which includes many types of chemical materials and nutrients. The construction of dams or barriers brings the accumulation of water to one place, which indirectly lowers the quality of the water. In other words, the waters are faced with degradation at many places and for various reasons.

Some ask, "Do we not have a countermeasure? Do we not have the wisdom to avert these crises? Can we not forecast the phenomena?" The answer is "Yes!". We do have countermeasures, wisdom, and the technology to face such challenges. However these countermeasures are still in the process of development; they have not been completed yet. The author believes that there is an order to coping with these problems. Firstly, we must watch, listen, investigate, and experiment on the phenomena. Secondly, we must understand them and make the mechanisms clear. Thirdly, we must reproduce them with fidelity and verify the process of their reproduction. Finally, we must play alternative scenarios and forecast the impact of various interests. These steps will lead to the ultimate goal.

The research in this thesis is concerned with the second, third, and final steps. Al-

though there are many approaches to dealing with the respective steps, the author has used the numerical approach. Consequently, the aim of this study is to build numerical models which can grasp the phenomena and assess the environmental impact of human activities.

Waters that are treated can be classified into four types by their characteristics; i.e., estuarine waters, man-made reservoirs, lakes, and irrigation tanks. They all have their own characteristics that are inadmissible to the others. Therefore, it is difficult to treat them in a completely similar fashion. The four numerical models presented in this thesis are built for the four classes of water. However, numerical strategies for the shallowness of the waters, density stratification, etc., which emphasize the superiority of the models, are the common characteristics. Above all, it is most important that they are approached with one common goal.

1.4 Constitution of the Thesis

This thesis consists of seven chapters, four of which describe original researches. Three chapters supplement the former chapters and make them consistent with the purpose of the thesis.

The introductory chapter explains the need for numerical modelling in environmental hydraulics and the aim of this thesis.

Chapter 2 reviews the literatures on modelling of stratified waters, water quality and ecosystems. Particular emphasis is given to the methodologies that tackle the large aspect ratio of the spatial domain of interest.

Chapter 3 presents a three-dimensional finite element modelling for hydrothermal computations in relatively small shallow waters. Heat exchanges through a water surface are of great interest in this research. The model is verified by applying it to a hypothetical reservoir and a real irrigation tank.[46]

Chapter 4 describes a three dimensional finite element modelling of density driven currents using the velocity correction method. The major strategies of this model are the treatment of the solenoidal condition and the non-linear effects of temperature and

salinity on the density, which are of great importance in brackish waters where trivial maldistribution of density works drastically on the currents. The capability of the model is tested on three different hypothetical waters.[25]

Chapter 5 and 6 present a side-view finite element modelling for thermally stratified reservoirs. The aim of the modelling is to develop a synthetic model, in other words, a model which includes flow, water temperature, water quality, and an ecosystem, and is applied to a long-term analysis. The close relation between vertical distributions of density and dissolved oxygen plays an important role in the model. Demonstrative computations are carried out for two different real reservoirs.[24, 28, 27]

Chapter 7 summarizes this study in a conclusion and gives an opinion regarding follow-up studies.

Chapter 2

LITERATURE REVIEW

2.1 Introduction

In the present study, four kinds of water bodies, viz., an irrigation tank, a lake, a man-made reservoir, and coastal waters are considered. The common feature of these bodies of water is that the density of the fluid has a great influence on the movement of the waters. Although density of the fluid usually depends on water temperature and salinity, the movement of water works on the thermal and salinity distributions conversely. Moreover, the movement and temperature of water affects water quality seriously and vice versa. Thus, the relations of components in water bodies are very complex.

In the following sections, reviews on models of stratified waters as a fundamental of a hydro-environment and those of water quality and ecosystems as applications are made briefly.

2.2 Modelling Stratified Waters

At first, 'stratified waters' of our interest should be defined simply for an easy understanding of this section.

Density stratification occurs in various situations of fluids, including bodies of water. Depending on the approach to the phenomena and the scale of the phenomena, there are some differences in the objectives of the studies. The movement of heated water in

a cavity is one of the most popular density-induced flow problems. Bènard-Rayleigh's convection may be the most famous experiment of density-driven currents. The size of their scale is relatively small, in other words 'micro problems', which are of benefit to theoretical development and become the fundamentals of numerical strategies. However, they are not our objectives. Compared with them, the phenomena of our interest are 'macro problems',which are on a relatively large scale.

Then, what are 'macro problems'? In the field of water resources engineering, problems such as salt water wedge in a river mouth, the thermal plume near the outfall of industrial plants, muddy or cold water intrusion into reservoirs, high salinity water accumulation on brackish lake beds, topographic heat accumulation, etc. are often considered. Of course these phenomena exist on a micro scale, but attention is paid only to resultant macro phenomena in most studies.

In environmental hydraulics, the salt water wedge in estuarine waters might be the first research theme. In this context various studies have been presented both theoretically and numerically for almost half a century. Initially, Ippen, A.T. *et al.* (1951)[36] believed that fresh and salt water layers exist simultaneously unmixed in brackish water and create a salt water wedge.

Later on, studies on stratification developed to include not only the above-mentioned two-layer flow but also waters with the maldistribution of density which is mathematically expressed by diffusion, dispersion, and advection equations. Bowden, K.F. (1965)[6], Holley, E.R.*et al.* (1970)[29] and others presented dispersion models for channel flows. Following them, many models were developed and applied to various problems. For example, Harashima *et al.* (1981) [20] and Yanagi *et al.* (1990)[88] tried to model the thermohaline front in coastal waters, Huyakorn (1987)[35] and Cooley (1983)[9] computed the coastal groundwater flow, Harleman *et al.* (1972) [22] treated a thermal plume and Oonishi (1975) [73] explained the heat accumulation. In addition energetic studies including Wang *et al.* (1997) [86] and Leendertse *et al.* (1978)[58] extended the models to two or three-dimensional configurations for estuarine and coastal waters. The major merits of the extensions are briefly explained as 1) They enable the accurate reproduction of the effects of stratification. 2) They enhance the ability to compare the model output

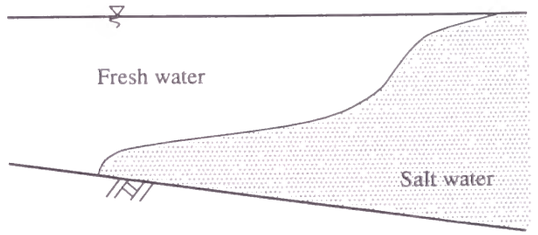

Figure 2.1: Salt water wedge at a river mouth

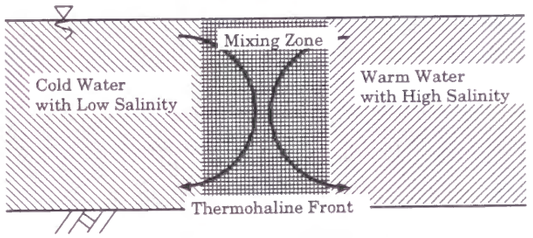

Figure 2.2: Thermohaline front by Caballing effect

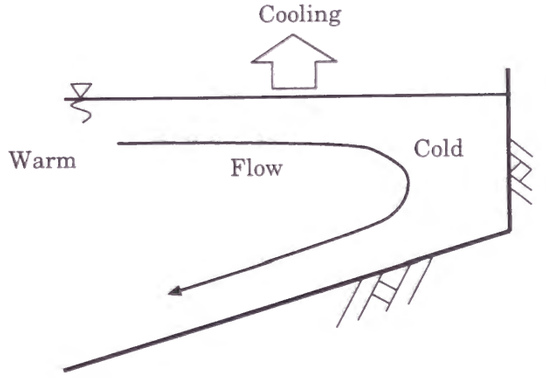

Figure 2.3: Topographic heat accumulation effect

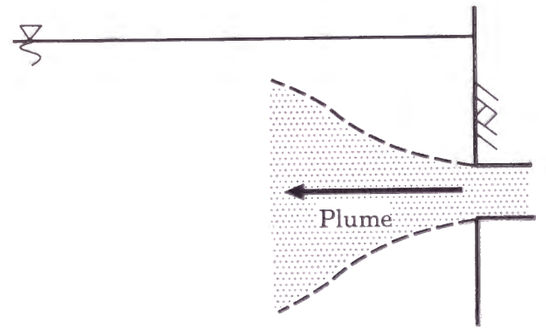

Figure 2.4: Thermal plume

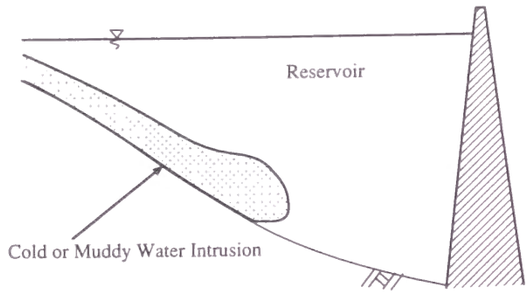

Figure 2.5: Cold or muddy water intrusion

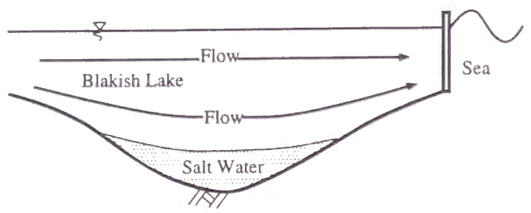

Figure 2.6: Salt water accumulation on bed

with the field data at whatever spatial location and time the data was obtained.

Ban, M. *et al.* (1989)[4] and Kawachi, T. (1990)[44] have brought important meaning to methodology by the models employed in this thesis. They divided the domain of interest into horizontal and vertical directions and used different finite element approximations for them. This enhanced the accuracy of the computation even when the magnitude of length in the horizontal direction was much larger than that in the vertical direction and the aspect number was quite large.

Similarly, density-driven current problems have been discussed in irrigation and water resources engineering. Stratification is mainly due to the salinity in coastal and estuarine waters, whereas the maldistribution of temperature is a main cause of stratification in limnic waters. For example, a thermal stratification in a reservoir is one of the major problems. To prevent cold water damage, an urgent countermeasure was required and simultaneous elucidation of the phenomena was also of great importance in the 1950's and 1960's. However, it was in the 1970's when numerical modelling strategies came to bear successful results. The representative strategy is called the MIT model, and it

was developed for horizontally isothermal reservoirs by Huber,W.C. *et al.* (1972) [33]. Following the concept of the MIT model, many models were developed and presented, and yet, the same is to be modified according to regional hydrological or geometric characteristics.

In modelling stratified waters, the identifications and parameterization of vertical eddy viscosity and diffusivity are two of the major interests. Munk *et al.* (1948)[69] adopted Richardson number as an index in the identification of diffusivity. Mamayev, O.I. (1958)[63] proposed that diffusivity should be expressed by an exponential function of Richardson number. Rossby *et al.* gave a power function of it. These methods using Richardson number give quite appropriate value in the flowing water. However, due to original definition of Richardson number, they cannot estimate the value in quiet waters. Osborn *et al.* (1972)[74] used Cox number, which makes it possible to estimate the value only by thermal distributions and turbulence. The dependence of eddy diffusion on buoyancy frequency was pointed out by Welander (1968)[87] and others. Welander derived an expression relating the diffusivity to the square of the Brunt-Väisälä frequency. Hondzo, M. *et al.* (1991) [30] developed Welander's concept and gave appropriate coefficients and functions. When the vertical convective mixing of water is also included in the vertical diffusion, the diffusivity may be expressed in an exponential function of the Brunt-Väisälä frequency.

2.3 Modelling Water Quality and Ecosystems

Although water quality encompasses many constituents, water quality in this section means mainly refers to dissolved oxygen. The history of studies on dissolved oxygen dates back to the 1920's. Streeter and Phelps (1925)[81] related it to the natural purification of a river, especially focusing on oxidation and reaeration. Their pioneering model is based on an empirical formula. Since then, a number of studies have been carried out to identify the parameter of natural purification. Among them, O'Connor *et al.* (1956)[72] is important, for they treated natural purification and its parameters in a theoretical manner. The development in theory started from inducing that the reaeration should

be considered a turbulence flow problem. Paying attention to just the applicability of the numerical model, reaeration is recently considered to also be a function of wind and flow. Banks, R.B. *et al.* (1997) [5] and Mackay *et al.* (1983) [61] introduced a wind speed 10 m above the water surface, Thomann *et al.* (1987)[82] used velocity of flow, water depth, and wind speed. At present, it can be said that they are the most popular and appropriate estimation methods.

Photosynthesis greatly influences the concentration of dissolved oxygen, as well as reaeration, which was pointed out by Streeter and Phelps (1925) [81]. In the early stages, some elements that seemed to be most dominant to the plankton ecosystems were chosen. Then a simple equation was used to estimate the photosynthesis. O'Conner, D.J. *et al.* (1970)[71] expressed the increase and decrease of plankton simply by a periodical steady function. Auer, M.T. *et al.* (1989) [1] used a function of light intensity. Goda *et al.* (1977)[19] also gave a one-variable function for the amount of phytoplankton. However, Di Toro *et al.* (1971)[12] and Chen *et al.* (1975)[7] introduced phytoplankton dynamics and nutrient kinetics into their models. The model by Di Toro*et al.* (1971) [12] consists of phytoplankton, zooplankton, and inorganic nitrogen compartments. That by Jørgensen, S.E. (1976)[40] is a little more complex having six compartments including phosphorus. Various models have been proposed, some of which are illustrated in Figure 2.7[67].

Kishi *et al.* (1978)[51], Iwasa *et al.* (1979)[38] and Kishi (1994)[50, 52] introduced flow models into their ecosystem models. Considering the important influence of advection, convection, and diffusion on the constituents, it is worth appreciating the combination of hydrodynamics, water quality, and phytoplankton dynamics. Walters, R.A. (1980)[85] is also worthy of notice, for they developed an eutrophication model with a vertical distribution of water temperature. Considering the influence of thermal stratification on the constituents and the dependency of them on water temperature, its extension has a great meaning. Kumagai *et al.* (1986)[55] clarified the mechanism of the formation of an anoxic layer in a hypolimnion and pointed out the close relationship between the vertical distribution of water temperature and dissolved oxygen. It is also meaningful that they took note of the function of vertical diffusivity of the dissolved oxygen.

Thus, major systems of water quality and ecosystems have been established quite

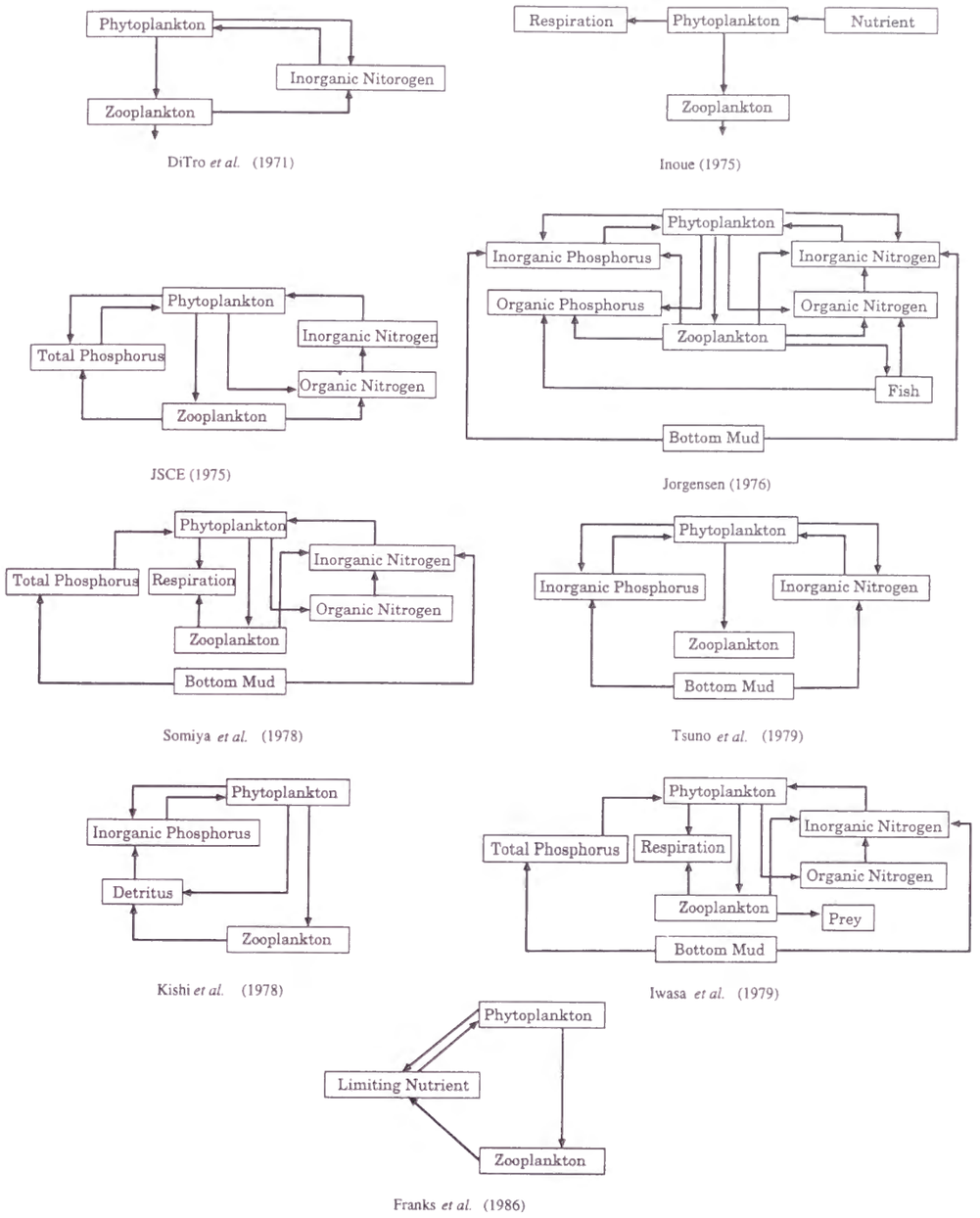

Figure 2.7: Comparison of Eutrophication models

well. The next task includes their application to real bodies of water and a continuous renovation of the parameters to enhance the modelling strategies.

Chapter 3

THREE DIMENSIONAL FINITE ELEMENT MODELLING OF THERMAL STRATIFICATION IN SHALLOW WATERS

3.1 Introduction

The increasing concern to environmental problems is making the models of environmental hydraulics developed. Seemingly the significant advances in the environmental model have reached the point where it is feasible to use models to make comparative risk assessment of alternative environmental management scenarios. And remarkable development of the computational efficiency spurs the models to apply three dimensional (3-D configurations.

Water temperature is one of the most important factors in assessing environmental problems, for its influences to water quality, especially eutrophication and ecological impact on aquatic livings is very significant. Thus the thermal modelling is overriding in building a water quality model.

Despite great importance of fully 3-D modelling in large bodies of shallow water, e.g., reservoirs of lakes, earlier works [e.g.,42,89] for the prediction of water temperature distribution mostly developed the vertically 2-D models based on the laterally averaged equations. Thus 3-D thermal stratification modelling seems so rudimentary that we cannot precisely investigate the stratification regime in real waters, e.g., behavior of waste heat rejected as a point or line source into a cooling pond, and influence of surface water intake on the stratification in an irrigation dam.

This chapter aims to develop a 3-D thermal stratification model that may be qualified as an easy to operate and versatile implement for accurate environmental assessment. The model interpolates solutions over the depth by continuous polynomials in a significant extension of the 3-D density stratified flow model[44, 45] to the thermal problem. The model is therefore characterized by its benefits: (1) discretization over the depth is not required, (2) the degree of approximations in the vertical can freely be specified, (3)indiscrete vertical distributions of the quantities of direct interest can be obtained and (4) complex bathymetry can easily be represented. With special considerations on heat transport through the water surface, details of the model and solution procedures are presented. Applicability and validity of the model are then investigated by solving different two thermal problems: bottom water cooling and surface water heating problems.

3.2 Governing Equations

The thermally stratified flow in a large body of water can be represented by the equations of continuity, momentum, heat transport and state. If the water body is hydraulically shallow, it is justified to neglect the vertical acceleration and the horizontal momentum exchange. Due to the former, the water motions are predominantly horizontal and the resultant vertical velocities characterize the vertical circulation of water and heat. The density is taken as dependent only on the temperature and included in the equations of momentum to describe the baroclinic water motions. The internal absorption of solar radiation through the water surface can be taken in the equation of heat transport. We can thus write the governing equation as;

$$\frac{\partial \zeta}{\partial t} + \frac{\partial}{\partial x}\int_0^h u dz + \frac{\partial}{\partial y}\int_0^h v dz = 0 \tag{3.1}$$

$$w = \frac{\partial}{\partial x}\int_z^h u dz + \frac{\partial}{\partial y}\int_z^h v dz \tag{3.2}$$

$$\frac{\partial u}{\partial t} + u\frac{\partial u}{\partial x} + v\frac{\partial u}{\partial y} + w\frac{\partial u}{\partial z} - \Omega v = -g\frac{\partial \zeta}{\partial x} - \frac{g}{\rho}\frac{\partial}{\partial x}\int_0^z \rho dz + \frac{\partial}{\partial z}\left[N_{zx}\frac{\partial u}{\partial z}\right] \tag{3.3}$$

$$\frac{\partial v}{\partial t} + u\frac{\partial v}{\partial x} + v\frac{\partial v}{\partial y} + w\frac{\partial v}{\partial z} + \Omega u = -g\frac{\partial \zeta}{\partial y} - \frac{g}{\rho}\frac{\partial}{\partial y}\int_0^z \rho dz + \frac{\partial}{\partial z}\left[N_{zy}\frac{\partial v}{\partial z}\right] \tag{3.4}$$

$$\frac{\partial \theta}{\partial t} + \frac{\partial (u\theta)}{\partial x} + \frac{\partial (v\theta)}{\partial y} + \frac{\partial (w\theta)}{\partial z} = \frac{\partial}{\partial x}\left[K_{xy}\frac{\partial \theta}{\partial x}\right] + \frac{\partial}{\partial x}\left[K_{xy}\frac{\partial \theta}{\partial y}\right] + \frac{\partial}{\partial x}\left[K_z\frac{\partial \theta}{\partial z}\right] - \frac{1}{\rho c_w}\frac{\partial Q^*}{\partial z} \tag{3.5}$$

$$\rho = \rho_0 \left(1 - \alpha_T (\theta - \theta_0)\right) \tag{3.6}$$

where x,y,z= Cartesian coordinates positive eastward, northward and downward, respectively, t= time, u,v,w= respective velocity components, θ= water temperature, h= undistributed water depth, ζ= water surface elevation above the depth h, ρ= water density, ρ_0= water density at reference temperature θ_0(= 4°C), α_T= volumetric expansion coefficient, Ω= Coriolis parameter, g= gravitational acceleration, N_{zx},N_{zy}= vertical eddy viscosity coefficients, K_{xy},K_z= horizontal and vertical turbulent diffusion coefficients, respectively, c_w= specific heat of water and Q^*= heat flux of internally absorbed radiation.

To obtain unambiguous solutions to Eqn.(3.1) through Eqn.(3.6), the following natural and essential boundary conditions are considered.

(a) Open Boundary (Γ_o)

$$\zeta = \zeta^*(t) \tag{3.7}$$

$$\theta = \theta^*(t) \quad \text{for} \quad u n_x + v n_y < 0 \tag{3.8}$$

$$\text{or} \quad K_{xy}\frac{\partial \theta}{\partial x} n_x + K_{xy}\frac{\partial \theta}{\partial y} n_y = 0 \quad \text{for} \quad u n_x + v n_y \geq 0 \tag{3.9}$$

(b) Inflow/Outflow Boundary (Γ_q)

$$u = u^*(z,t) \tag{3.10}$$

$$\theta = \theta^*(t) \quad \text{for} \quad \text{inflow} \tag{3.11}$$

$$\text{or} \quad K_{xy}\frac{\partial \theta}{\partial x} n_x + K_{xy}\frac{\partial \theta}{\partial y} n_y = 0 \quad \text{for} \quad \text{outflow} \tag{3.12}$$

(c) Insulating Land Boundary (Γ_h)

$$un_x + vn_y = 0 \tag{3.13}$$

$$\text{or} \quad K_{xy}\frac{\partial\theta}{\partial x}n_x + K_{xy}\frac{\partial\theta}{\partial y}n_y = 0 \tag{3.14}$$

(d) Non-Insulating Free Surface Boundary (Λ_h)

$$-\rho N_{zx}\left.\frac{\partial u}{\partial z}\right|_{z=0} = \tau^*_{sx}(t) \quad , \quad -\rho N_{zy}\left.\frac{\partial v}{\partial z}\right|_{z=0} = \tau^*_{sy}(t) \tag{3.15}$$

$$-\rho c_w K_z\left.\frac{\partial X}{\partial z}\right|_{z=0} = Q^*_{sur} \tag{3.16}$$

(e) Insulating Bottom Boundary (Λ_b)

$$-\rho N_{zx}\left.\frac{\partial u}{\partial z}\right|_{z=h} = k_b(\rho u)_{z=h} = \tau_{bx} \quad , \quad -\rho N_{zy}\left.\frac{\partial u}{\partial z}\right|_{z=h} = k_b(\rho v)_{z=h} = \tau_{by} \tag{3.17}$$

$$-\rho K_z\left.\frac{\partial\theta}{\partial z}\right|_{z=h} = 0 \tag{3.18}$$

where n_x,n_y= components of the outward normal to the boundary surface, ζ^*,θ^*,u^*,v^*= respective prescribed boundary values, τ^*_{sx},τ^*_{sy}= components of the prescribed shearing stress at the surface, k_b= bottom resistance coefficient under the assumption of linear inadhesive condition and Q^*_{sur}= heat flux absorbed and released at the water surface. In application of the boundary conditions, the following is assumed.

$$\Gamma_o \cup \Gamma_q \cup \Gamma_h \cup \Lambda_f \cup \Lambda_b = S$$

$$\Gamma_o \cap \Gamma_q \cap \Gamma_h \cap \Lambda_f \cap \Lambda_b = \emptyset \tag{3.19}$$

where S is the whole surface of the three-dimensional domain V and $\emptyset$ is the empty set.

Their vertical diffusivities N_{zx},N_{zy} and K_z can be assumed to exponentially decrease with the increasing local Richardson number[63], i.e.,

$$N_{zx} = N^0_z \exp\left\{-\mu_1 \frac{g\frac{\partial\rho}{\partial z}}{\rho\left(\frac{\partial u}{\partial z}\right)^2}\right\}$$

$$N_{zy} = N^0_z \exp\left\{-\mu_1 \frac{g\frac{\partial\rho}{\partial z}}{\rho\left(\frac{\partial v}{\partial z}\right)^2}\right\}$$

$$K_{zx} = K^0_z \exp\left\{-\mu_2 \frac{g\frac{\partial\rho}{\partial z}}{\rho\left[\left(\frac{\partial u}{\partial z}\right)^2\left(\frac{\partial v}{\partial z}\right)^2\right]}\right\} \tag{3.20}$$

where μ_1,μ_2= undetermined empirical constants ($\mu_1 = 4.0$,$\mu_2 = 18.0$[39]) and the neutral diffusivities N^0_z and K^0_z are given resorting to the Reynolds analogy and the mixing length theory as

$$N^0_z = K^0_z = L^2\left[\left(\frac{\partial u}{\partial z}\right)^2 + \left(\frac{\partial v}{\partial z}\right)^2\right]^{1/2} \tag{3.21}$$

with $L = k(h-z)(z/h)^{1/2}$ (k: Von Karman constant).

In an analogy to the momentum transfer, the diffusivity K_{xy} can be identified with the sub-grid scale (SGS) eddy viscosity[79, 80] expressed in terms of the local velocity deformation and the mesh spacing, which leads to

$$K_{xy} = (s\Delta)^2\left[\left(\frac{\partial u}{\partial x} - \frac{\partial v}{\partial y}\right)^2 + \left(\frac{\partial u}{\partial x} + \frac{\partial v}{\partial y}\right)^2\right]^{1/2} \tag{3.22}$$

where s= dimensionless constant (close to 0.1[11, 59]) and Δ= mesh spacing.

3.3 Heat Exchange and Absorption

3.3.1 Normal Specification of Heat Fluxes Q^* and Q^*_{sur}[41]

The specification of the fluxes Q^* and Q^*_{sur} can generally be based on the following heat budget equation that describes the heat exchange through the water surface.

$$Q = Q_s - Q_{sr} + Q_a - Q_{ar} - Q_{br} - Q_e - Q_c \tag{3.23}$$

where Q= net heat flux, Q_s= short wave radiation, Q_a= long wave radiation, Q_{br}= released long wave radiation, Q_e= latent heat, Q_c= sensible heat and the added subscript (r) indicates reflection.

As Eqn.(3.23) states, the incoming solar radiation consist of a short wave component Q_s and a long wave component Q_a. The former can fractionally penetrate the water surface and be internally absorbed, while the latter is completely absorbed very near the surface. When conveniently separating Q_s into a fraction β absorbed at the surface and a fraction $1-\beta$ absorbed internally, the net flux Q can be rewritten as

$$Q = (1-\beta)(Q_s - Q_{sr}) + \{\beta(Q_s - Q_{sr}) + Q_a - Q_{ar} - Q_{br} - Q_e - Q_c\} \tag{3.24}$$

where β= fraction of incident light absorbed by the water surface. The second term on the left hand side of Eqn.(3.24) is associated with the heat absorbed and released at the surface and thus identified with Q^*_{sur} to be specified in accordance with Eqn.(3.16), i.e.

$$Q^*_{sur} = \beta(Q_s - Q_{sr}) + Q_a - Q_{ar} - Q_{br} - Q_e - Q_c \tag{3.25}$$

On the other hand, the internal absorption is exponentially decreased with depth as defined by the Lambert-Bouger low. The solar radiation Q^* at depth z can therefore be given as

$$Q^* = (1-\beta)(Q_s - Q_{sr})^{-\nu z} \tag{3.26}$$

where ν= extinction coefficient.

When the meteorological forcing conditions are specified, the heat exchange elements in Eqns.(3.25) and (3.26) can be estimated by use of the well-established relations[76];

$$Q_s = Q_{s0}\left(1 - \bar{a}n^{\bar{b}}\right) \tag{3.27}$$

$$Q_{sr} = \alpha_s Q_s \tag{3.28}$$

$$Q_a = \sigma_S \Theta_a^4 \left(\bar{c} + \bar{d}\sqrt{e_a}\right) \tag{3.29}$$

$$Q_{ar} = \alpha_a Q_a \tag{3.30}$$

$$Q_{br} = 0.97\sigma_S \left(\Theta|_{z=0}\right)^4 \tag{3.31}$$

$$Q_e = \left\{0.095\left(\Delta\theta_v\right)^{1/3} + 0.108W\right\}(e_w - e_a)\left(594.9 - 0.51\,\theta|_{z=0}\right) \tag{3.32}$$

$$Q_c = \rho_a c_a k_c \left(\theta|_{z=0} - \theta_a\right) W \tag{3.33}$$

where Q_{s0}= amount of short wave radiation on a clear day (4.1868 J/m^2·s), n_c= amount of cloud, $\bar{a}$,$\bar{b}$,$\bar{c}$,$\bar{d}$= empirical constants, α_s, α_a= albedo (reflectivity), σ_S= Stefan-Boltzman constant (=5.67×10^{-8}W/m^2·K^4), Θ_a, Θ= absolute temperatures of air and water, respectively (K), s=0.97, θ_a,e_a= temperature (°C) and vapor pressure of air (hPa), e_w= saturated vapor pressure (hPa) for θ at z=0, ρ_a,c_a= density and specific heat of air, respectively, k_c= heat transfer coefficient, W= wind speed (m/s) and $\Delta\theta_v$= a function of θ at z=0, θ_a,e_a,e_w and atmospheric pressure.

3.3.2 Modified specification

Usually the flux Q^*_{sur} estimated by Eqn.(3.25) is negative and therefore reflects the heat loss upward from the surface. As a result, the surface is somewhat cooler than the water below to which the flux Q^* is transported according to Eqn.(3.26), thus producing a layer of limited depth with densimetric (gravitational) instability. In shallow water reality, however, such a unstable layer is by no means observed. This is interpreted as a necessary consequence of the vertical convective mixing by the kinetic energy that is generated by free convection and/or wind stress. Unfortunately the mathematical model represented by Eqns(3.1) through (3.6) lacks expression of this convective phenomenon, though it has the capability of expressing an enhancement of turbulent diffusion which results from the unstable temperature gradient since the negative local Richardson number leads to an enlargement of K_z. Namely the vertical velocities resulting from occurrence of the horizontal velocities, represented by Eqn.(3.2), are those which may induce mixing of injected water through the boundaries Γ_0 or Γ_q with indigenous water, i.e., mixing by forced convection, but not those which may eliminate the unstable thermal stratification caused by the heat exchange at the surface.

In order to compensate for this lack of the model, earlier model[33] employed an approximate numerical technique that renders solutions of the temperature in a surface layer of densimetric instability uniform (T_a in Fig.(3.1)(a)) within so presumable thickness, based on an instantaneous thermal energy balance caused by the convective mixing. This poses an awkward problem, however, that the temperature gradient near the surface which Γ_0 or Γ_q may cause is also made to vanish.

Now the alternative is proposed that prior to solving Eqns.(3.1) through (3.6) the upward heat flux Q^*_{sur} is cancelled by appropriately modifying the distribution of the downward heat flux Q^*. The distribution $Q^{**}(z) = -\partial Q^*/\partial z$ is then modified as

$$\begin{aligned} \text{For} \quad 0 \geq z \geq z_l : \qquad & Q^{**}(z) = (1-\beta)(Q_s - Q_{sr})\nu \exp(-\nu z_l) \\ \text{For} \quad z_l < z : \qquad & Q^{**}(z) = (1-\beta)(Q_s - Q_{sr})\nu \exp(-\nu z) \end{aligned} \tag{3.34}$$

with a depth z_l necessary for cancellation of Q^*_{sur} (See Fig.(3.1)(b)) that can be found by solving the following equation with the aid of the bisection method.

$$\int_0^{z_l} (1-\beta) Q_s \nu \{\exp(-\nu z) - \exp(-\nu z_l)\} dz = Q^*_{sur} \tag{3.35}$$

In computational practice, Eqn.(3.34) is applied to Eqn.(3.5) and Q^*_{sur} in Eqn.(3.16) is set equal to zero, discarding Eqn(3.26) and Eqn.(3.25), respectively. This technique exerts no influence on the solution subject to the boundary conditions and must therefore be an undoubtedly better alternative to the above-mentioned one.

3.4 Model Building

For finite element representations of Eqn.(3.1) through (3.6), the primitive variables are first approximated by the following series including the Chebyshev polynomials as depth-dependent basis functions.

$$\begin{aligned} u &= A_r(x,y,t)T_r(H) \\ v &= B_r(x,y,t)T_r(H) \\ \theta &= C_r(x,y,t)T_r(H) \end{aligned} \tag{3.36}$$

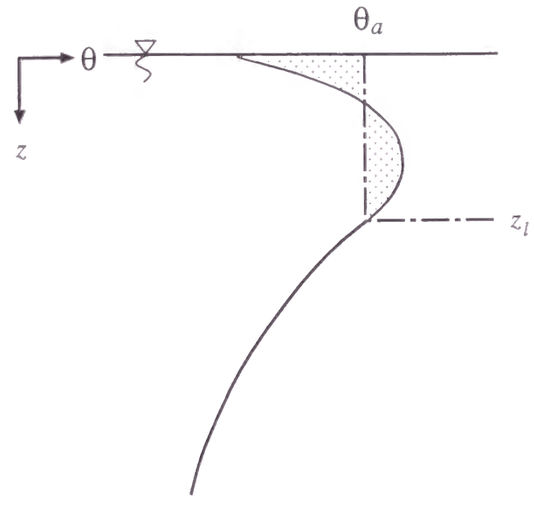

(a) MIT model

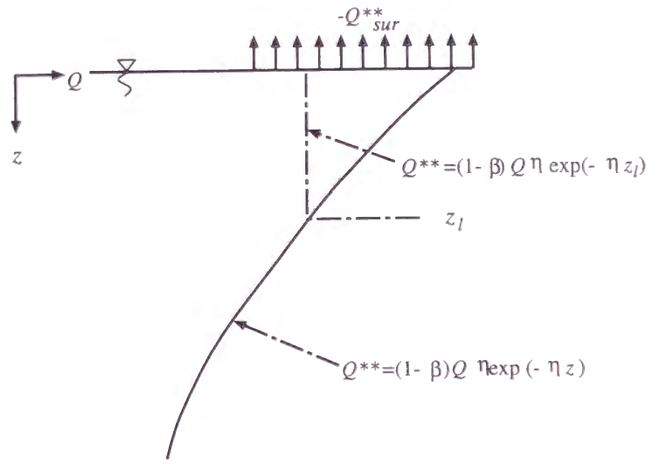

(b) Present model

Figure 3.1: Convective mixing of surface water

where $r(=0,1,2,\cdots,m)$= repeated subindex implying summation and $T_r(H)$= Chebyshev polynomials given by the recurrence relation;

$$\begin{aligned} r=0 \quad &: \quad T_0(H)=1 \\ r=1 \quad &: \quad T_1(H)=H \\ r\geq 2 \quad &: \quad T_r(H)=2HT_{r-1}(H)-T_{r-2}(H) \end{aligned} \tag{3.37}$$

$$H=\frac{2z-h}{h} \qquad (-1\geq H\geq 1) \tag{3.38}$$

Assuming that the temperature distribution arising from the last term on the right hand side of Eqn.(3.5) can be interpolated by the Chebyshev polynomial, the term is also approximated by

$$\frac{1}{\rho c_w}\frac{\partial Q^*}{\partial z}=Q_r^{**}(x,y,t)T_r(H) \tag{3.39}$$

Substituting Eqn.(3.36) into Eqns.(3.3) and Eqn.(3.4) and Eqns.(3.36) and (3.39) into Eqn.(3.5), and applying the Galerkin approximation with the weighting function $T_k(H)$ $(k=0,1,2,\cdots,m)$ to the resulting equations achieve vertical integrations with elimination of the partial derivatives with respect to depth coordinate. In this approximation the depth-dependent second order derivatives are integrated by parts to accommodate the natural boundary conditions Eqns.(3.15),(3.16),(3.17) and (3.18) in the respective equations. Eqns.(3.1) and (3.2) are also cast into the approximate ones by direct introduction of Eqn.(3.36) with a variable conversion from z to H. In consequence we have a suite of the following equations.

$$\frac{\partial\zeta}{\partial T}=-\frac{\partial\bar{A}}{\partial x}-\frac{\partial\bar{B}}{\partial y} \tag{3.40}$$

$$W=-\frac{\partial\bar{A}_H}{\partial X}-\frac{\partial\bar{B}_H}{\partial Y} \tag{3.41}$$

$$\frac{\partial A_k}{\partial t}=-\frac{\partial A_k^u}{\partial x}-\frac{\partial A_k^v}{\partial y}-A_k^w+\Omega B_k-gb_k\frac{\partial\zeta}{\partial x}-\frac{\partial C_k^0}{\partial x}-A_k^z-T_k^h\phi^h+T_k^0\phi^0 \tag{3.42}$$

$$\frac{\partial B_k}{\partial t}=-\frac{\partial B_k^u}{\partial x}-\frac{\partial B_k^v}{\partial y}-B_k^w-\Omega A_k-gb_k\frac{\partial\zeta}{\partial y}-\frac{\partial C_k^0}{\partial y}-B_k^z-T_k^h\psi^h+T_k^0\psi^0 \tag{3.43}$$

$$\frac{\partial C_k}{\partial t}=-\frac{\partial C_k^u}{\partial x}-\frac{\partial A_k^x}{\partial x}-\frac{\partial C_k^v}{\partial y}-\frac{\partial B_k^y}{\partial y}+C_k^w+C_k^{w'}+\frac{\partial^2 C_k^s}{\partial x^2}-\frac{\partial^2 C_k^s}{\partial y^2}-C_k^z+T_k^0\delta^s-Q_k^{**} \tag{3.44}$$

where

$$\bar{A}=\frac{1}{2}h\left[\int_{-1}^{1}T_r dH\right]A_r \quad , \quad \bar{B}=\frac{1}{2}h\left[\int_{-1}^{1}T_r dH\right]B_r$$

$$\bar{A}_H=\frac{1}{2}h\left[\int_{H}^{1}T_r dH\right]A_r \quad , \quad \bar{B}_H=\frac{1}{2}h\left[\int_{H}^{1}T_r dH\right]B_r$$

$$\bar{M}_{ks}=\left[\int_{-1}^{1}T_kT_s dH\right]^{-1} \quad , \quad b_k=\bar{M}_{ks}\int_{-1}^{1}T_s dH$$

$$A_k^u=\left[\bar{M}_{ks}\int_{-1}^{1}T_s\left(A_pT_p\right)T_r dH\right]A_r \quad , \quad B_k^u=\left[\bar{M}_{ks}\int_{-1}^{1}T_s\left(A_pT_p\right)T_r dH\right]B_r$$

$$C_k^u=\left[\bar{M}_{ks}\int_{-1}^{1}T_s\left(A_pT_p\right)T_r dH\right]C_r \quad , \quad A_k^v=\left[\bar{M}_{ks}\int_{-1}^{1}T_s\left(B_pT_p\right)T_r dH\right]A_r$$

$$B_k^v=\left[\bar{M}_{ks}\int_{-1}^{1}T_s\left(B_pT_p\right)T_r dH\right]B_r \quad , \quad C_k^v=\left[\bar{M}_{ks}\int_{-1}^{1}T_s\left(B_pT_p\right)T_r dH\right]C_r$$

$$A_k^w=\left[\bar{M}_{ks}\int_{-1}^{1}T_s w\frac{2}{h}\frac{\partial T_r}{\partial H}dH\right]A_r \quad , \quad B_k^w=\left[\bar{M}_{ks}\int_{-1}^{1}T_s w\frac{2}{h}\frac{\partial T_r}{\partial H}dH\right]B_r$$

$$C_k^w=\left[\bar{M}_{ks}\int_{-1}^{1}T_s w\frac{2}{h}\frac{\partial T_r}{\partial H}dH\right]C_r \quad , \quad C_k^0=\frac{\alpha_T gh}{2}\left[\bar{M}_{ks}\int_{-1}^{1}T_s\frac{\int_{-1}^{H}T_r dH}{1-\alpha_T\left\{C_pT_p-\theta_0\right\}}dH\right]C_r$$

$$A_k^z=\frac{4}{h^2}\left[\bar{M}_{ks}\int_{-1}^{1}N_{zx}\frac{dT_s}{dH}\frac{dT_r}{dH}dH\right]A_r \quad , \quad B_k^z=\frac{4}{h^2}\left[\bar{M}_{ks}\int_{-1}^{1}N_{zy}\frac{dT_s}{dH}\frac{dT_r}{dH}dH\right]B_r$$

$$C_k^z=\frac{4}{h^2}\left[\bar{M}_{ks}\int_{-1}^{1}K_z\frac{dT_s}{dH}\frac{dT_r}{dH}dH\right]C_r \quad , \quad A_k^x=\left[\bar{M}_{ks}\int_{-1}^{1}T_s\left(C_pT_p\right)T_r dH\right]A_r$$

$$B_k^y=\left[\bar{M}_{ks}\int_{-1}^{1}T_s\left(C_pT_p\right)T_r dH\right]B_r \quad , \quad C_k^s=\left[\bar{M}_{ks}\int_{-1}^{1}K_zT_sT_r dH\right]C_r$$

$$C_k^{w'}=\bar{M}_{ks}\frac{2}{h}\left\{T_s(1)T_k(1)w(1)-T_s(-1)T_k(-1)w(-1)\right\}C_k$$

$$T_k^h = \bar{M}_{ks} T_s(+1) \quad , \quad T_k^0 = \bar{M}_{ks} T_s(-1)$$

$$\phi^h = \frac{2\tau_{bx}}{\rho_h h} \quad , \quad \phi^0 = \frac{2\tau_{sx}}{\rho_0 h} \quad , \quad \psi^h = \frac{2\tau_{by}}{\rho_h h} \quad , \quad \psi^0 = \frac{2\tau_{sy}}{\rho_0 h} \quad , \quad \delta^0 = \frac{2Q^*_{sur}}{\rho_0 c_w h}$$

$$\rho_h = \rho_0 \left\{1 - \alpha_T \left(C_p T_p(+1) - \theta_0\right)\right\} \quad , \quad \rho_0 = \rho_0 \left\{1 - \alpha_T \left(C_p T_p(-1) - \theta_0\right)\right\}$$

with the repeated indices p, r and s (=0,1,2,$\cdots$,m) implying summation.

Secondly an entire set of Eqns.(3.40) through (3.44) is integrated over the horizontal domain by reuse of the Galerkin process. Variations of the k-th components of the unknown coefficients A_r, B_r and C_r are then assumed linear within a triangular element, i.e.,

$$\begin{aligned} A_k &= G_j(x,y) A_{kj}(t) \\ B_k &= G_j(x,y) B_{kj}(t) \\ C_k &= G_j(x,y) C_{kj}(t) \end{aligned} \tag{3.45}$$

where j= repeated subindex implying summation (j=1,2,3) and G= linear basis function. Similarly Q_k^{**}, ζ and w are expressed as;

$$\begin{aligned} Q_k^{**} &= G_j(x,y) Q_{kj}^{**}(t) \\ \zeta &= G_j(x,y) \zeta_j(t) \\ w &= G_j(x,y) w_j(t) \end{aligned} \tag{3.46}$$

The Galerkin integration is performed with the weighting function $G_j(x,y)$ (j=1,2,3), and the natural boundary conditions Eqns.(3.8), (3.10) and (3.12) are then satisfied. Thus we have a set of ordinary differential equations in time and the algebraic local continuity equation;

$$M_{ij} \frac{d\zeta_j}{dt} = -P_{ij}^x \bar{A}_j - P_{ij}^y \bar{B}_j \tag{3.47}$$

$$\begin{aligned} M_{ij} \frac{dA_{kj}}{dt} = &-P_{ij}^x A_{kj}^u - P_{ij}^y A_{kj}^u - M_{ij} A_{kj}^w + \Omega M_{ij} B_{kj} - g b_k P_{ij}^x \zeta_j \\ &-P_{ij}^x C_{kj}^0 - M_{ij} A_{kj}^z - T_k^h M_{ij} \phi_j^h + T_k^0 M_{ij} \phi_j^0 \end{aligned} \tag{3.48}$$

$$\begin{aligned} M_{ij} \frac{dB_{kj}}{dt} = &-P_{ij}^x B_{kj}^u - P_{ij}^y B_{kj}^u - M_{ij} B_{kj}^w - \Omega M_{ij} A_{kj} - g b_k P_{ij}^y \zeta_j \\ &-P_{ij}^y C_{kj}^0 - M_{ij} B_{kj}^z - T_k^h M_{ij} \psi_j^h + T_k^0 M_{ij} \psi_j^0 \end{aligned} \tag{3.49}$$

$$\begin{aligned} M_{ij} \frac{dC_{kj}}{dt} = &-P_{ij}^x C_{kj}^u - P_{ij}^x A_{kj}^x - P_{ij}^y C_{kj}^v - P_{ij}^y B_{kj}^y - M_{ij} C_{kj}^w - M_{ij} C_{kj}^{w'} \\ &-D_{ij} C_{kj}^s - M_{ij} C_{kj}^z + T_k^0 M_{ij} \delta_j^0 - M_{ij} Q_{kj}^{**} \end{aligned} \tag{3.50}$$

$$M_{ij} w_j = P_{ij}^x \bar{A}_{Hj} \pm P_{ij}^y \bar{B}_{Hj} \tag{3.51}$$

where

$$M_{ij} = \int_A G_i G_j dA \quad , \quad P_{ij}^x = \int_A G_i \frac{\partial G_j}{\partial x} dA \quad , \quad P_{ij}^y = \int_A G_i \frac{\partial G_j}{\partial y} dA$$

$$D_{ij}^x = \int_A \left[\frac{\partial G_i}{\partial x} \frac{\partial G_j}{\partial x} + \frac{\partial G_i}{\partial y} \frac{\partial G_j}{\partial y} \right] dA$$

For integration of Eqn.(3.47) through (3.50), time is stepwise advanced in quite the same manner as in the referring works [44, 45]: Eqns.(3.47) through (3.49) are integrated by the Kawachi scheme, while Eqn(3.50) by the forward time scheme. Since both schemes are of explicit type where only two time stages $t = n$ and $t = n + 1$ are considered, the mass matrix M_{ij} at $t = n + 1$ which impedes explicit determination of the unknowns is diagonalized by the lumped mass approximation. On the other hand, the mass matrix at $t = n$ is replaced with the generalized mass matrix that permits us to selectively damp the useless short waves generated by numerical disturbances. After proper assembly of the resulting algebraic equations over an entire domain of interest, all the solutions at $t = n + 1$ are, in conjunction with Eqn.(3.51), obtainable one after another without solving huge simultaneous equations.

3.5 Applications

Applicability and validity of the model are tested by simulating two thermal stratification problems: (1) bottom water cooling by cold water discharge in hypothetical reservoir, (2) surface water heating by solar radiation in a real irrigation tank. Throughout these two simulations the order of the Chebyshev polynomials is fixed to be four.

3.5.1 Hypothetical Reservoir

The reservoir of rectangular expanding cross section is considered to make a demonstrative simulation of the bottom water cooling problem. As shown in Fig.3.2, the solution domain is in the horizontal discretized into a total of 140 elements jointed at the 100 common nodes. The inlet plane on the left side of the reservoir where the cold water is introduced is treated as Γ_q-boundary, while the opposite plane as Γ_0-boundary. The remainder is of Γ_h-boundary.

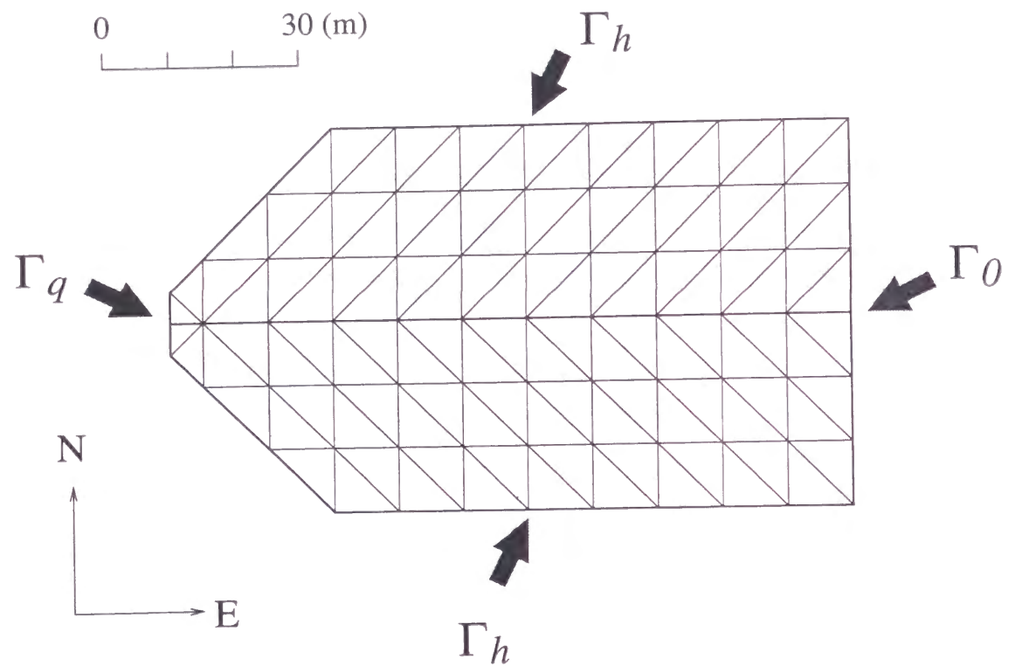

Figure 3.2: Finite element spatial discretization of hypothetical reservoir

The water in the reservoir is initially quiescent and at a uniform temperature of 25°C. During the simulation, the cold water at 10°C is introduced into the whole of the inlet plane at a rate of 0.02 m/s. At the opposite plane the water level is specified as $\zeta = 0$ and temperature is specified as 25°C only for the inflow which occurs by the density-induced counter flow. In this case no heat exchange through the water surface

is considered. Thus the simulation considers the situation of cold river water flowing in an impoundment.

Part of the results obtained are illustrated in Fig.3.3 and Fig.3.4 which include the temperature and velocity distributions at selected three times stages along the center line of the reservoir, respectively. Note that a mixture of the temperature boundary conditions at the right end plane where counter flow occurs, i.e., the essential conditions for the upper inflow and the natural conditions for the lower outflow, is successfully achieved even by the polynomial function.

3.5.2 Irrigation Tank

To verify the model in an actual case, a small-scale irrigation tank with an are of about 2,270m^2 and a maximum depth of 1.6m, called Benten-Ike pond, is taken as the object for the simulation. The tank is located on the premises of Kanto-Gakuin University, and therefore the intensive field investigation of its water temperature and heat budget was conducted by the research group of the university and the results and relevant date were in detail published in the literature[77]. The tank has just one inlet and one outlet. The capacity of the outlet is big enough, compared to the inflow, to keep the water surface fluctuation within the range of 5cm. There are some small springs and infiltrations in the restricted portions of the tank bed, and they perceptibly regulate local heat budget.

Using the topographical and bathymetrical maps available, the domain is discretized into 151 elements jointed at the 97 common nodes, as shown in Fig.3.5, and the variable water depth is given at the nodes. The date of May 12,1980 when the vertical temperature distributions at some selected locations were observed is considered in the simulation, thus taking the meteorological conditions as cloudy weather, θ_a= 23.2°C and W=1.0m/s(east). Daily mean discharge of the outflow which is specified at the inlet is 53.61ℓ/min. The water level and water temperature specified at the inlet are the normal retention level of the tank and 16.1°C, respectively.

The numerical experiments executed to identify the parameters ν and β showed that β was far less sensitive to the solutions than ν and consequently ν=2.5m^{-1} and β=0.10 were best at reproducing the observed water temperature distributions. Such a relatively

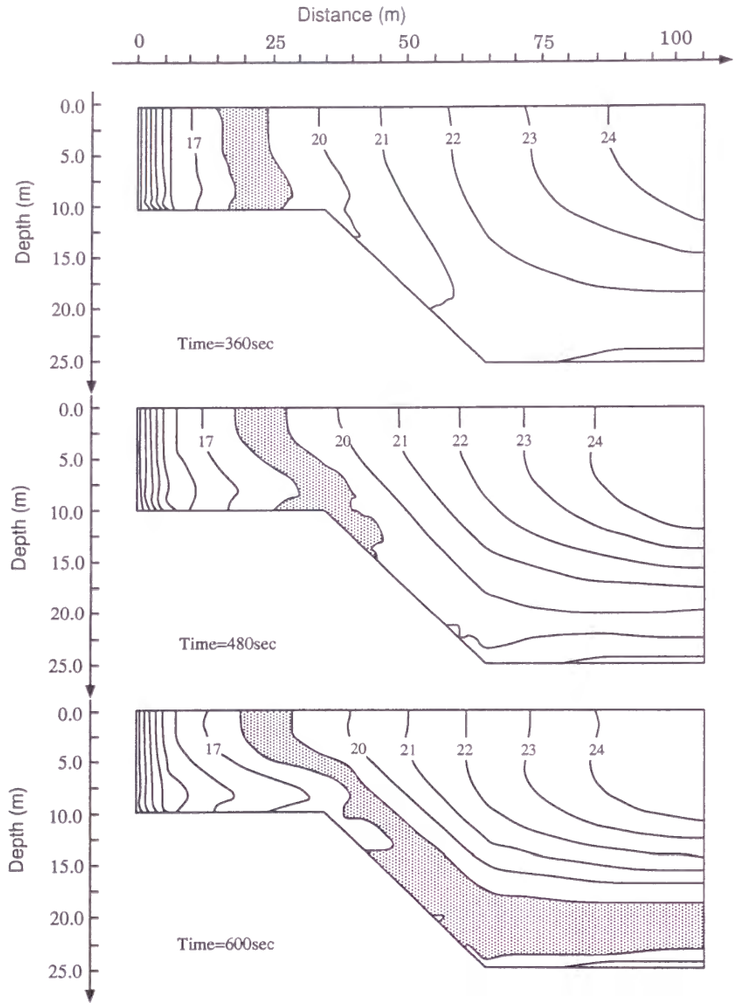

Figure 3.3: Time-varying temperature profiles

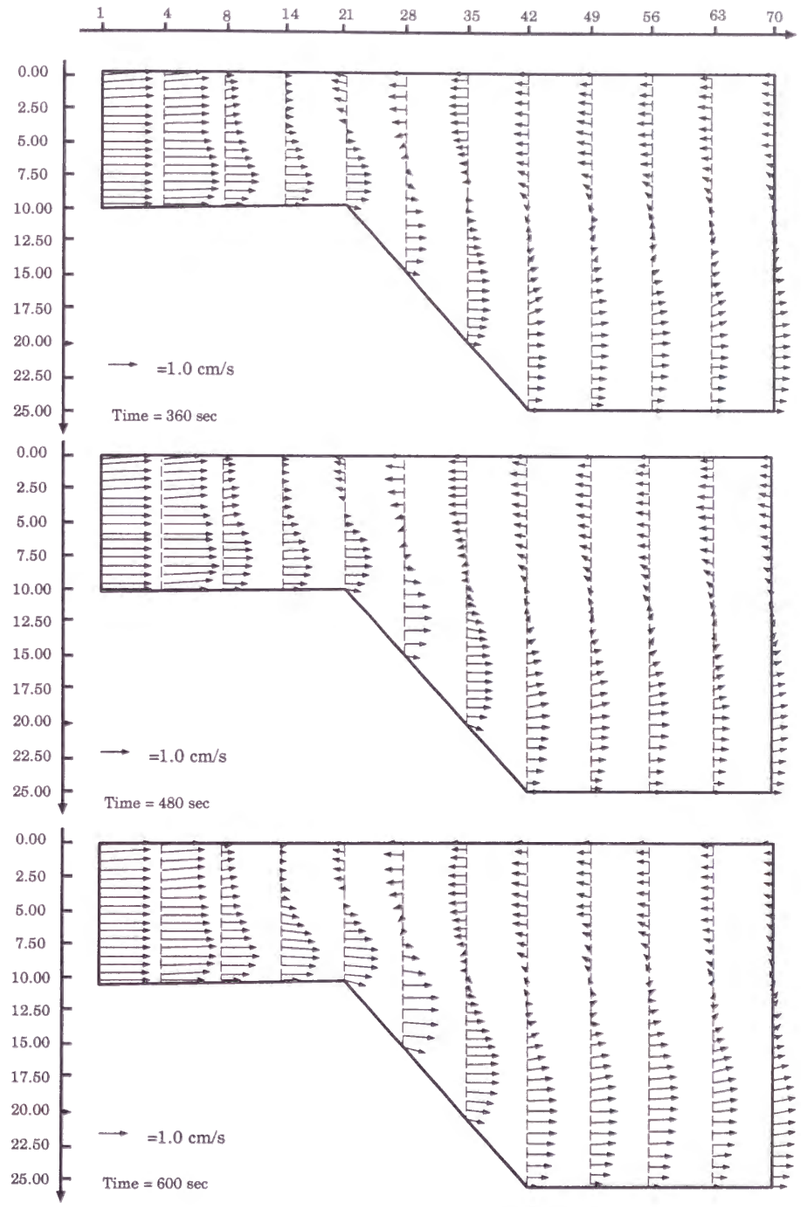

Figure 3.4: Water motion along the center line

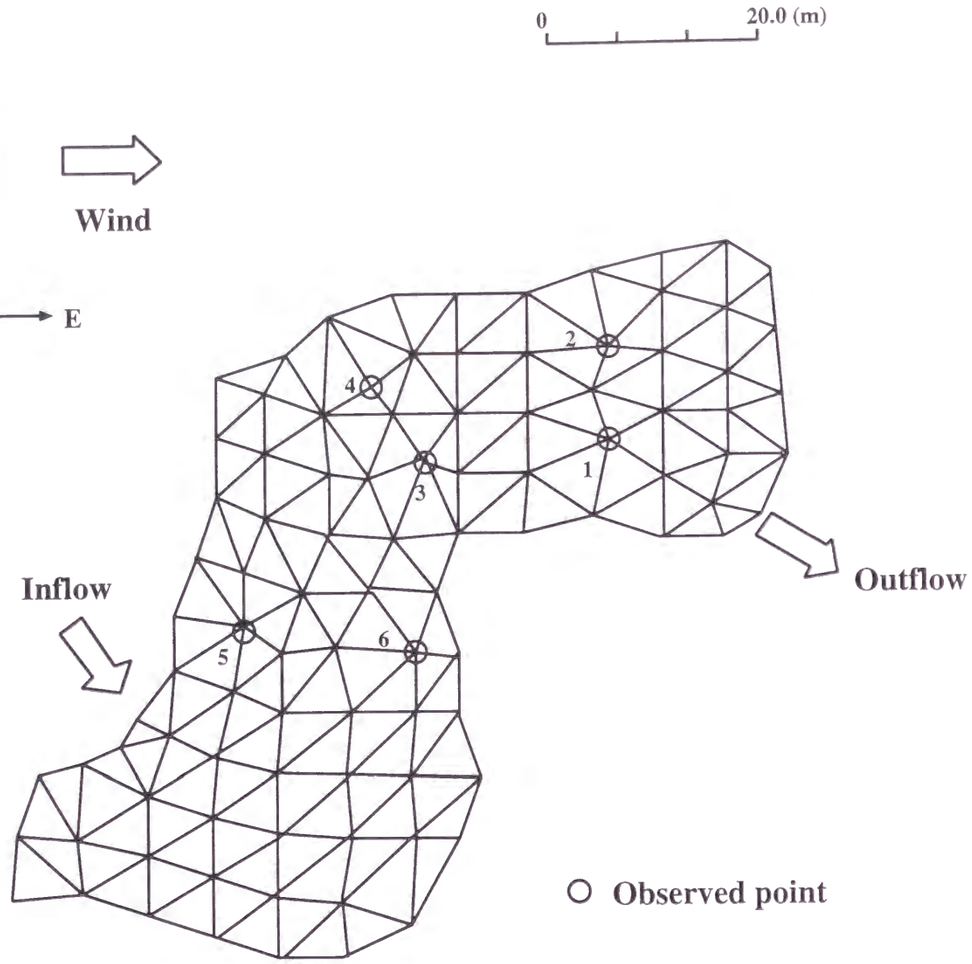

Figure 3.5: Finite element spatial discretization of irrigation tank

large ν-value may be justified by the fact that in general a small and shallow pond like the present irrigation tank has very low transparency and thereby renders the incident light extinct in a shallow level of the depth. Comparison of the computed steady-state temperature distributions under these identified value with the observed ones is given in Fig.3.6. For all except one at the point No.1 under the influence of the cold spring, the computed results are in good agreement with the observed ones that have a band of ± 0.5°C as an observational error. The computed water motions are illustrated in Fig.3.7 for the three levels of water depth.

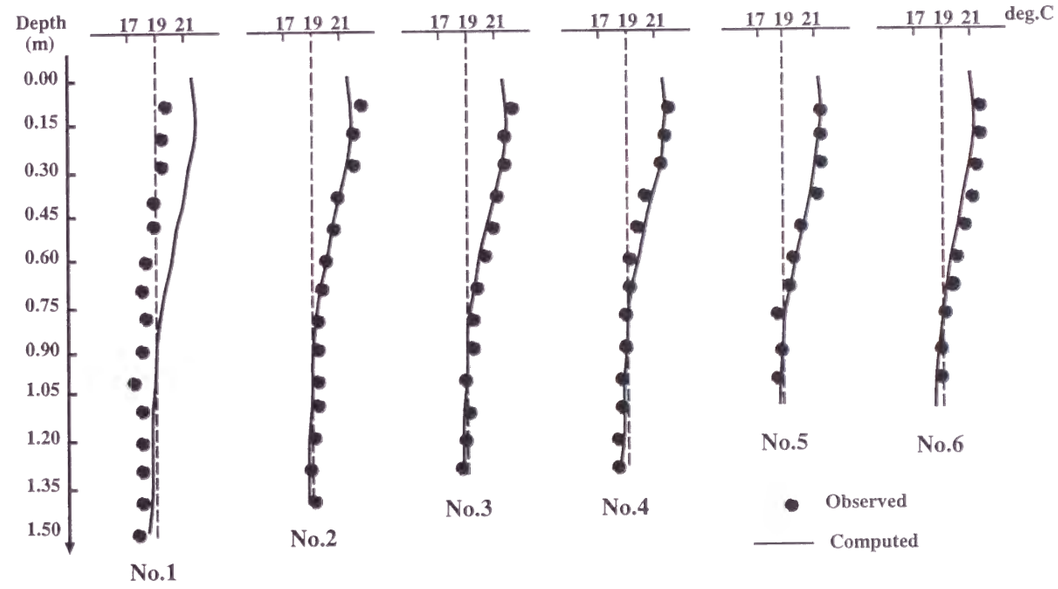

Figure 3.6: Vertical temperature distributions

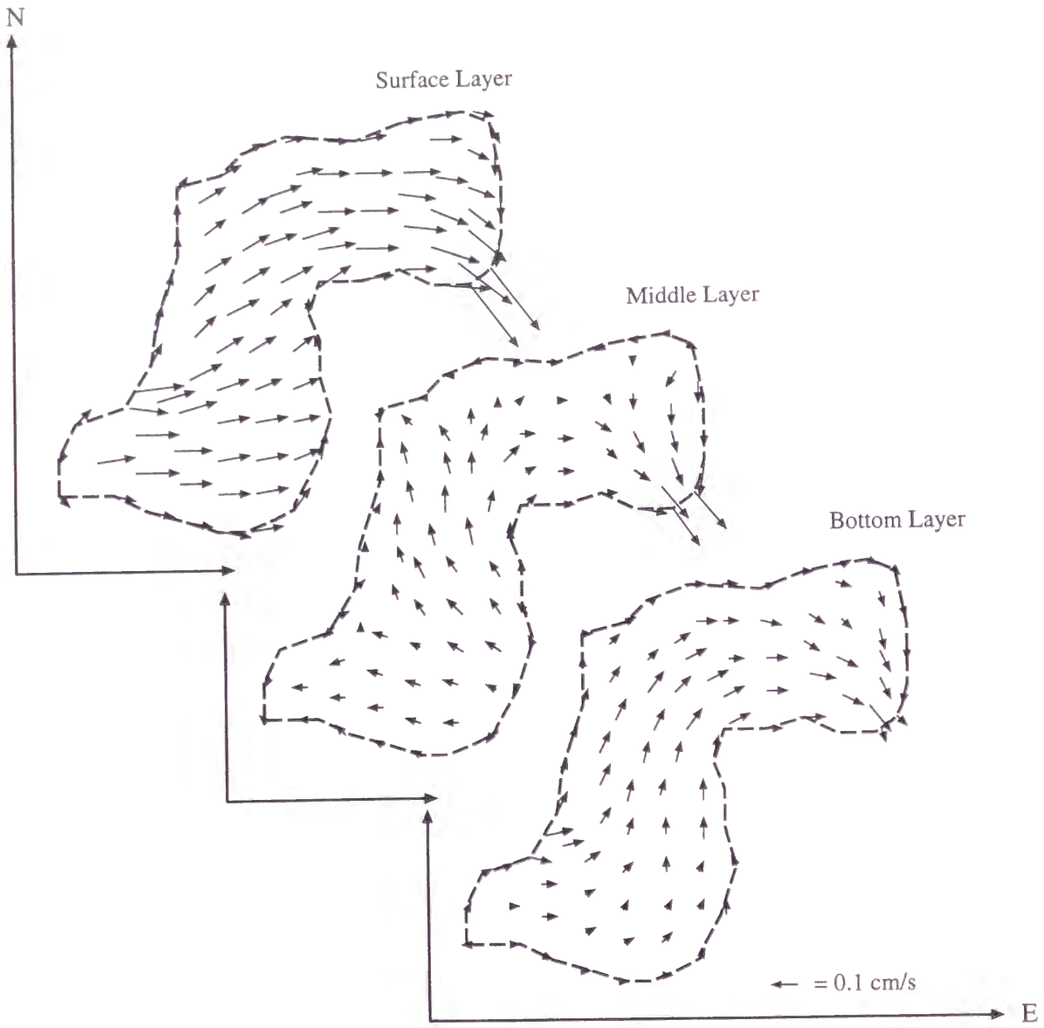

Figure 3.7: Three-dimensional water motion

3.6 Conclusions

A 3-D finite element model for flow and temperature studies has been presented. Through an advance modification of the distribution of internally absorbed heat flux, this model allows for the effect of free and/or wind-induced convection in a surface layer. The model also allows for depth dependency of the vertical viscosity and diffusion coefficients and SGS dependency of the horizontal diffusivities, based on the turbulence transfer theories commonly accepted. Due to these inclusion and the finite element formulation, we can predicate of this model that it has a high level of generality. And its operation is easy and flexible being free from depthwise discretization and capable of specifying the accuracy of solution profile by only a parametric change of the order of the polynomials.

Extending the model to include other water quality constituents is relatively straightforward, but increasingly expensive with the increase in number of the constituents to be solved. Nevertheless this extension is considered extremely significant since for water quality and hydro-environmental studies numerical models are in many aspects much more attractive than empirical hydraulic model.

Chapter 4

POLYNOMIAL FINITE ELEMENT SOLUTION OF 3-D DENSITY-DRIVEN CURRENTS USING THE VELOCITY CORRECTION METHOD

4.1 Introduction

In recent years three-dimensional (3-D) mathematical models for the description of time-dependent flow problems have been investigated using a variety of methods. However, most of them applied to lakes, estuaries and/or coastal sea neglect the acceleration of the vertical velocity. Since the quality of water is often related to the vertical density structure, it is required to express the vertical velocity not via horizontal velocities in accessing environmental problems. Though some methods are proposed to satisfy the solenoidal condition and reveal vertical accelerations, they are inadequate yet for the shallow water computation, including some problems awaiting solution.

For the development of 3-D hydraulic and environmental model of large water bodies, the author attempts the combined use of the 3-D Galerkin finite element method and the velocity correction method. The velocity correction method is one of the most hopeful methods to satisfy the solenoidal condition. The aim of the study is to combine it with the 3-D polynomial model successfully and make a versatile fully 3-D finite element flow model coupled with salinity and heat effects.

In the finite element modelling horizontally two-dimensional well-defined basis sets and vertically Chebyshev polynomial basis sets are applied. By the use of depth-dependent polynomial basis functions the computational volume can be saved, com-

pared with fully 3-D discretization by tetrahedral or cubic elements. At the same time the model can avert the large "aspect ratio" that often arises in discretizing shallow waters and induces numerical inaccuracies. In the time marching procedure the explicit Kawachi and FT schemes with the velocity correction method which is a branch of the fractional step method are applied. This method satisfies the incompressible condition through the pressure Poisson equation without neglecting the depthwise acceleration of the flow and makes it feasible to compute the flow stably with no smoothing technique and mixed interpolation method.

The present model is based on the earlier works of 3-D polynomial models [44, 45] to take over their merits, namely, (1) easy to operate, especially in discretizing even complex geometries, (2) indiscrete vertical distributions of the quantities of direct interest can be obtained and the degree of approximations in the vertical can freely be specified, (3) easy to introduce surface boundary conditions with depthwise exponential intrusion of short wave radiation and other heat exchanges.

Applicability is tested through analyzing caballing effects and topographic heat accumulation effects with/without the Coriolis effects in hypothetical water bodies.

4.2 Algorithm

4.2.1 Governing Equations

Considering three-dimensional spatial domain V with x, y, z representing the coordinates positive eastward, northward, downward, respectively and accepting the Boussinesq approximation, the mathematical description of motion for transient viscous incompressive fluid is given by the Navier-Stokes equations and the continuity equation as;

$$\frac{\partial \boldsymbol{u}}{\partial t} + (\boldsymbol{u} \cdot \nabla)\boldsymbol{u} = \frac{\rho}{\rho_0}\boldsymbol{F} - \frac{1}{\rho_0}\nabla \cdot (p\boldsymbol{I}) + \boldsymbol{\mu}\nabla^2 \boldsymbol{u} \tag{4.1}$$

$$\nabla \cdot \boldsymbol{u} = 0 \tag{4.2}$$

where ρ, ρ_0, $\boldsymbol{u}(= [u, v, w]^T), p$, $\boldsymbol{I}$, $\boldsymbol{F}(= \Omega[-v, u, 0]^T), \Omega$ and $\boldsymbol{\mu}$ are density, reference density, velocity, pressure, identity tensor, body force, Coriolis parameter and eddy viscosity [44], respectively.

Assuming that the density variation depends only on salinity and temperature, salinity S, temperature θ and the state of density ρ are related by the following advection-diffusion equations and Eckart's formula [14].

$$\frac{\partial S}{\partial t} + \nabla \cdot (\boldsymbol{u}S) = \nabla \cdot (\boldsymbol{K}_s \nabla S) \tag{4.3}$$

$$\frac{\partial \theta}{\partial t} + \nabla \cdot (\boldsymbol{u}\theta) = \nabla \cdot (\boldsymbol{K}_\theta \nabla \theta) \tag{4.4}$$

$$\rho = \frac{m_0 + m_1 S}{\bar{m}_0 + \bar{m}_1 S} \tag{4.5}$$

$$m_0 = (5890.0 + 38.0 \times \theta - 0.375 \times \theta^2) \times 10^3$$

$$m_1 = 3.0 \times 10^3$$

$$\bar{m}_0 = (5890.72 + 37.774 \times \theta - 0.33625 \times \theta^2) \times 10^3$$

$$\bar{m}_1 = -1.706 - 0.001 \times \theta$$

where $\boldsymbol{K}_s$, $\boldsymbol{K}_\theta$, and Q^* are eddy diffusivities and heat source term relating to heat exchange through the surface, respectively.

And the position of the surface is governed by the following equation.

$$\frac{\partial \zeta}{\partial t} + \left(\boldsymbol{u}^0 \cdot \nabla\right)\zeta = 0 \tag{4.6}$$

where ζ is the surface elevation measured from the reference level and $\boldsymbol{u}^0$ is the velocity at the surface.

4.2.2 Boundary Conditions

For the complete mathematical description of the governing equations above, appropriate boundary conditions must be specified. Let Γ be a piecewise smooth boundary of a horizontal domain Ω and Λ be surface and bottom boundaries of a vertical domain over water depth h.

Γ is composed of the following three boundaries.

(a) Open Boundary (Γ_o)

$$\eta = \eta^*(t) \tag{4.7}$$

(b) Inflow/Outflow Boundary (Γ_q)

$$\boldsymbol{u} = \boldsymbol{u}^*(z,t) \tag{4.8}$$

(c) Insulating Land Boundary (Γ_h)

$$\boldsymbol{u} \cdot \boldsymbol{n} = 0 \tag{4.9}$$

where $\boldsymbol{n}$ is the components of the outward unit vector normal to the boundary surface Γ, and the superscript (*) indicates the boundary value specified. On these boundaries the following conditions regarding salinity and temperature are given.

$$X = X^*(t) \quad \text{for} \quad \boldsymbol{u} \cdot \boldsymbol{n} < 0 \tag{4.10}$$

$$\boldsymbol{K}_h(\boldsymbol{n} \cdot \nabla)X = \sigma_f^* = 0 \quad \text{for} \quad \boldsymbol{u} \cdot \boldsymbol{n} \geq 0 \tag{4.11}$$

where X is a substitute for S and θ, and σ_f^* is the diffusion transport to vanish for the flow leaving the domain.

On the surface boundary, the heat exchange including the intrusion of the short wave radiation, subjected to the Lambert-Beer low, is handled through the convective adjustment technique. And on the bottom boundary geographical feature is well-considered by the 3-D treatment.

(d) Non-Insulating Free Surface Boundary (Λ_s)

$$-\rho\mu_z \left.\frac{\partial \boldsymbol{u}}{\partial z}\right|_{z=0} = \tau_s^* \tag{4.12}$$

$$-K_z \left.\frac{\partial X}{\partial z}\right|_{z=0} = \sigma_s^* \tag{4.13}$$

(e) Insulating Bottom Boundary (Λ_b)

$$-\rho\mu_z \left.\frac{\partial \boldsymbol{u}}{\partial z}\right|_{z=h} = \tau_b^* \tag{4.14}$$

$$-K_z \left.\frac{\partial X}{\partial z}\right|_{z=h} = \sigma_b^* \tag{4.15}$$

$$\boldsymbol{u} \cdot \boldsymbol{n} = 0 \tag{4.16}$$

where $\boldsymbol{n}$ is the outward unit vector normal to the boundary surface, and τ and σ are the components of the shearing stress and the salt and/or heat flux, respectively.

4.2.3 Velocity Correction Method

The algorithm of this method[13, 49, 68, 75, 78] which is based on Helmholtz's decomposition theorem is formulated as follows. Applying the forward Eulerian Scheme to the time derivative terms leads Eqns.(4.1) and (4.2) to;

$$\frac{\boldsymbol{u}^{n+1} - \boldsymbol{u}^n}{\Delta t} + (\boldsymbol{u}^n \cdot \nabla)\,\boldsymbol{u}^n = \frac{\rho^n}{\rho_0}\boldsymbol{f}^n - \frac{1}{\rho_0}\nabla \cdot \left(p^{n+1}\boldsymbol{I}\right) + \mu\nabla^2\boldsymbol{u}^n \tag{4.17}$$

$$\nabla \cdot \boldsymbol{u}^{n+1} = 0 \tag{4.18}$$

where Δt is the time increment between current (n) and advanced $(n+1)$ time stages.

Herein the pressure is divided into the hydrostatic pressure p_s and the hydrodynamic pressure $p_d^{n+1/2}$, and the velocity $\boldsymbol{u}^{n+1/2}$ is considered, where $(n+1/2)$ means intermediate time stages. Then we can have $\boldsymbol{u}^{n+1/2}$ and p_s defined as;

$$\frac{\boldsymbol{u}^{n+1/2} - \boldsymbol{u}^n}{\Delta t} + (\boldsymbol{u}^n \cdot \nabla)\,\boldsymbol{u}^n = \frac{\rho^n}{\rho_0}\boldsymbol{f}^n - \frac{1}{\rho_0}\nabla \cdot (p_s^n\boldsymbol{I}) + \mu\nabla^2\boldsymbol{u}^n \tag{4.19}$$

$$p_s = g\int_0^z \rho dz \tag{4.20}$$

Note that $\boldsymbol{u}^{n+1/2}$ i n Eqn.(4.19) does not satisfy the solenoidal condition. Subtracting Eqns.(4.17) from (4.19) yields the relationship between the u^{n+1} and $u^{n+1/2}$;

$$\boldsymbol{u}^{n+1} = \boldsymbol{u}^{n+1/2} - \frac{\Delta t}{\rho_0}\nabla \cdot \left(p_d^{n+1/2}\boldsymbol{I}\right) \tag{4.21}$$

And getting rid of the divergence from Eqn.(4.21), the pressure Poisson equation, or

$$\nabla^2 p_d^{n+1/2} = \frac{\rho_0}{\Delta t}\nabla \boldsymbol{u}^{n+1/2} \tag{4.22}$$

can be obtained. Solving Eqns.(4.19),(4.21) and (4.22), we can determine $\boldsymbol{u}^{n+1}$ from $\boldsymbol{u}^n$. Then $\boldsymbol{u}^{n+1/2}$ serves as a predictor and $p_d^{n+1/2}$ as a corrector.

4.3 Solution Procedure

The governing equations including the pressure Poisson equation are spatially discretized by the finite element method in two steps, viz., vertical and horizontal steps. At the first step the primitive variables, u, v, w, S, θ, ρ and p_d are in the vertical interpolated by the Chebyshev polynomial basis set as;

$$\begin{aligned} u &= A_r(x,y,t)T_r(H), \qquad & v &= B_r(x,y,t)T_r(H) \\ w &= C_r(x,y,t)T_r(H), \qquad & \rho &= D_r(x,y,t)T_r(H) \\ S &= R_r(x,y,t)T_r(H), \qquad & \theta &= O_r(x,y,t)T_r(H) \\ & & p_d &= P_r(x,y,t)T_r(H) \end{aligned} \tag{4.23}$$

where $r(=0,1,2,\cdots,m)$ is repeated subindex implying summation and $T_r(H)$ is the Chebyshev polynomial expressed in terms of the normalized variable $H\ (=(2z-h)/h)$. Application of the Galerkin procedure with the weighting function of the same polynomial to Eqn.(4.19) regarding the u-component leads to the following form.

$$\frac{\partial A_k}{\partial t} = -\frac{\partial A_k^u}{\partial x} - \frac{\partial A_k^v}{\partial y} - A_k^w + \omega B_k^d - g b_k^d \frac{\partial \zeta}{\partial x} - \frac{\partial D_k^0}{\partial x} - A_k^z - T_k^h \phi^h + T_k^0 \phi^0 \tag{4.24}$$

where

$$\begin{aligned} A_k^u &= \left[\bar{M}_{ks}\int_0^h T_s(A_pT_p)T_r dz\right] A_r, & A_k^v &= \left[\bar{M}_{ks}\int_0^h T_s(B_pT_p)T_r dz\right] A_r, \\ A_k^w &= \left[\bar{M}_{ks}\int_0^h T_s(C_pT_p)\frac{\partial T_r}{\partial z}dz\right] A_r, & B_k^d &= \left[\bar{M}_{ks}\int_0^h T_s\frac{(D_pT_p)}{\rho_0}T_r dz\right] B_r, \\ b_k^d &= \bar{M}_{ks}\int_0^h T_s\frac{(D_pT_p)}{\rho_0}dz, & D_k^0 &= \left[\bar{M}_{ks}\int_0^h T_s\frac{g}{\rho_0}\left\{\int_0^z T_r dz\right\}dz\right] D_r, \end{aligned}$$

$$A_k^z = \left[\bar{M}_{ks}\int_0^h T_s\frac{\partial}{\partial z}\left\{N_{zx}\frac{\partial T_r}{\partial z}\right\}dz\right] A_r, \quad \bar{M}_{ks} = \left[\int_{-1}^1 T_k T_s dH\right]^{-1},$$
$$T_k^h\phi^h = \bar{M}_{ks}T_s(h)\frac{\tau_{bx}}{\rho_h}, \quad T_k^0\phi^0 = \bar{M}_{ks}T_s(0)\frac{\tau_{sx}}{\rho_0}$$

with the repeated indices p, r and s implying summation and the degree of polynomial k. Eqns.(4.3), (4.4), (4.6), (4.20), (4.21) and the remaining components of Eqn.(4.18) are integrated similarly to the processes above mentioned.

At the secondary step the equations obtained from the former step are integrated over the horizontal domain by the use of the Petrov Galerkin Process, which successfully dampens the numerical oscillation caused in the advection dominant flows[34]. The unknowns in the former step are approximated by the well-defined linear shape function G within the horizontally projected triangular elements. And the asymmetric weighting function is given as;

$$W_i = G_i + 3\left(\alpha_j G_k G_i - \alpha_k G_j G_i\right) \tag{4.25}$$

where (i,j,k) is $(1,2,3)$, $(2,3,1)$ or $(3,1,2)$ and α is the damping factor. An optimal value of α is written in the form;

$$\alpha_{opt} = \coth\left[\frac{Vl}{2\mu}\right] - \frac{2\mu}{Vl} \tag{4.26}$$

where l is the length of an elemental side, V is the component of an average velocity along the side (i,j). The sign of α is determined in accordance with;

$$\alpha > 0 \quad \text{if} \quad V > 0 \qquad \text{and} \quad \text{vice versa.} \tag{4.27}$$

Thus spatial discretization is implemented to have, for instance, the equation regarding the u-component;

$$\begin{aligned} \left[M_{ij}\frac{\partial A_{kj}}{\partial t}\right]^{n,n+1/2} = \Big[&-P_{ij}^x A_{kj}^u - P_{ij}^y A_{kj}^v - M_{ij}A_{kj}^w + \omega M_{ij}B_{kj}^d - g b_k^d P_{ij}^x \zeta_j \\ &- P_{ij}^x D_{kj}^0 - M_{ij}A_{kj}^z - T_k^h M_{ij}\phi_j^h + T_k^0 M_{ij}\phi_j^0\Big]^n \end{aligned} \tag{4.28}$$

where

$$M_{ij} = \int_A W_i G_j dA, \qquad P_{ij}^x = \int_A W_i \frac{\partial G_j}{\partial x}dA, \qquad P_{ij}^y = \int_A W_i \frac{\partial G_j}{\partial y}dA$$

The vertically integrated equations of v, w, θ, S, ζ and the correcting equation are integrated in the similar manners.

Also the Poisson equation, in which a Dirichlet boundary of pressure is transformed to the Neuman boundary of inflow and/or outflow velocity in the finite element formulation using the Gauss' theorem, is rewritten as;

$$\left[-N_{ij}P_{kj} - M_{ij}P^z_{kj}\right]^{n+1/2} = \left[F^x_{ij}A_{kj} + F^y_{ij}B_{kj} + T^h_k M_{ij}\xi^h_j - T^0_k M_{ij}\xi^0_j\right]^n - \left[P^x_{ij}A^\zeta_{kj} + P^y_{ij}B^\zeta_{kj} - M_{ij}C^\zeta_{kj}\right]^{n+1/2} \tag{4.29}$$

where

$$F^x_{ij} = \frac{\rho_0}{\Delta t}\int_\Gamma G_i G_j d\Gamma, \qquad F^y_{ij} = \frac{\rho_0}{\Delta t}\int_\Gamma G_i G_j d\Gamma$$
$$\xi^0_j = \frac{2\rho_0}{h\Delta t}w^s_j, \qquad \xi^h_j = \frac{2\rho_0}{h\Delta t}w^b_j$$
$$A^\zeta_{kj} = \frac{\rho_0}{h\Delta t}A_{kj}, \qquad B^\zeta_{kj} = \frac{\rho_0}{h\Delta t}B_{kj}$$
$$C^\zeta_{kj} = \frac{2\rho_0}{h\Delta t}\left[\bar{M}_{ks}\int_{-1}^{1}\frac{\partial T_s}{\partial z}T_r dH\right]C_{rj}$$

Here, note that the left hand-side of the equation can be written,

$$-N_{ij}P_{kj} - M_{ij}P^z_{kj} = -\int_A\left[\frac{\partial G_i}{\partial x}\frac{\partial G_j}{\partial x} + \frac{\partial G_i}{\partial y}\frac{\partial G_j}{\partial y}\right]dA\ E_{kr}P_{rj} - M_{ij}\left[\bar{M}_{ks}\int_0^h \frac{\partial T_s}{\partial z}\frac{\partial T_r}{\partial z}dz\right]P_{rj} \tag{4.30}$$
$$= -N(3,3)E(r,r)P(r,3) - M(3,3)F(r,r)P(r,3) \tag{4.31}$$

where E is a unit matrix and the indices (m, m) express the matrix size. To solve the Poisson equation, "N and E" and "M and F" in Eqn.(4.30) must be united. However, it is impossible to multiply each other directly due to their different sizes. Here the following technique is introduced to overcome this inconsistency.

$$N(3,3)[E(r,r)P(r,3)]^T = \begin{bmatrix} N_{11}(E(r,r)) & N_{12}(E(r,r)) & N_{13}(E(r,r)) \\ N_{21}(E(r,r)) & N_{22}(E(r,r)) & N_{23}(E(r,r)) \\ N_{31}(E(r,r)) & N_{32}(E(r,r)) & N_{33}(E(r,r)) \end{bmatrix}\begin{bmatrix} (P(r,1) \\ (P(r,2) \\ (P(r,3) \end{bmatrix} \tag{4.32}$$

Consequently, the size of the matrix becomes to be $(3r, 3r)$. And "M and F" are also united in the same manner.

The computational procedure is shown in Fig.4.1. The explicit Kawachi and FT schemes, of which combination has been proved to exhibit well performance in earlier works, are employed in time discretization. Storing the symmetrized and decomposed coefficient matrix of spatially discretized Poisson equation in memory makes it possible to advance time-steps smoothly.

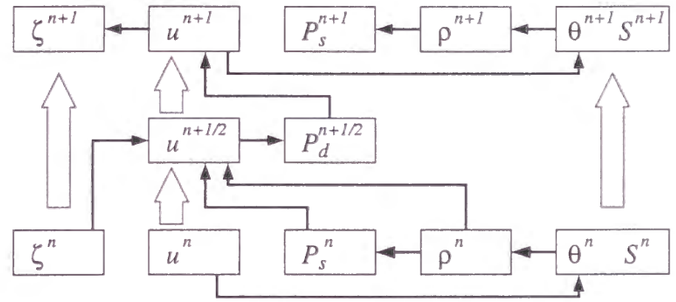

Figure 4.1: Time-marching procedure

4.4 Demonstrative Computations

4.4.1 Caballing Effect

Consider a mixture of two different water bodies of equal density in an impoundment which are initially separated by a vertical partition at the center; one on the left is a cold water with low salinity and the other on the right is warm water with high salinity. When they are mixed by instantaneous removal of the partition, the mixture becomes heavier than the original waters as a result of well known "caballing effect"[88]. This effect sometimes contributes the generation of a thermohaline front which is generally considered as an osculation of two different natured fluid.

As a demonstrative testing of the capability of the model presently developed, repro-

Table 4.1: Initial conditions for reproduction of caballing effect

Side	Left-hand side	Right-hand side
Initial Salinity	5.45 psu	9.74 psu
Initial Temperature	5.0 °C	25.0 °C
Initial Density (σ_t)	4.184	4.184

ducibility of the caballing effect is investigated. The impoundment of a simple rectangle with unit width, 45m long and 30m deep, is initially filled with two different stationary waters whose respective initial conditions for salinity, temperature and density are listed in Table 4.1. The diffusive heat transport in the vertical is assumed dependent on the eddy diffusivities expressed in terms of the vertical density gradient as;

$$K_z = a(A_s)^b(N^2)^c \tag{4.33}$$

where a, b, c are empirical constants (8.17, 0.56 and -0.43, respectively), A_s is surface area in km^2 and N^2 is $-(\partial\rho/\partial z)(g/\rho)$[31]. The computational results obtained are shown in Figs.4.2,4.3,4.4 and 4.5 which represent the profiles of current, temperature, salinity and density at a certain time stage after a commencement of mixing, respectively. From these figures, it can readily be seen that the model is capable of describing the two adjoining vertical circulations quite well and clearly reproducing the absolute increase in density of the mixing zone, viz., an increase of more than $5.6\times10^{-}4$ g/cm^3 due to the caballing effect.

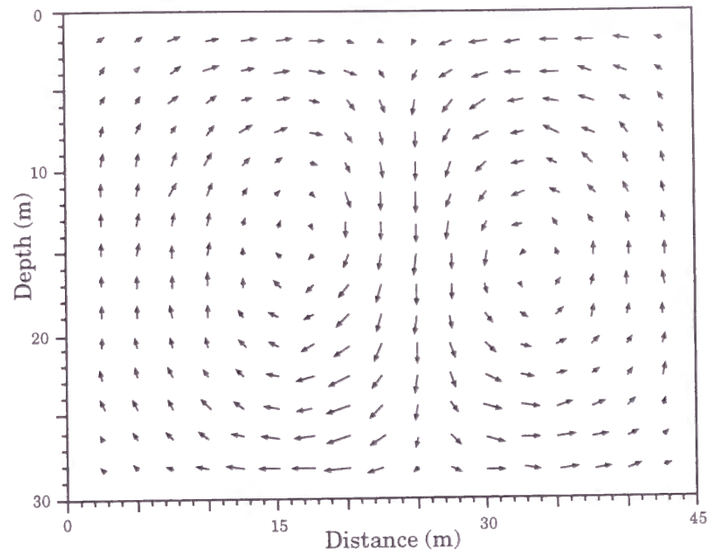

Figure 4.2: Flow profile

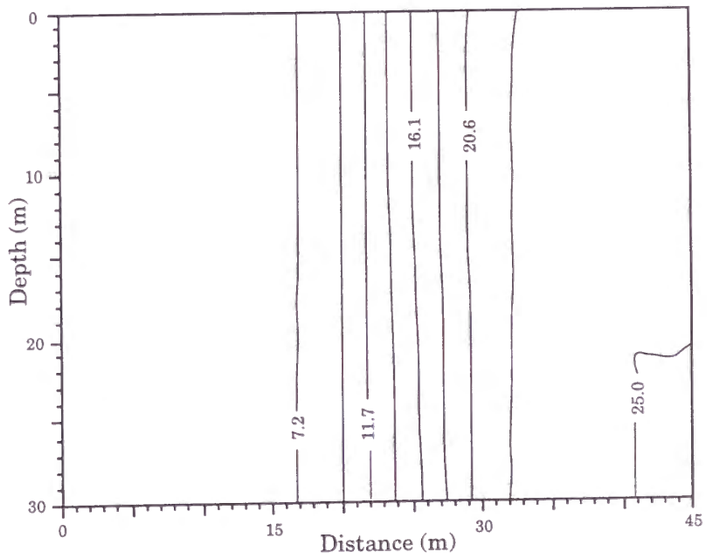

Figure 4.3: Temperature distribution(°C)

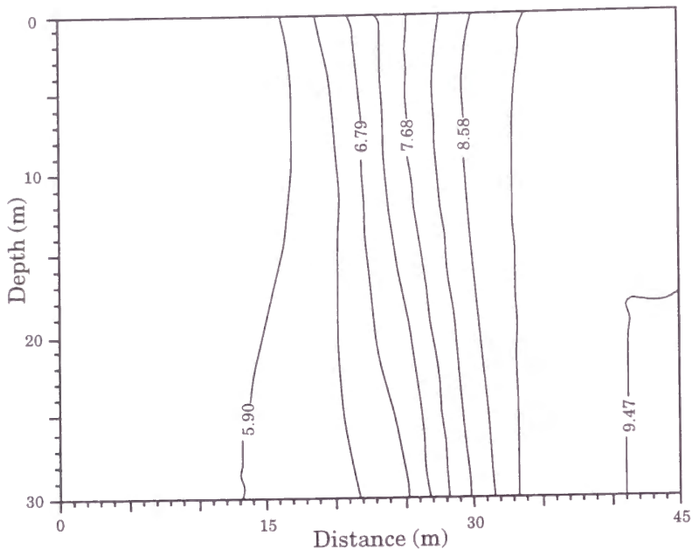

Figure 4.4: Salinity distribution(psu)

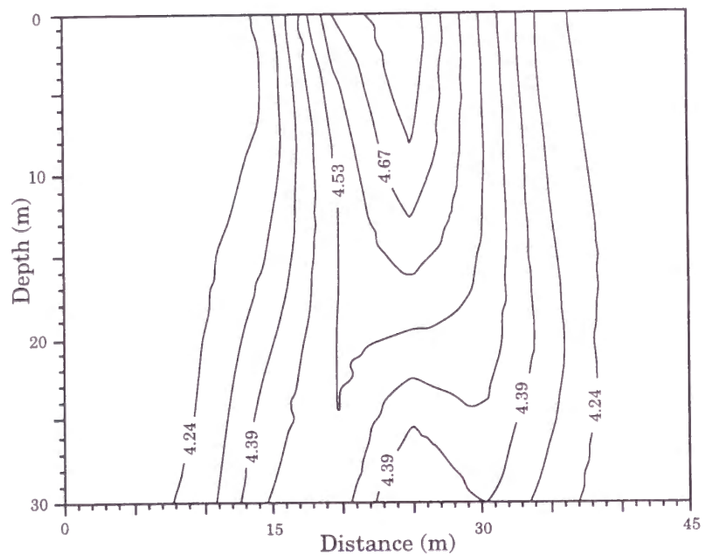

Figure 4.5: Density distribution(σ_t)

4.4.2 Topographic Heat Accumulation Effect

Maldistribution of temperature is often caused in the water body, even if water surface is warmed or cooled uniformly in horizontal domain, because different water depths have different heat accumulation budgets. This heat accumulation resulting from topographic irregularity is considered to have an important effect on the flows in lakes or coastal sea.

The second testing is associated with reproduction of this particular phenomenon. Now consider the case of negative heat accumulation that surface is being cooled. It is then anticipated that colder water in the shallow region flows into the lower layer of warmer water in the deep region, and contrarily the warmer in the deep region flows into the shallow region. Such an exchange of waters results in vertical water circulations, and moreover in perceptible horizontal circulations when spatiotemporal scale is large enough to accept the Coriolis force.

First, testing is carried out for a simple spatial domain of octagonal cone-shaped basin. The key parameters are; initial temperature:25°C, heat loss by surface cooling: 1256.0J/cm^2/day. For comparison, two extremes of the Coriolis parameter, $\Omega = 0$ and $\Omega = 0.00075$[1/s] (unrealistically magnified), are considered. The varying diffusivities are also given according to Eqn.(4.33). Reproduction of the phenomenon requires a sufficient cooling period in which heat can be conveyed upward to the surface, therefore the results at t=96 hrs. are employed to depict the typical currents induced by the heat accumulation. Fig.4.6 are the currents in surface, middle and bottom layers [of which non-dimensional depths are 0.1, 0.5, 0.9, respectively] for Ω=0 and Fig.4.7 is the corresponding current profile in the centered west-east plane to visualize occurrence of the symmetric inverse gravitational circulations. Fig.4.8 are the horizontal circulations driven by the magnified Coriolis effect to be contrasted with Fig.4.6.

Next, another illustrative computation is made for a real closed lake shown in Fig.4.9. The given conditions associated with surface cooling, initial temperature and vertical diffusivities are the same as in the preceding testing. The Coriolis parameter Ω=0.00075 [1/s] is also employed. The computed horizontal currents in selected three layers at t=72 hrs. are illustrated in Fig.4.10. Additionally Fig.4.11 is inserted to show water motion in a vertical plane.

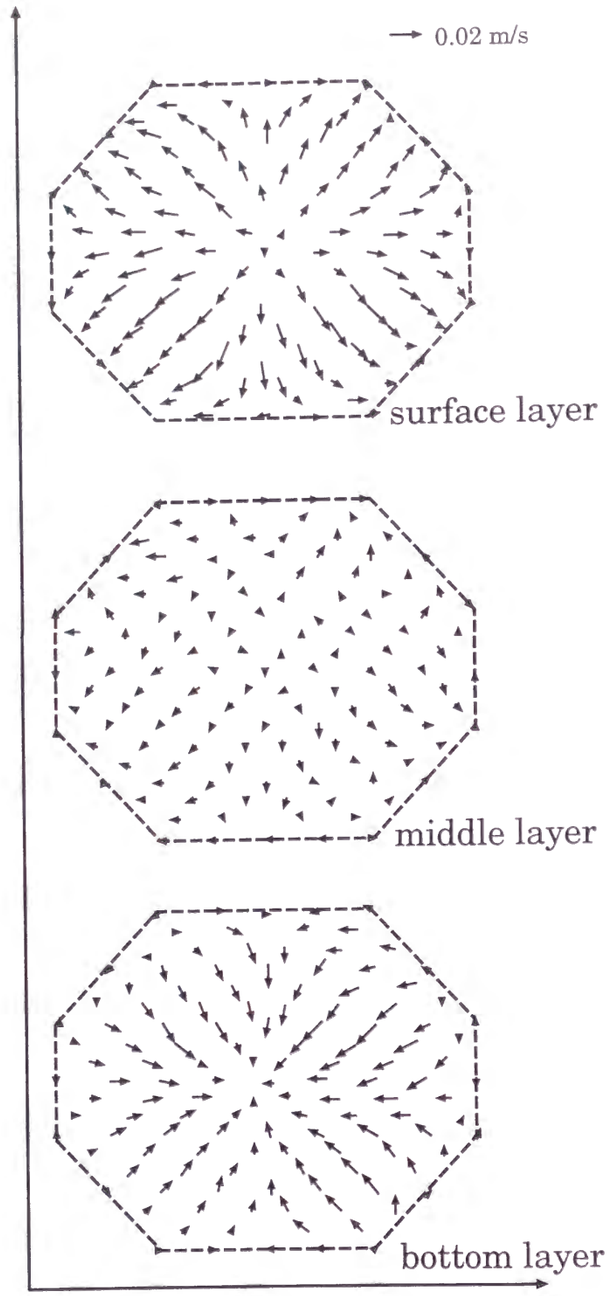

Figure 4.6: Water motion without Coriolis effect, time=96hrs.

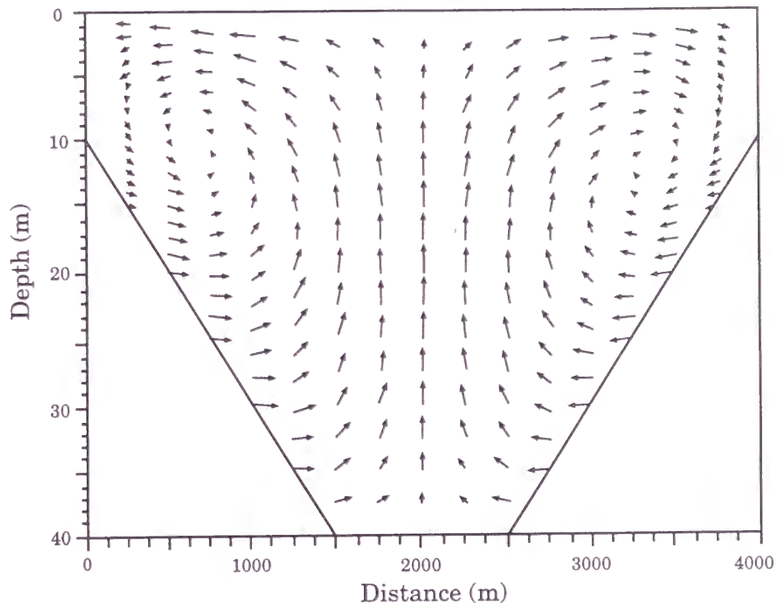

Figure 4.7: Current profile of cone-shaped basin, time=96hrs.

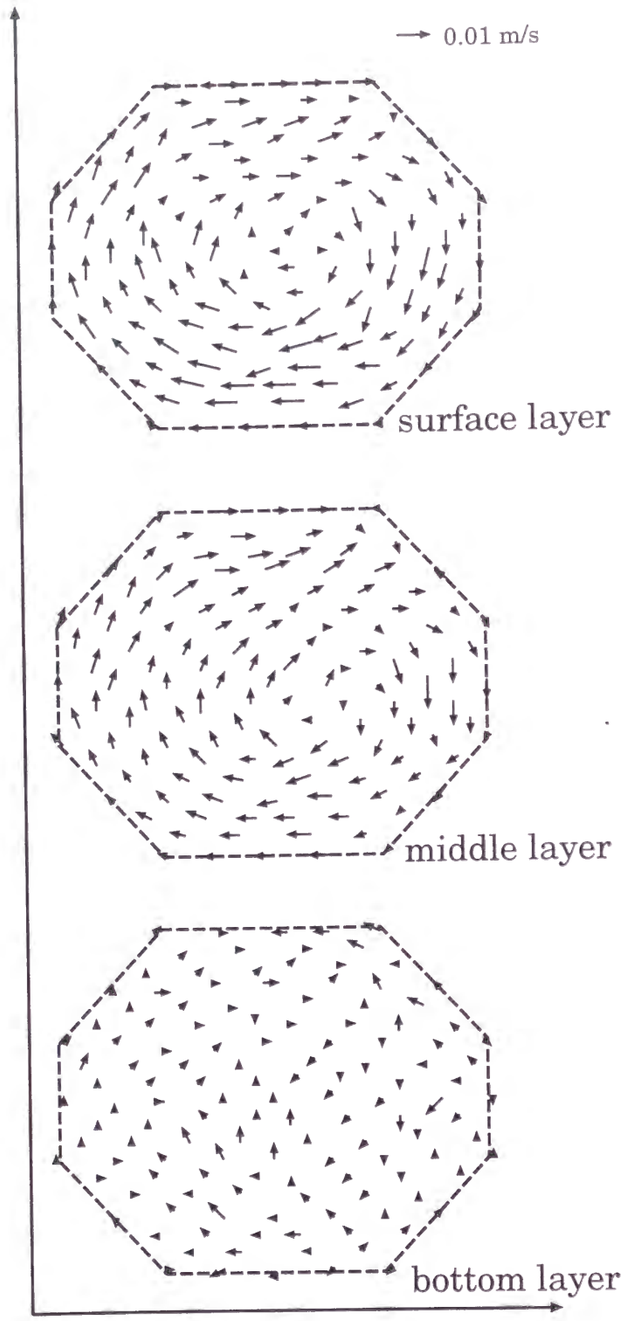

Figure 4.8: Water motion with Coriolis effect, time=96hrs

The results from both testings are well illustrative of colder water creeping into deep regions and warmer water upwelling into shallow regions.

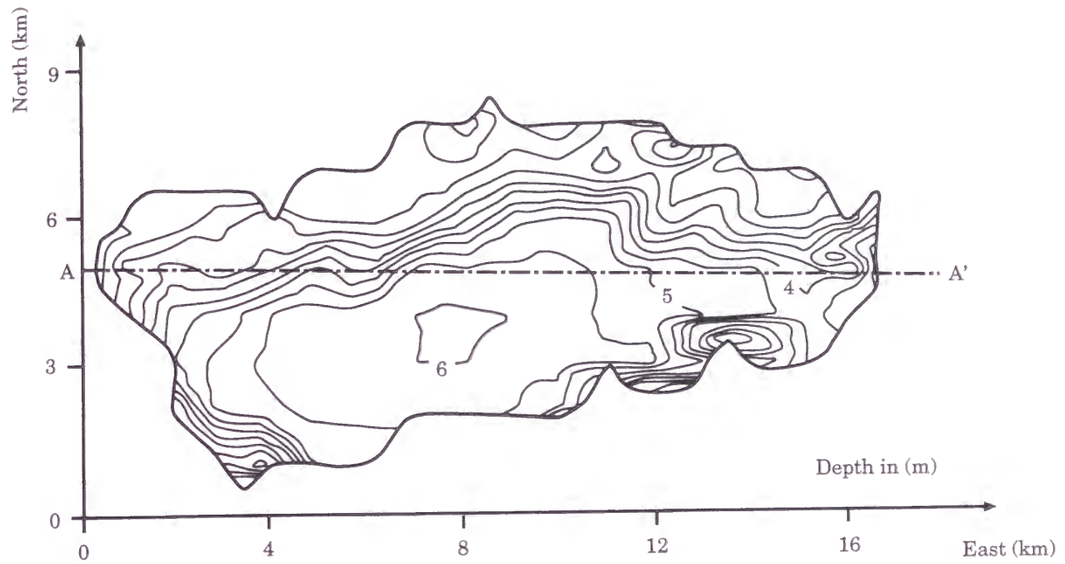

Figure 4.9: Depth contour of a real lake (m)

4.5 Conclusions

A fully 3-D polynomial finite element model, non-stacked and non-layered, has been presented for the solution of the hydraulic and environmental problems. The fractional step scheme, combined with the explicit time-marching scheme, has successfully been incorporated into the model to satisfy the incompressibility in dynamic pressure that arises from retaining the acceleration of vertical velocity in the equation of motion. Some device for substantial reduction of computer storage and run-time have been made.

The model presently developed is of more time-consuming in computer implementation than the model developed in the previous chapter under the hydrostatic assumption. Instead its applicability is expanded to the hydraulic events often encountered with the

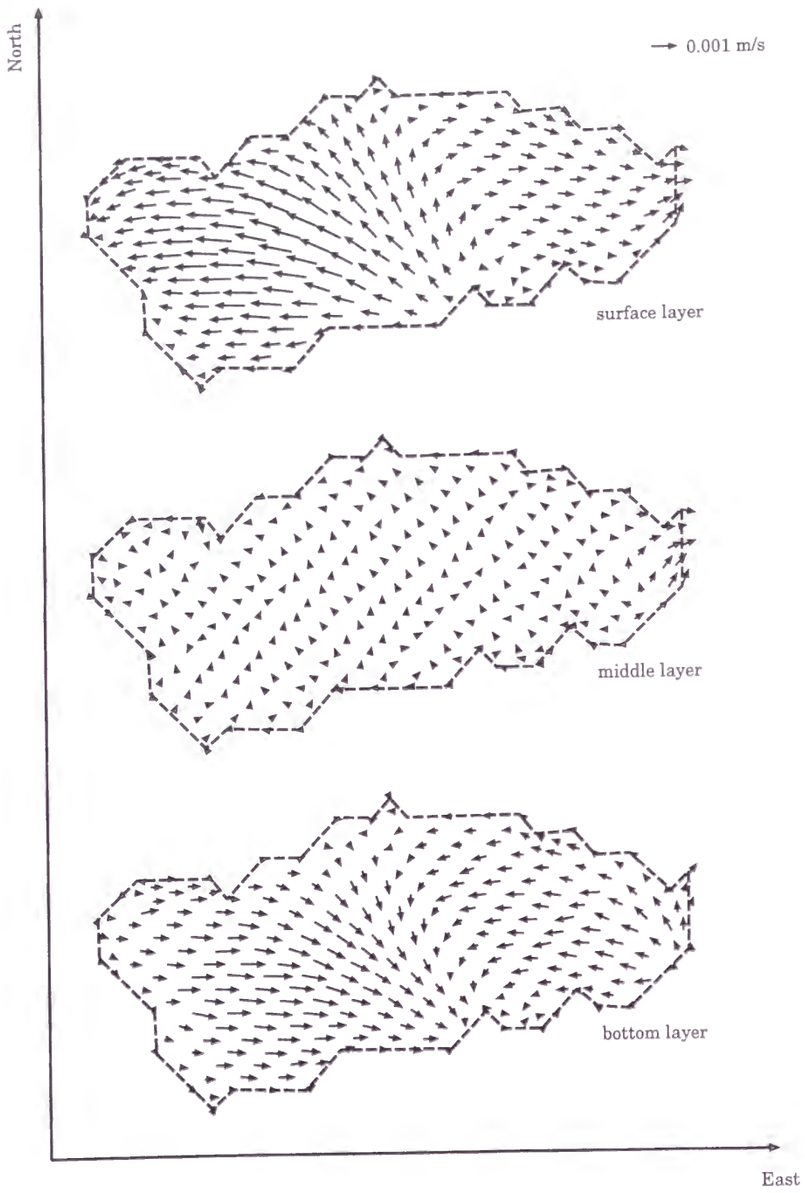

Figure 4.10: Water motion in a real lake, time=72hrs.

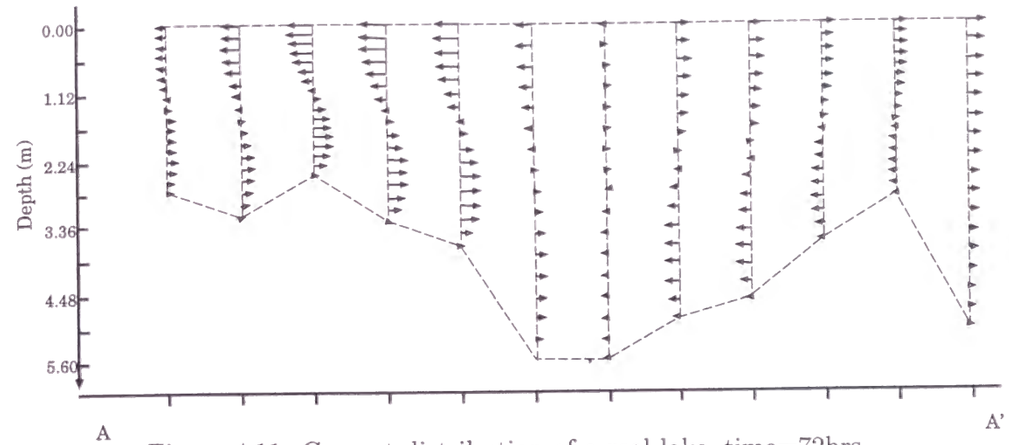

Figure 4.11: Current distribution of a real lake, time=72hrs

effects such as "caballing effect" or "topographic heat accumulation effect", where such an assumption might be invalid.

For the evolution of refined water quality modelling, it is imperative to develop in advance such a sophisticated hydraulic model that detailed flow structures in the vertical as well as in the horizontal, in which salinity and/or thermal effects are woven based on reality, can be quantified. From this viewpoint, the present modelling is considered as a significant progress toward the implementation of refined water quality modelling, although estimation of the eddy diffusivities and checking the solution accuracies remain as matters for future research.

Chapter 5

A MODIFIED SIDE-VIEW MODEL FOR HYDRO-THERMAL ANALYSIS IN MAN-MADE RESERVOIRS

5.1 Introduction

Water temperature is one of the most important indices in assessing environmental problems in reservoirs, for its influence on water quality is very significant. Thermal stratification inhibits vertical mixing of water and has great influence on the behavior of plankton, nutrients and other water quality constituents. Quantifications of turbulent mixing through thermocline and cancellation of densimetric instability due to the surface cooling are of great interest in hydrothermal and water quality analysis.

Considering the geometry and hydraulic properties of a man-made reservoir in which the scale of lateral width is quite small compared with that of longitudinal length and the vertical factors play important roles in its hydraulic environment, several finite element models [e.g.,3,4,10,25,45,53,54] have been proposed. Among them a side-view model is one of the most suitable models for the hydraulic analysis of thermally stratified reservoir, because it enables us to cancel the numerically inaccurate result due to the large aspect ratio of element and it can accept the complex geometry conditions.

In this chapter, the laterally averaged two dimensional side-view model for hydrothermal analysis is developed with newly introduced parameterization of vertical eddy diffusivity and the reasonable treatments of bottom boundary conditions and internal confluence boundary condition. Accuracy of the model is tested through two demon-

strative examples, i.e., 1) Comparison with the analytical solution in a hypothetical rectangular reservoir and demonstration in a hypothetical reservoir with a confluence, 2) Comparison with the observed data in a man-made reservoir.

5.2 Side-View Model

5.2.1 Basic Equations

Accepting the Boussinesq approximation and hydrostatic approximation, the laterally averaged basic equations of continuity, longitudinal momentum and thermal conservation can be represented as;

$$\frac{\partial}{\partial x}(bu) + \frac{\partial}{\partial z}(bw) = 0 \tag{5.1}$$

$$b\frac{\partial u}{\partial t} + bu\frac{\partial u}{\partial x} + bw\frac{\partial u}{\partial z} + \frac{b}{\rho}\frac{\partial p}{\partial x} - \frac{\partial}{\partial x}\left(bE_x\frac{\partial u}{\partial x}\right) - \frac{\partial}{\partial z}\left(bE_z\frac{\partial u}{\partial z}\right) + \lambda|u|u = 0 \tag{5.2}$$

$$b\frac{\partial \theta}{\partial t} + bu\frac{\partial \theta}{\partial x} + bw\frac{\partial \theta}{\partial z} - \frac{\partial}{\partial x}\left(bK_x\frac{\partial \theta}{\partial x}\right) - \frac{\partial}{\partial z}\left(bK_z\frac{\partial \theta}{\partial z}\right) + \frac{1}{\rho c_w}\frac{\partial Q^*}{\partial z} = 0 \tag{5.3}$$

$$p = p_0 + g\int_z^\eta \rho d\beta = p_0 + P_t + P_c \tag{5.4}$$

$$P_t = \rho_0 g\eta \ , \ P_c = g\int_z^{h_0} \rho d\beta$$

$$\rho = \rho_0\left(1 - \alpha_T(\theta - \theta_0)\right) \tag{5.5}$$

where, x, z=horizontal and vertical (positive upward) coordinates, respectively, t=time, u=longitudinal velocity, w=vertical velocity, b=flow width, p= hydrostatic pressure, ρ= fluid density, λ=dimensionless coefficient of side-wall, c_w=specific heat of water, E_x, E_z=horizontal and vertical eddy viscosities, respectively, K_x, K_z=horizontal and vertical eddy diffusivities, respectively, θ=water temperature, θ_0=reference temperature (=4 ° C), α_T=volumetric expansion coefficient(=0.00021), Q^*=heat flux of internally absorbed radiation, p_0=atmospheric pressure on the surface, g= gravitational acceleration, η=vertical displacement of the free-surface from mean water level, P_t=barotropic pressure, P_c= baroclinic pressure and ρ_0=reference density(1000kg/m^3).

When the reservoir is hydraulically shallow, the vertical acceleration can be neglected because it is much smaller than the gravitational one. Then, integrating the continuity equation over the depth, we have the equations of the vertical velocity and the surface elevation as;

$$b_0\frac{\partial \eta}{\partial t} + \frac{\partial}{\partial x}\left(\int_{h_n}^{\eta} bud\beta\right) = 0 \tag{5.6}$$

$$b_k w_k + \frac{\partial}{\partial x}\left(\int_{h_n}^{h_k} bud\beta\right) - b_k u_k\frac{\partial h_k}{\partial x} = 0 \tag{5.7}$$

where b_0 is the surface width and the variables with subscript k(=0,1,2,3$\cdots$) denote those at $z = h_k$ ($k = 0$ at the surface, $k = n$ at the bottom, See Fig.5.2).

5.2.2 Boundary Conditions and Parameters

To obtain unambiguous solution to Eqn.(5.1) through Eqn.(5.7), the following boundary conditions are considered.

a)velocity boundary

$$u = \hat{u}(z,t) \tag{5.8}$$

b)elevation boundary

$$\eta = \hat{\eta}(t) \tag{5.9}$$

c)surface boundary

$$\rho E_z\frac{\partial u}{\partial z} = \tau_s = \rho_a C_a^2|W|W \tag{5.10}$$

$$-K_z\frac{\partial \theta}{\partial z} = \hat{Q}_{sur} \tag{5.11}$$

d)bottom boundary

$$\rho E_z\frac{\partial u}{\partial z} = \hat{\tau}_b \tag{5.12}$$

e)inflow/outflow boundary

$$\theta = \hat{\theta}(z,t) \quad for \quad inflow \tag{5.13}$$

$$K_x\frac{\partial \theta}{\partial x} = 0 \quad for \quad outflow \tag{5.14}$$

f)insulating heat boundary

$$K_x\frac{\partial\theta}{\partial x} = K_z\frac{\partial\theta}{\partial z} = 0 \tag{5.15}$$

where τ_s, τ_b=share stresses on the surface and bottom, respectively, W=wind speed, ρ_a=atmospheric density, C_a=coefficient of wind stress and the circumflex " ˆ " indicates the prescribed value.

The relationship between the heat fluxes Q^* and $\hat{Q}_{sur}$ are represented by the following heat budget equations[23, 46, 60].

$$\begin{aligned} Q &= (1-\beta)(Q_s - Q_{sr}) + \{\beta(Q_s - Q_{sr}) + Q_a \\ &\quad -Q_{ar} - Q_{br} - Q_e - Q_c\} \\ &= Q^* + \hat{Q}_{sur} \end{aligned} \tag{5.16}$$

where Q=net heat flux, Q_s=short wave radiation, Q_a=long wave radiation, Q_{br}=released long wave radiation, Q_e=latent heat, Q_c=sensible heat, β=fraction of incident light absorbed by the water surface and (r) indicates reflection.

The internal absorption of heat Q^* conforms to the following Lambert-Beer law.

$$Q^* = (1-\beta)(Q_s - Q_{sr})e^{-\nu z} \tag{5.17}$$

where ν is the extinction coefficient of light. These budget terms are conceptually illustrated in Fig.5.1.

Though the conventional parameterization using exponential function of the Richardson number is quite proper in the reproduction of the densimetric stratification[63], the thermal instability caused by the surface cooling cannot be cancelled. Several methods[33, 37], which modify the temperature or heat flux distribution directly not via diffusivity, have been proposed to cope with such a situation. If it is possible to cancel the instability via diffusivity, however, the model can be more simple[25, 30, 31, 66]. Thus, newly proposed parameterization of the vertical eddy diffusivity and viscosity is introduced using the exponential function of Brunt-Väisälä frequency (N^2) as;

$$E_z = K_z = K_z^0 \exp\left(\mu N^2\right) + c \tag{5.18}$$

$$N^2 = -\frac{\partial\rho}{\partial z} \tag{5.19}$$

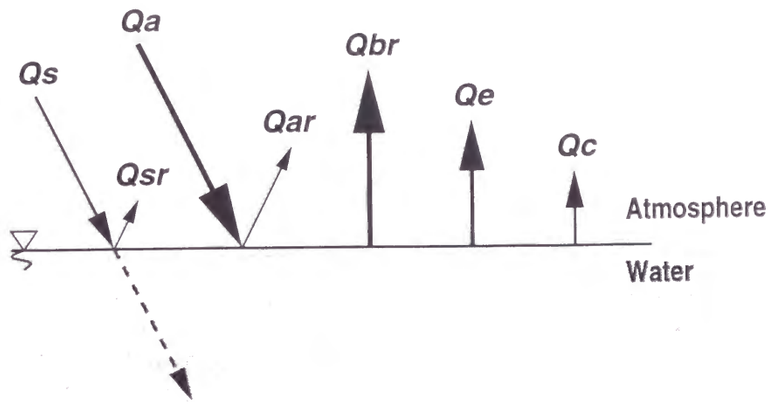

Figure 5.1: Heat balance through the surface

where K_z^0=neutral diffusivity, μ= empirical constant($\simeq$ 1000 according to our tests) and c= constant. In addition, if the value of diffusivity exceeds the maximum value decided beforehand for stable computations, it is replaced by the maximum value (=10m^2/sec).

5.2.3 Finite Element Formulation

The computational domain is discretized into rectangular, trapezoidal and triangular elements as shown in Fig.5.2. However, in order to avert numerical inaccuracy caused by baroclinic term, a rectangular element is preferable except the bottom elements sided by sloping bed.

With subindex for summation (i, j), the field variables $\Psi(= u, \theta)$ are approximated within a rectangular and/or trapezoidal element by;

$$\Psi(\xi,\zeta) = \Phi_j\Psi_j = M_i N_{ij}\Psi_j \tag{5.20}$$
$$(i = 1,2 \quad , \quad j = 1,2,3,4)$$

$$M = [1 - \xi/L \quad \xi/L] \tag{5.21}$$

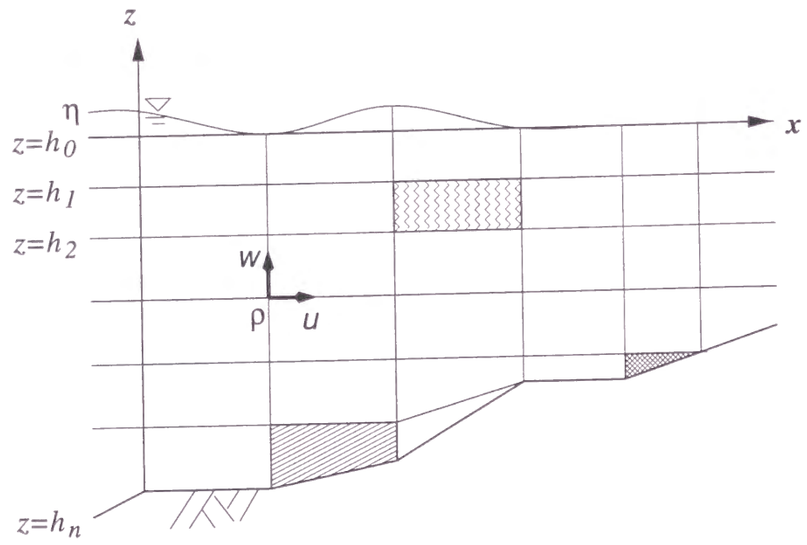

Figure 5.2: Discretization and nodal arrangement in side-view model

$$N = \begin{bmatrix} \zeta/d & 1-\zeta/d & 0 & 0 \\ 0 & 0 & \zeta/d & 1-\zeta/d \end{bmatrix} \tag{5.22}$$

$$\Phi = M_i N_{ij} = \begin{bmatrix} (1-\xi/L)(\zeta/d) & (1-\xi/L)(1-\zeta/d) \\ (\xi/L)(\zeta/d) & (\xi/L)(1-\zeta/d) \end{bmatrix} \tag{5.23}$$

And within a triangular element Φ is approximated by;

$$\Phi = M_i N_{ij} = \begin{bmatrix} (1-\xi/L)(\zeta/d) & (1-\xi/L)(1-\zeta/d) & (\xi/L) & 0 \end{bmatrix} \tag{5.24}$$

where ξ, ζ=the local coordinates within an element, L and d= horizontal and vertical distances between two segments of an element, respectively.

In addition the following internal boundary condition is introduced to be consistent with other quadrilateral elements.

$$\Psi_3 - \Psi_4 = 0 \tag{5.25}$$

where subscripts 3 and 4 indicate the node at an acute angle of the triangle.

When an element is trapezoidal or triangular one, d is also written with an interpolation function as;

$$d = M_i D_i \tag{5.26}$$

where D_1, D_2 are the length of vertical segments.

If an element near the bottom is not rectangular, P_c at a lower corner of the shallow side is replaced by;

$$P_c = g\int_{z_s}^{h_0} \rho d\beta + g\int_{z_d}^{z_s} \hat{\rho} d\beta \tag{5.27}$$

where z_s, z_d=vertical coordinates of shallow side and deep side, respectively, and $\hat{\rho}$= averaged density within the element. Then, the resultant velocity is divided into horizontal and vertical components according to the bed slope. The vertical components are introduced to Eqn.(5.7) as a boundary condition.

And the rest variable η, w_k are approximated horizontally as;

$$\eta = M_i \cdot \eta_i \quad , \quad w_k = M_i \cdot w_{ki} \tag{5.28}$$

Eqns.(5.1) through (5.3) are integrated by means of the weighted residual method to have the following suit of the equations;

$$\boldsymbol{A}\frac{d\boldsymbol{\Psi}}{dt} + \boldsymbol{B}\boldsymbol{\Psi} = \boldsymbol{T} \tag{5.29}$$

$$\boldsymbol{A} = \begin{bmatrix} A_1 & 0 & 0 \\ 0 & A_2 & 0 \\ 0 & 0 & A_2 \end{bmatrix} \qquad \boldsymbol{\Psi} = \begin{bmatrix} \eta \\ u \\ \theta \end{bmatrix}$$

$$\boldsymbol{B} = \begin{bmatrix} 0 & B_1 & 0 \\ B_2 & B_3 & B_4 \\ 0 & 0 & B_5 \end{bmatrix} \qquad \boldsymbol{T} = \begin{bmatrix} 0 \\ T_1 \\ T_2 \end{bmatrix}$$

$$A_1 = \int_L M b_0 M d\xi \ , \qquad A_2 = \int_L \int_d \Phi b \Phi d\zeta d\xi$$

$$B_1 = \sum_{m=0}^{n}\left(\int_L G_m d\xi\right), \qquad B_2 = g\int_L\int_d \Phi b\frac{\partial \Phi_0}{\partial \xi}d\zeta d\xi$$

$$B_3 = \int_L\int_d\left\{\Phi\left(bu\frac{\partial\Phi}{\partial\xi}+bw\frac{\partial\Phi}{\partial\zeta}+\lambda|u|\Phi\right)+bE_z\frac{\partial\Phi}{\partial\zeta}\frac{\partial\Phi}{\partial\zeta}\right\}d\zeta d\xi$$

$$B_4 = \frac{-\alpha_T g}{2}\int_L\int_d\left[\Phi b\frac{\partial}{\partial\xi}\left\{(d-\zeta)(\Phi+\Phi_0)+H_m\Phi\right\}\right]d\zeta d\xi$$

$$B_5 = \int_L\int_d\left\{\Phi\left(bu\frac{\partial\Phi}{\partial\xi}+bw\frac{\partial\Phi}{\partial\zeta}\right)+b\left(K_x\frac{\partial\Phi}{\partial\xi}\frac{\partial\Phi}{\partial\xi}+K_z\frac{\partial\Phi}{\partial\zeta}\frac{\partial\Phi}{\partial\zeta}\right)\right\}d\zeta d\xi$$

$$T_1 = \int_L \Phi_0 b_0\tau_s d\xi, \qquad T_2 = \int_L \Phi_0 b_0 Q_s d\xi$$

where n indicates bottom (See Fig.5.2) and H_m means water depth from the surface to the element. In a global matrix formation, $[H_m \times \theta]$ will be replaced by;

$$\sum_{k=1}^{m}(\theta_{k-1}+\theta_k)(h_{k-1}-h_k)/2.$$

where m indicates the layer of the element.

The weighted residual equation for w_k is given as;

$$\int_L Mb_k Md\xi\cdot w_k + \sum_{m=k}^{n}\left(\int_L G_m u_m d\xi\right) + \frac{dh_k}{d\xi}\int_L Mb_k Md\xi\cdot u_k = 0 \tag{5.30}$$

where

$$G_m = M\frac{\partial}{\partial\xi}\left\{d_m\left(\frac{b_{m-1}u_{m-1}+b_m u_m}{2}\right)M\right\}$$
$$(m = 1,2\cdots n-1)$$

5.2.4 Confluence[48]

Since the vertically projected domain of interest is one-dimensionally approximated in this model, an internal junction boundary condition is newly introduced to consider the stream with a confluence.

$$\Upsilon_1 = \eta_i - \eta_j = \eta_i - \eta_k = 0 \tag{5.31}$$

$$\Upsilon_2 = b_i u_i - b_j u_j - b_k u_k = 0 \tag{5.32}$$

where i means the downstream and j, k mean the upstream.

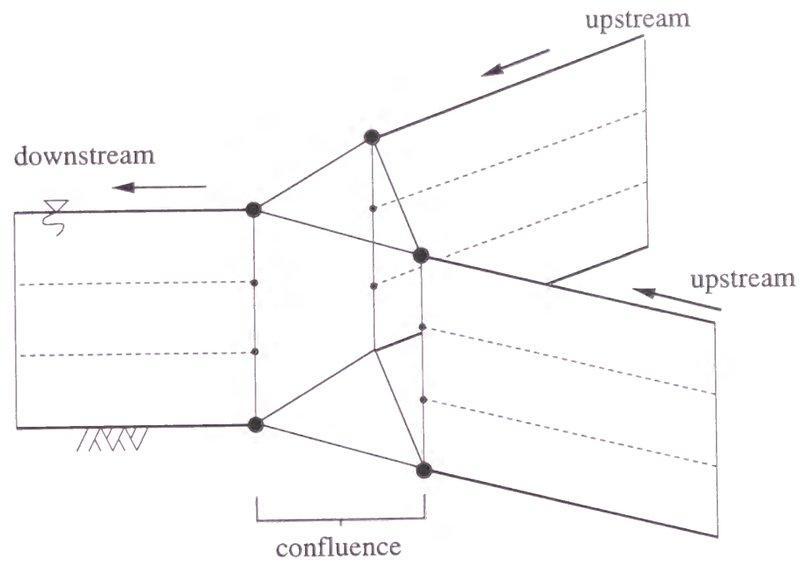

Figure 5.3: Image of confluence

Fig.5.3 shows the image of confluence. These equations are directly introduced into the global matrix equation which is built by the finite element procedure.

5.3 Demonstrative Computations

5.3.1 Hypothetical Reservoirs[44]

The accuracy of numerical solution is examined in comparison with the analytical solution in a rectangular basin shown in Fig.5.4 (case-1). If E_z is constant and water is homogeneous in density, the profile of wind-induced flow at the central point of the basin is given by;

$$u = \frac{h}{6\bar{\rho}E_z}\left[-\frac{1}{4}\tau_s^* - \frac{3}{2}\tau_s^* H + \frac{3}{4}\tau_s^* H^2\right] \tag{5.33}$$

where τ_s^*=wind stress, h=depth of the basin, $\bar{\rho}$=density, H=normalized depth.

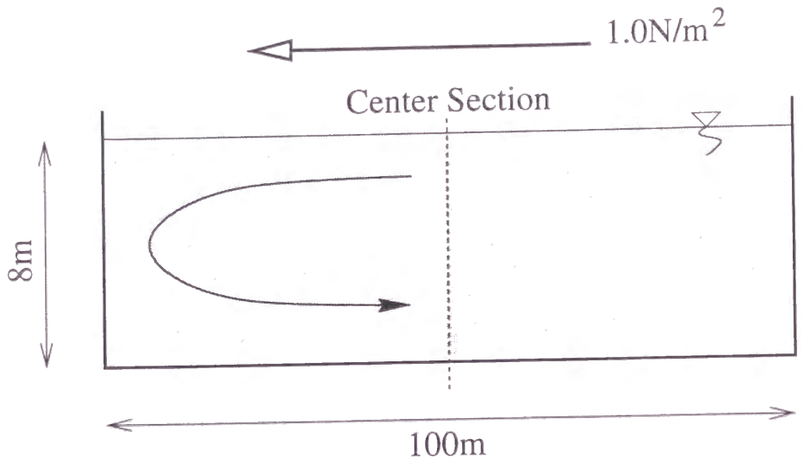

Figure 5.4: Closed rectangular basin for model verification (case-1)

Good agreement between the analytical and the computed solutions are shown in Fig.5.5.

Another test (case-2) is carried out for a hypothetical reservoir with a confluence, shown in Fig.5.6, in order to demonstrate the newly introduced confluence treatment. Computed profiles of flow and water temperature (θ) are shown in Fig.5.7, which displays that the confluence treatment works well.

5.3.2 Verification in real reservoirs[47]

In order to demonstrate the applicability, the model is applied to the analysis in the Osakabe Reservoir (Fig.5.8). This reservoir is a typical reservoir located in hilly rural area. The period of the analysis is from March to October in 1988 with relatively small water surface fluctuations. Observed atmospheric temperature is directly used in this analysis. Wind speed, extinction coefficient, fraction β and amount of cloud are assumed to be constant during the entire computations (1.0[m/s], 0.4[m^{-1}], 0.4 and 0.1,respectively). Other parameters used are: K_x=10.0[m^2/s], λ=0, Δt(time increment)=60[min]. Though the direct influence of rainfall is not considered, fluctuation of solar radiation partially

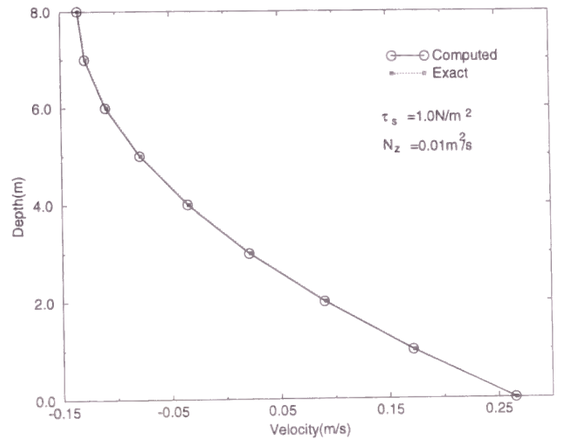

Figure 5.5: Comparison between analytical and computed solutions (case-1)

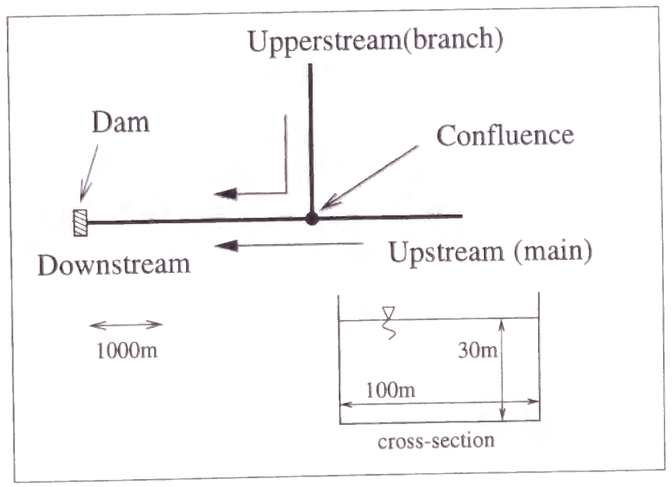

Figure 5.6: Definition of a hypothetical reservoir (case-2)

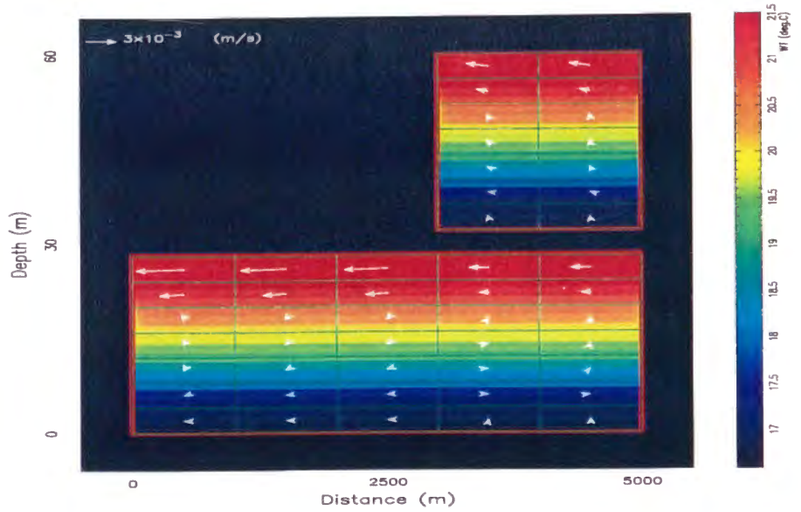

Figure 5.7: Computed distributions of flow and water temperature (case-2)

includes its effects, since solar radiation on rainy days is set to be 1/10 of usual days. The computed profiles of flow and water temperature at the selected stages of April 21 and July 25 are shown in Fig.5.9(a)~(b). Profiles of water temperature at reference sections (near the dam-site) are illustrated in Fig.5.10(a)~(f) in comparison with the observed ones. Thermocline appears vaguely at the end of March and develops as the month advances. Time varying water temperatures at depth=0.5m and 15m below the water surface of the reference sections are also shown in Fig.5.11 (a)~(g). This simulation is executed with monthly averaged inflow discharge Q and water temperature, which are listed in Table 5.1 without considering unusual flood inflow and/or events and with outflow discharge to maintain the water surface level constant, so that the computed values of water temperature often deviate from the observed ones. However, they show quite a similar tendency over a long period of time, except ones at the deeper reference point in September. The reason why the computed results and the observed ones differ in September is not clear, but there might be unexpected cold inflow into the lower layers.

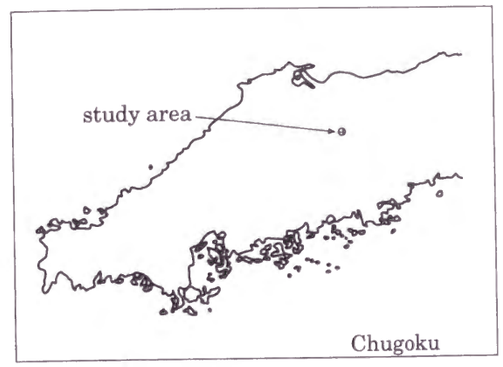

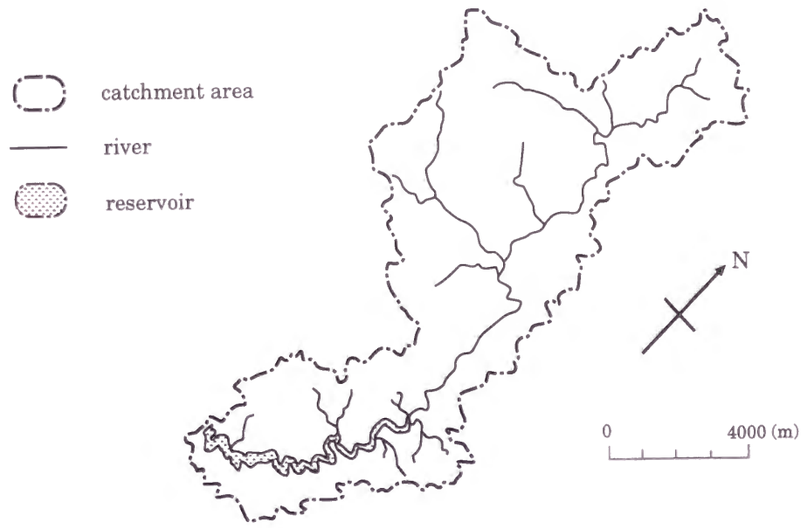

Figure 5.8: Topography of Osakabe Reservoir

Table 5.1: Monthly discharge and water temperature of inflow

Month	Apr	May	Jun	Jul	Aug	Sep
$Q[m^3/s]$	4.93	6.98	14.43	9.23	4.46	4.93
$\theta[^\circ C]$	12.5	17.7	20.1	19.5	23.8	18.8

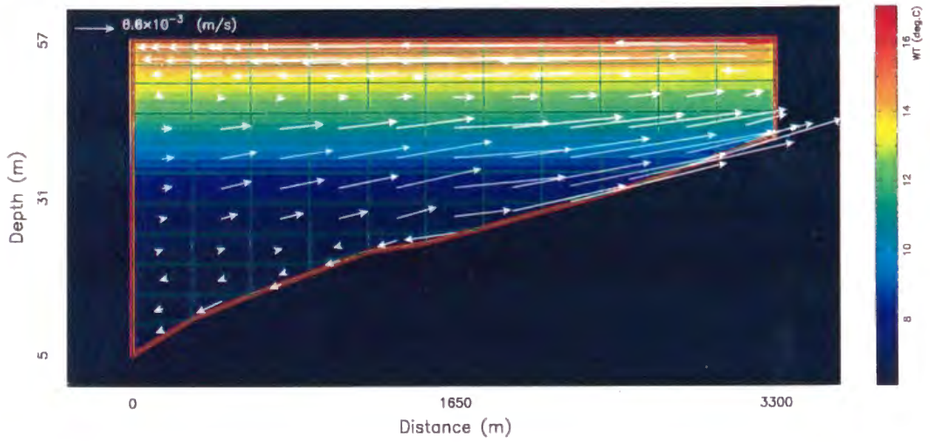

Temperature distribution in Osakabe reservoir

(a) 21 April

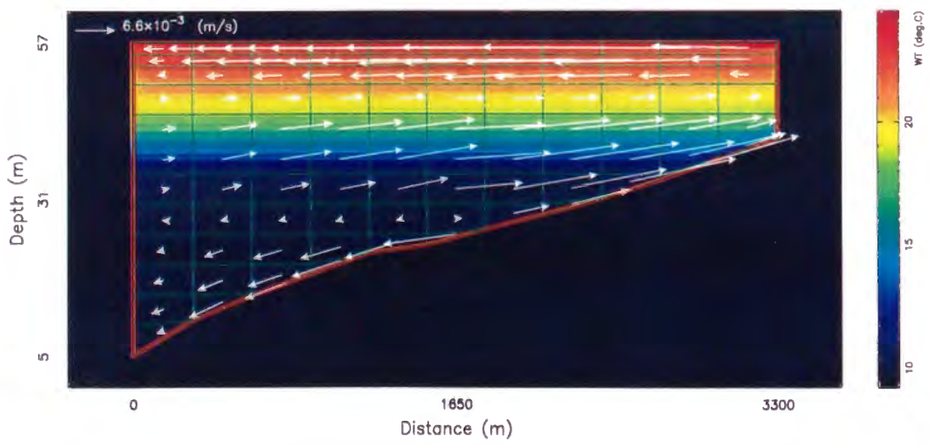

Temperature distribution in Osakabe reservoir

(b) 25 July

Figure 5.9: Computed profiles of flow and water temperature (Osakabe Reservoir)

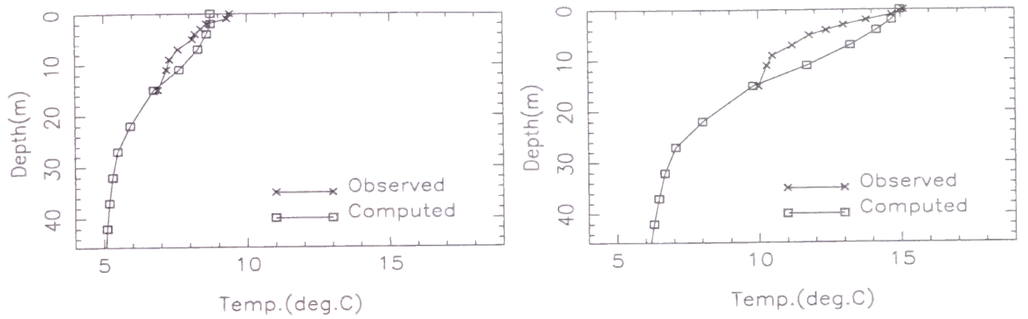

(a) 29th March

(b) 21st April

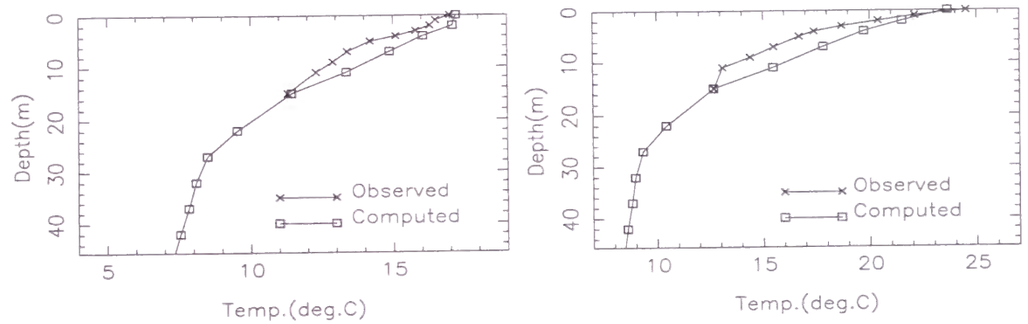

(c) 6th May

(d) 15th June

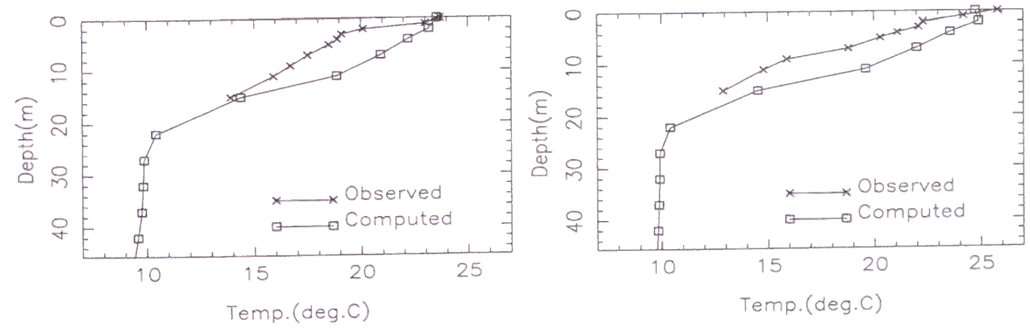

(e) 25th July

(f) 25th August

Figure 5.10: Comparison between computed and observed water temperature at reference sections (Osakabe Reservoir)

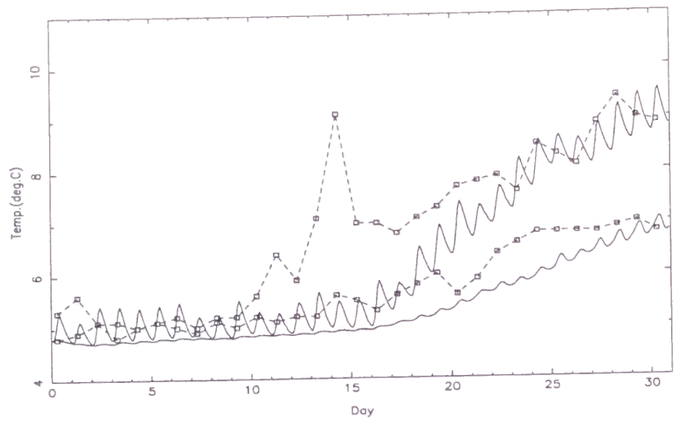

(a) March

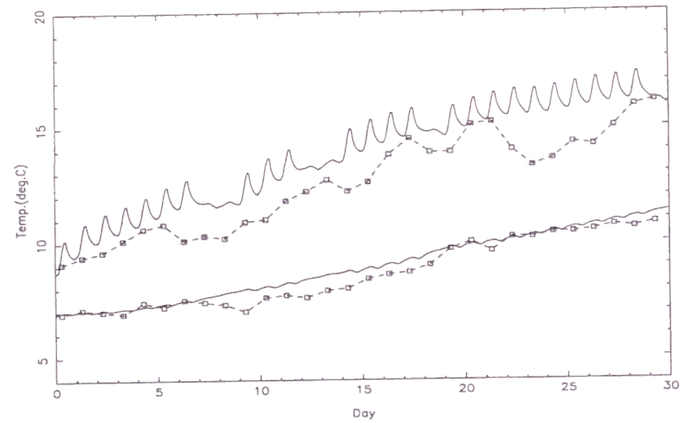

(b) April

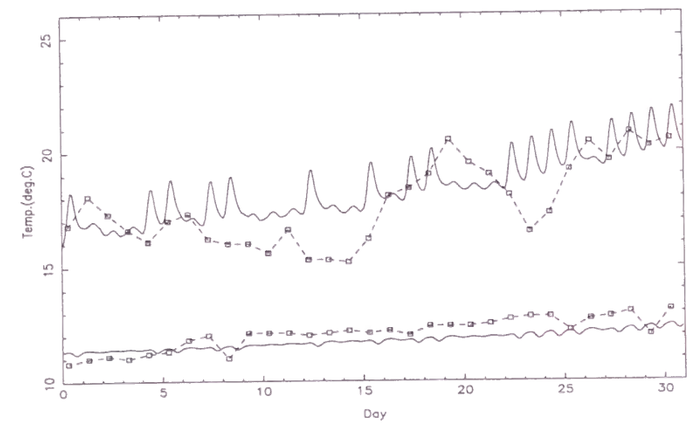

(c) May

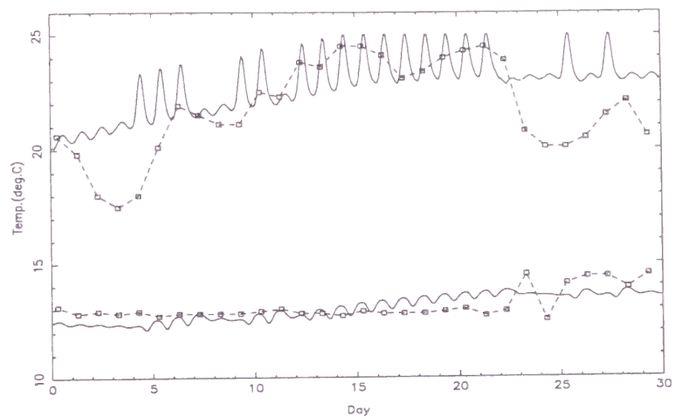

(d) Jun

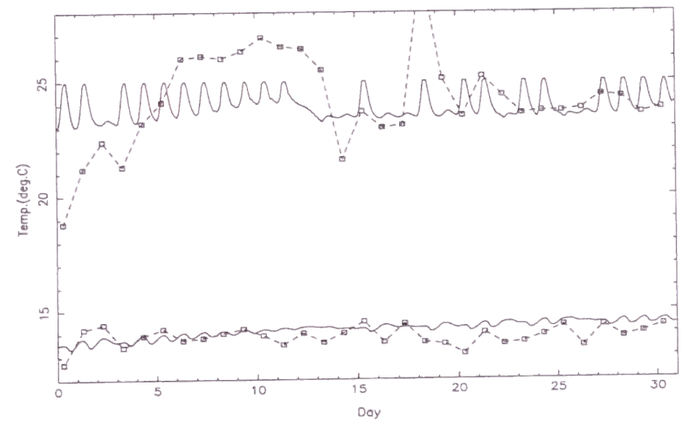

(e) July

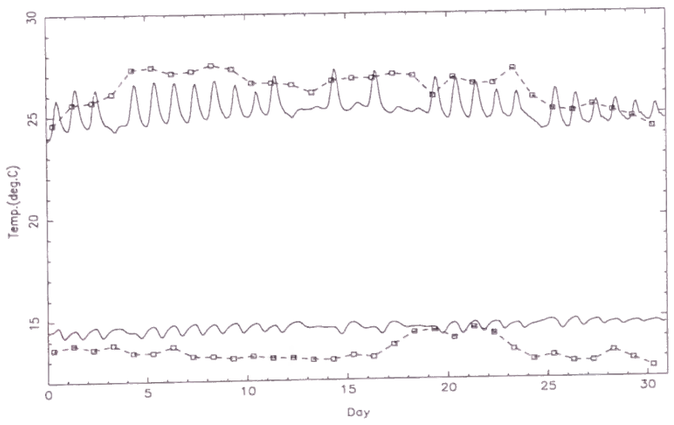

(f) August

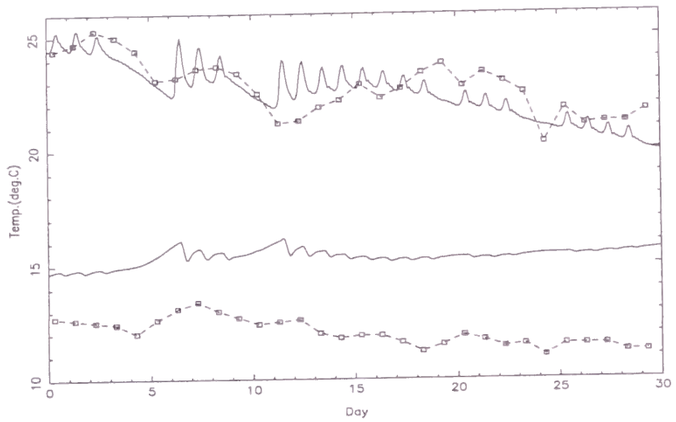

(g) September

Figure 5.11: Comparison between computed and observed time-varying water temperatures (upper; 0.5m below the surface, lower;15m below the surface) (solid lines; computed, dashed lines;observed)

5.4 Conclusions

The concluding remarks are summarized as;

(a) The model developed gives satisfactory results compared with exact and/or observed data. However, its response to climatic changes is quite dull, for it does not consider rainfall, variation of wind and cloud and fluctuations of inflow discharge and reservoir water depth.

(b) The model is confirmed to be one of the most suitable methods for hydro-thermal analysis in a reservoir which has a large aspect ratio, in terms of accuracy, stability and applicability.

(c) Newly introduced confluence treatment and the modified bottom boundary condition work efficiently. These enhance model applicability to the reservoirs with complex geometry.

(d) The proposed parameterization of vertical eddy diffusivity gives satisfactory results. It can eliminate the densimetric instability smoothly and represent the appropriate thermal stratification. It can be an alternative parameterization in hydro-thermal analysis.

Thus, the side-view model presented herein could be considered as a useful tool for hydro-thermal analysis in a reservoir and expected to contribute toward the development of water quality models. However, some important parameters were not given theoretically, which obstructs the versatility of the model. In a future work appropriate parameterizations (e.g., the extinction coefficient should be a function of plankton and suspended solids) and countermeasures for climatic changes would be introduced.

Chapter 6

SIDE-VIEW MODELLING OF DISSOLVED OXYGEN IN THERMALLY STRATIFIED RESERVOIRS

6.1 Introduction

Dissolved oxygen (DO) is one of the most important indices in water quality problems. Extensive efforts have therefore been made to build numerical models for the prediction of DO [e.g.,14,16,51,52,53,61]. However, most of them are classified into budget models or depth-averaged models. While the vertical distribution of DO is not a simple feature and its representation is strongly required, there are still few DO models coupled with hydro-thermal model for determining the vertical distribution of DO in a reservoir.

Thermocline prevents not only the mixing of water but also that of water quality constituents. Our observed data in reservoirs certainly show that the distribution of DO is highly correlative with that of water temperature(θ). To build a DO model, therefore, a hydro-thermal model as its foundation is required. In addition the oxygen production by photosynthesis is not negligible[50]. Thus, the DO model consists of the following sub-models; Flow and Temperature sub-model (FT sub-model), Phytoplankton sub-model (PP sub-model) and DO sub-model.

In this chapter a modelling strategy is presented at first, and secondly its validity is tested through the demonstrative computations for the Osakabe and the Oso man-made Reservoirs.

6.2 Modelling Procedure

6.2.1 Basic Equations

6.2.1.1 Flow and Temperature Model[4, 24]

Accepting the Boussinesq approximation and hydrostatic approximation, the laterally averaged basic equations of continuity, longitudinal momentum and thermal conservation are represented as;

$$\frac{\partial}{\partial x}(bu) + \frac{\partial}{\partial z}(bw) = 0 \tag{6.1}$$

$$b\frac{\partial u}{\partial t} + bu\frac{\partial u}{\partial x} + bw\frac{\partial u}{\partial z} + \frac{b}{\rho}\frac{\partial p}{\partial x} - \frac{\partial}{\partial x}\left(bE_x\frac{\partial u}{\partial x}\right) - \frac{\partial}{\partial z}\left(bE_z\frac{\partial u}{\partial z}\right) + \lambda|u|u = 0 \tag{6.2}$$

$$b\frac{\partial \theta}{\partial t} + bu\frac{\partial \theta}{\partial x} + bw\frac{\partial \theta}{\partial z} - \frac{\partial}{\partial x}\left(bK_x\frac{\partial \theta}{\partial x}\right) - \frac{\partial}{\partial z}\left(bK_z\frac{\partial \theta}{\partial z}\right) + \frac{1}{\rho c_w}\frac{\partial Q^*}{\partial z} = 0 \tag{6.3}$$

where, x, z= horizontal and vertical (positive upward) coordinates, respectively, t= time, u= longitudinal velocity, w= vertical velocity, b= flow width, p= hydrostatic pressure, ρ= fluid density, c_w= specific heat of water,, E_x, E_z= horizontal and vertical eddy viscosities, respectively, K_x, K_z= horizontal and vertical eddy diffusivities, respectively, θ= water temperature(θ), θ_0= reference temperature, α_T= volumetric expansion coefficient, Q^*= heat flux of internally absorbed radiation and p_0= atmospheric pressure on the surface.

When the reservoir is hydraulically shallow, the vertical acceleration can be neglected since it is much smaller than the gravitational one. Then, integrating the continuity equation over the depth, we have the equations of the surface elevation and the vertical velocity as;

$$b_0\frac{\partial \eta}{\partial t} + \frac{\partial}{\partial x}\left(\int_{h_n}^{\eta} bud\beta\right) = 0 \tag{6.4}$$

$$b_k w_k + \frac{\partial}{\partial x}\left(\int_{h_n}^{h_k} bud\beta\right) - b_k u_k\frac{\partial h_k}{\partial x} = 0 \tag{6.5}$$

where b_0 is the surface width and the variables with subscript $k(= 0, 1, 2, 3\cdots)$ denote those at $z = h_k$ ($k = 0$ at the surface, $k = n$ at the bottom).

6.2.2 Phytoplankton Model [8, 15, 17, 40, 70, 84]

Contribution of the phytoplankton to DO is quite large [50] with remarkable diurnal variation. Therefore it is necessary to include phytoplankton sub-model to DO model. The sub-model is built under paying attention to the dynamics of phosphate among phytoplankton, zooplankton and nutrient(PO_4-P)(See Fig.6.1).

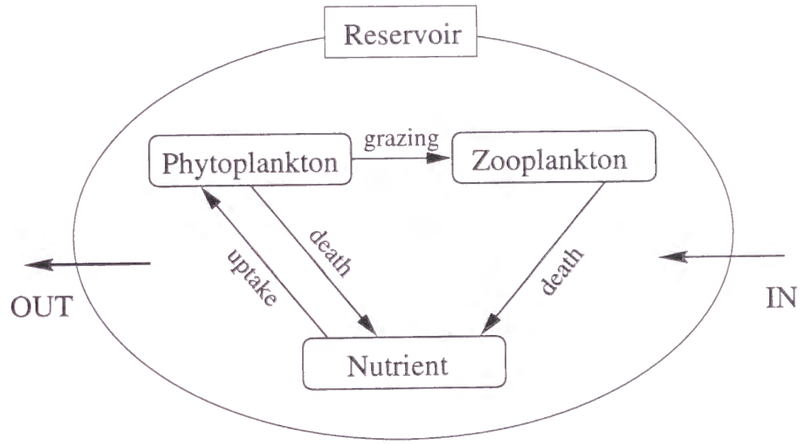

Figure 6.1: Conceptual diagram of phosphorus cycle

When lateral uniformity is assumed similarly to FT sub-model, the basic equations for the compartments of this sub-model are given as;

$$\frac{\partial X}{\partial t} + bu\frac{\partial X}{\partial x} + bw\frac{\partial X}{\partial z} - \frac{\partial}{\partial x}\left(bK_x\frac{\partial X}{\partial x}\right) - \frac{\partial}{\partial z}\left(bK_z\frac{\partial X}{\partial z}\right) + bR = 0 \tag{6.6}$$

where X is a substitute for P, Z and E, P, Z, and E are phosphate contents in phytoplankton, zooplankton and dissolved nutrient, respectively, and R is also a substitute for the following source terms.

$$\begin{aligned} R_P &= N_{UT} - G_{RA} - P_{DT} \\ R_Z &= (1-\gamma)G_{RA} - Z_{DT} \\ R_E &= -N_{UT} + \gamma G_{RA} + P_{DT} + Z_{DT} \\ N_{UT} &= V_{max}exp(\beta_T\theta)\frac{E}{k_n + E}\mu(I)P \end{aligned}$$

$$
\begin{aligned}
G_{RA} &= R_{max}\lambda_I\{1-exp(-\lambda P)\}PZ \\
P_{DT} &= \delta_p exp(-\beta_T\theta)P \\
Z_{DT} &= \delta_z exp(-\beta_T\theta)Z \\
\mu(I) &= \frac{I_0}{I_s}e^{-\alpha(h_0-z)}exp\left(1-\frac{I_0}{I_s}e^{-\alpha(h_0-z)}\right) \\
I &= I_0 e^{-\alpha(h_0-z)}
\end{aligned}
$$

where N_{UT}=term concerning the nutrient uptake by phytoplankton, G_{RA}=term concerning uptake by zooplankton, P_{DT}=term concerning mortality of phytoplankton, Z_{DT}=term concerning mortality of zooplankton, γ=unassimilated grazing fraction (= 0.3 [ℓ/μgP]), V_{max}= maximum uptake rate of phytoplankton (= 0.02 [hr^{-1}]), R_{max}= maximum grazing rate of zooplankton (=0.05 [hr^{-1}]), δ_v= mortality of phytoplankton (= 0.064[hr^{-1}]), δ_z= zooplankton death rate (= 0.032 [hr^{-1}]), β_T= temperature coefficient (=0.06931), λ_I= Ivlev constant (=0.080645 [ℓ/μg]), k_N= half-saturation constant for nutrient uptake (=3.1 [$\mu gP/\ell$]), I_{opt}= saturating intensity of light (=200 [cal/cm^2/day]) and I_{max}= maximum intensity of light (=783 [cal/cm^2/day]).

6.2.3 Dissolved Oxygen Model [1, 2, 43, 56, 57, 62, 64, 83]

The DO balance consists of about 10 components depicted in Fig.6.2. However, in this sub-model the components concerning waterweed, fish, benthos, NO_2-N and zooplankton are assumed to be negligible. Then oxygen flow becomes as in Fig.6.3. When NH_4-N is to be constant throughout the computation, the basic equations for this sub-model are given as;

$$b\frac{\partial X}{\partial t}+bu\frac{\partial X}{\partial x}+bw\frac{\partial X}{\partial z}\frac{\partial}{\partial x}\left(bK_x\frac{\partial X}{\partial x}\right)-\frac{\partial}{\partial z}\left(bK_z\frac{\partial X}{\partial z}\right)+bR=0 \qquad (6.7)$$

where X is a substitute for O and C, O, C and N are concentration of dissolved oxygen, COD and ammonia nitrogen, respectively, and R is also a substitute for the following source terms.

$$R_O = R_{O1}+R_{O2}+R_{O3}+R_{O4}$$

$$
\begin{aligned}
&= -\phi_c K_C C+\alpha_{OP}\mu P-\alpha_{OC}\gamma_r P-\alpha_N K_N N \qquad (6.8)\\
R_C &= (K_C+K_D)\,C \qquad (6.9)
\end{aligned}
$$

where R_{O1}= consumption by oxygenation by carbon, R_{O2}= production by photosynthesis, R_{O3}= consumption by respiration of phytoplankton, R_{O4}= consumption by nitrification, K_C= carbonaceous oxidation rate (=0.23[day^{-1}]), ϕ_c= ratio of TOD/COD (=5.1), α_N= the rate of oxygen uptake per unit of ammonia oxidation (=4.57[mg O /mg N]), K_N= nitrification rate (=0.1[day^{-1}]), α_{OP}= oxygen production rate of phytoplankton (=1000[kg O/kg chl.a]), μ= phytoplankton growth rate (=2.0[day^{-1}]), α_{OC}= oxygen uptake rate of phytoplankton(=1000[kg O/kg chl.a]), γ_r= respiration rate of phytoplankton (=0.1[m^{-1}]) and K_D= removal rate by sedimentation and absorption (=0.23[day^{-1}]).

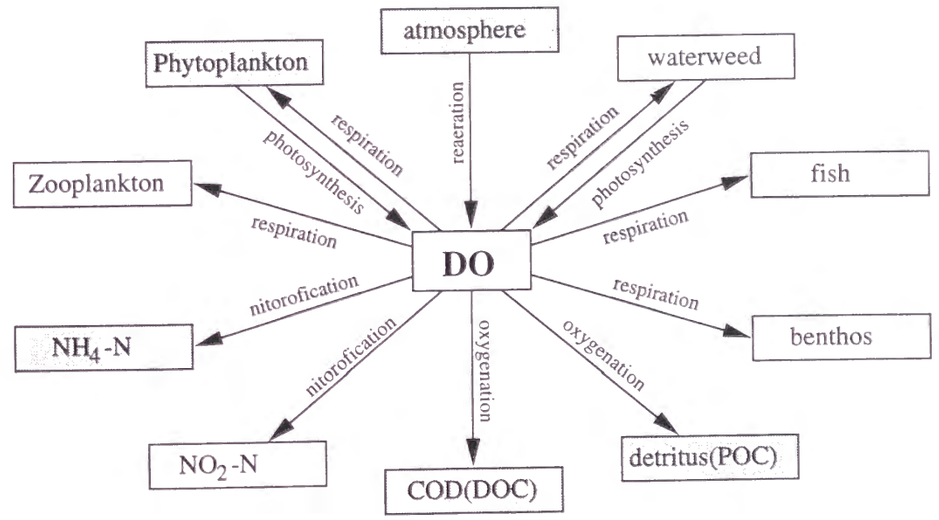

Figure 6.2: Conceptual diagram of oxygen flow

6.2.4 Time-Marching Procedure

At first flow and water temperature are obtained by FT sub-model. Secondly, the concentration of phytoplankton is computed by phytoplankton sub-model using the results

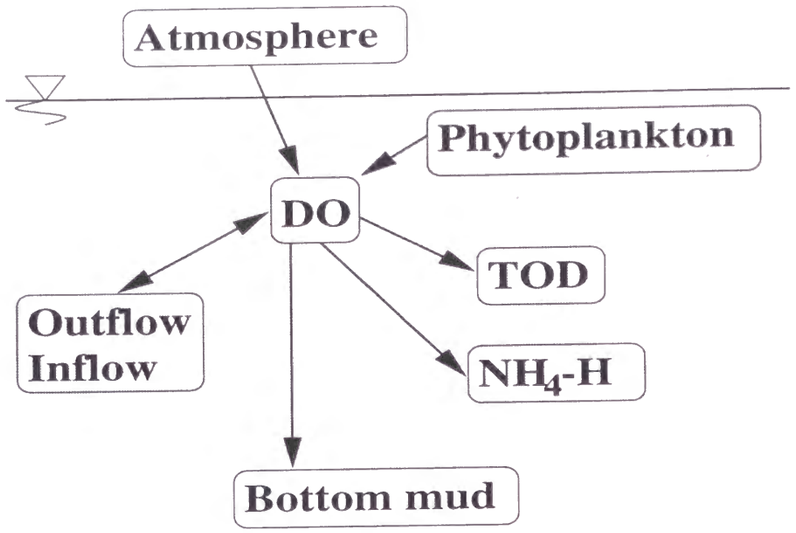

Figure 6.3: Schematic view of oxygen flow

of FT sub-model. Finally the concentration of DO is estimated in DO sub-model based on these two sub-models. In this procedure the influences of phytoplankton on the light transparency and those of DO on phytoplankton are assumed to be negligible. This time-marching procedure is illustrated in Fig.6.4.

6.2.5 Boundary Conditions and Parameters

6.2.5.1 Boundary conditions

To obtain unambiguous solution to Eqn.6.1 through Eqn.6.7, the following boundary conditions are considered.

a)velocity boundary

$$u = \hat{u}(z,t) \tag{6.10}$$

b)elevation boundary

$$\eta = \hat{\eta}(t) \tag{6.11}$$

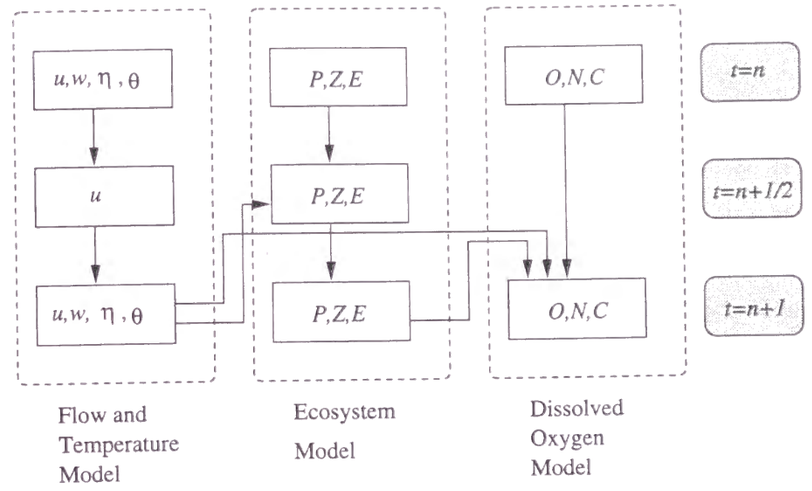

Figure 6.4: Time-marching procedure

c)surface boundary

$$\rho E_z \frac{\partial u}{\partial z} = \tau_s = \rho_a C_a^2 |W| W \tag{6.12}$$

$$-K_z \frac{\partial \theta}{\partial z} = \hat{Q}_{sur} \quad , \quad -K_z \frac{\partial X}{\partial z} = 0 \tag{6.13}$$

d)bottom boundary

$$\rho E_z \frac{\partial u}{\partial z} = \hat{\tau}_b \tag{6.14}$$

$$-K_z \frac{\partial \theta}{\partial z} = 0 \quad , \quad -K_z \frac{\partial X}{\partial z} = 0 \tag{6.15}$$

e)inflow/outflow boundary

$$\theta = \hat{\theta}(z,t) \qquad for \quad inflow \tag{6.16}$$

$$K_x \frac{\partial \theta}{\partial x} = 0 \qquad for \quad outflow \tag{6.17}$$

f)insulating boundary

$$K_x \frac{\partial \theta}{\partial x} = K_z \frac{\partial \theta}{\partial z} = 0 \tag{6.18}$$

g)flux boundary

$$K_x \frac{\partial X}{\partial x} = \hat{X}_f \tag{6.19}$$

where X=a substitute for P, Z, O, C, τ_s and τ_b= share stresses on the surface and bottom, respectively, W=wind speed, ρ_a=atmospheric density, C_a=coefficient of wind stress, X_f= flux value and the circumflex " ˆ " indicates the prescribed value.

6.2.5.2 Vertical diffusivities [31, 63]

Though the conventional parameterization using exponential function of the Richardson number is quite proper in the reproduction of the density stratification, the thermal instability caused by the surface cooling cannot be eliminated. Several methods, which modify the θ or heat flux distribution directly not via diffusivity, have been proposed to cope with such situation. However, if it is possible to eliminate the instability via diffusivity, the model can be much simpler. Here, newly proposed parameterization of the vertical eddy diffusivity and viscosity is introduced using the exponential function of Brunt-Väisälä frequency (N^2) as;

$$E_z = K_z = K_z^0 \exp\left(-\mu N^2\right) + c \tag{6.20}$$

$$N^2 = -\frac{g}{\rho}\frac{\partial \rho}{\partial z} \tag{6.21}$$

where K_z^0=the neutral diffusivity, μ= an empirical constant($\simeq$ 1000 through our tests) and c= a constant.

From Tables 6.1,6.2 and 6.3 designating the correlationship between the vertical distributions of θ and DO in reservoirs, it can readily be seen that both are highly correlative in spite of different boundary conditions. From this fact we can consider that the vertical eddy diffusivities of θ and DO are the same.

6.2.5.3 Others [32, 82, 61, 16]

To estimate saturated DO and liquid film transfer coefficient, the following equations are used.

$$C_s = exp[-17.015355 + 0.022629\theta + (3689.38/\theta) \tag{6.22}$$

$$K_r = 0.728W^{0.5} - 0.317W + 0.0372W^2 \tag{6.23}$$

And the time-varying variation of atmospheric temperature is approximated by;

$$\theta_a(t) = \theta_a^{min} + (\theta_a^{max} - \theta_a^{min}) sin^3(\frac{\pi t}{86,400}) \tag{6.24}$$

where θ_a= atmospheric temperature, θ_a^{max}= maximum atmospheric temperature, θ_a^{min}= minimum atmospheric temperature and t= time.

Cloudy days are assumed to appear according to the probability estimated from the past observed data. On cloudy day the solar radiation is reduced to one-third of that on clear day and direct influence of rain and snow is neglected.

Table 6.1: Correlation coefficient between water temperature and DO (Osakabe Reservoir, long term observation, 1988)

M/D	06/10	07/25	08/11	10/18
Gate	0.973	0.827	0.838	0.907
Center	0.989	0.971	0.945	0.986

Table 6.2: Correlation coefficient between water temperature and DO (Hiju Reservoir, 24hr observation, 88/08/07-08)

11:00	13:00	15:00	17:00	19:00	21:00	23:00
0.834	0.886	0.805	0.869	0.895	0.878	0.893
01:00	03:00	05:00	07:00	09:00	11:00	Ave.
0.898	0.833	0.891	0.854	0.888	0.875	0.807

Table 6.3: Correlation coefficient between water temperature and DO (Hiju Reservoir, long term observation, 1988-1989)

M/D	06/26	07/24	08/28
Gate	0.994	0.975	0.925
09/27	10/25	12/06	02/22
0.999	0.999	0.977	0.978

6.3 Demonstrative Computations

6.3.1 Osakabe Reservoir

A demonstrative computation is carried out for the Osakabe Reservoir and the results are compared with the observed data. The reservoir comprises the lowest terminus of the upper Takahashi river basin and has a storage of 15,624,000m^3 and a maximum depth of about 50m.

The computational and climatic conditions are shown in Tables 6.4,6.5 and 6.6. Figs.6.5~6.9 illustrate the distributions of DO, P,E and Z on June 10 and that of DO on July 15 in a vertical plane of the reservoir. Computed DO and water temperature of June 10 and July 15 are compared with observed ones, which are shown in Figs.6.10~6.13.

Table 6.4: Monthly value of atmospheric temperature (Osakabe Reservoir,1988,am9:00)

Month	Apr	May	Jun	Jul	Aug
Ave.	12.2	15.9	21.9	24.4	25.3

Table 6.5: Monthly frequency of clear and cloudy (rainy) days (Osakabe)

Month	Apr	May	Jun	Jul	Aug
Clear	24	17	17	21	24
Cloudy	6	14	13	10	7

Table 6.6: Monthly discharge and water quality of inflow (partly assumed) (Osakabe Reservoir)

Month	Apr	May	Jun	Jul	Aug
Q$[m^3/s]$	4.93	6.98	14.43	9.23	4.46
$\theta[^\circ C]$	12.5	17.7	20.1	19.5	23.8
COD$[mg/\ell]$	1.3	1.5	1.9	2.1	2.5
PO_4-P$[mg/l]$	.010	.010	.010	.010	.010

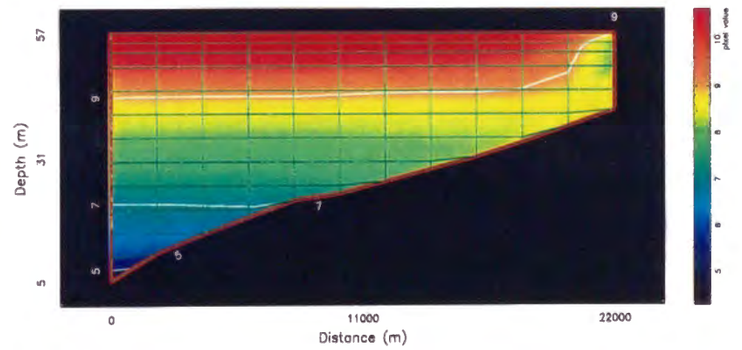

Figure 6.5: Distribution of DO in a vertical plane (June 10)

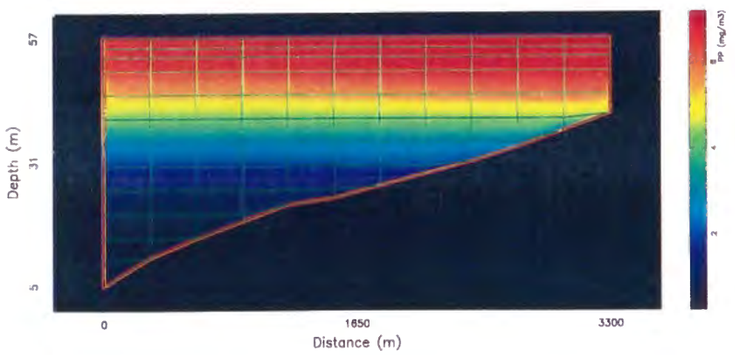

Figure 6.6: Distribution of P in a vertical plane (June 10)

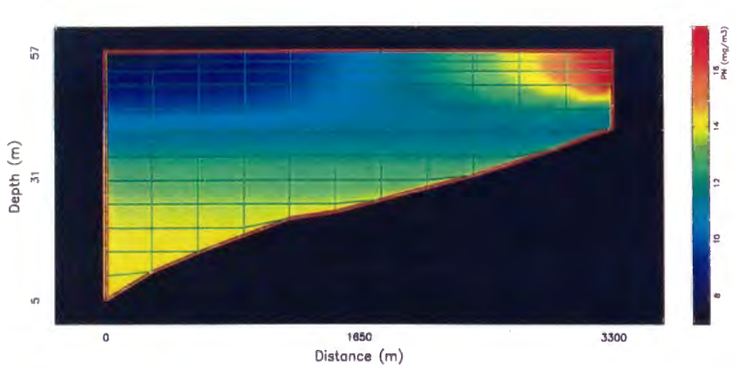

Figure 6.7: Distribution of E in a vertical plane (June 10)

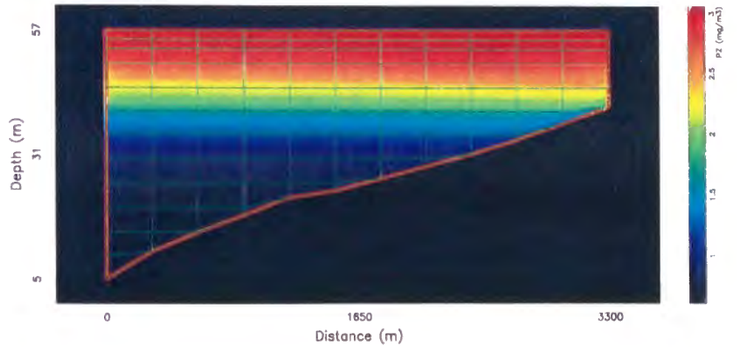

Figure 6.8: Distribution of Z in a vertical plane (June 10)

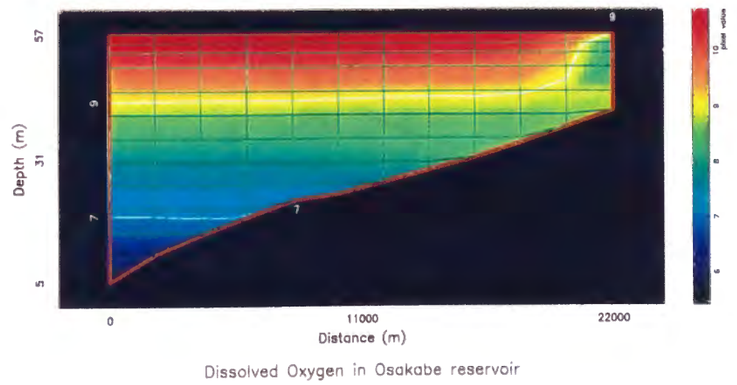

Figure 6.9: Distribution of DO in a vertical plane (July 25)

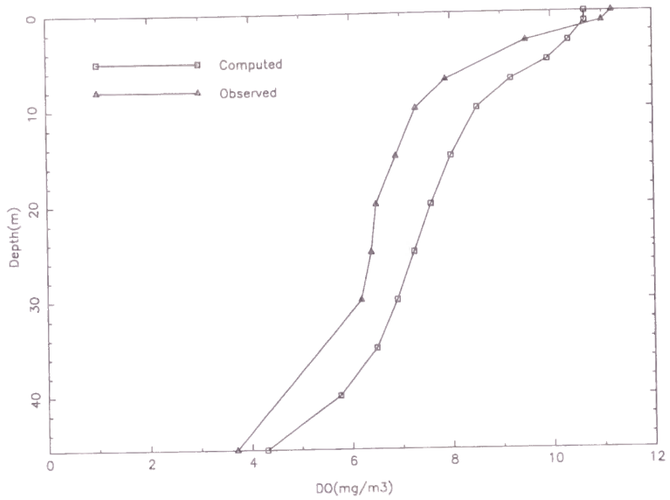

Figure 6.10: Comparison between computed and observed DO (June 10)

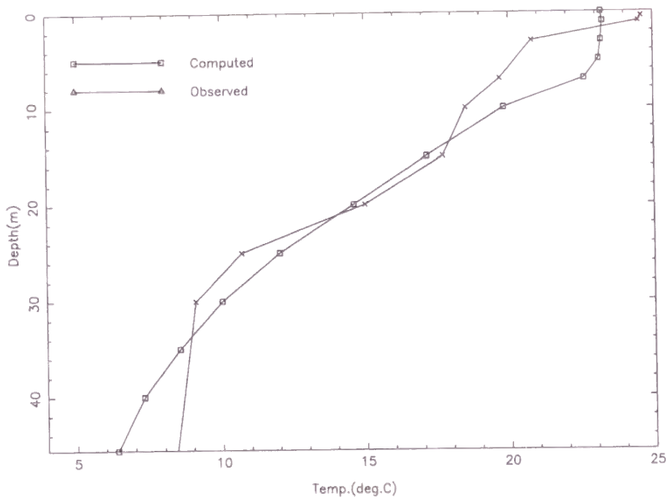

Figure 6.11: Comparison between computed and observed water temperature (June 10)

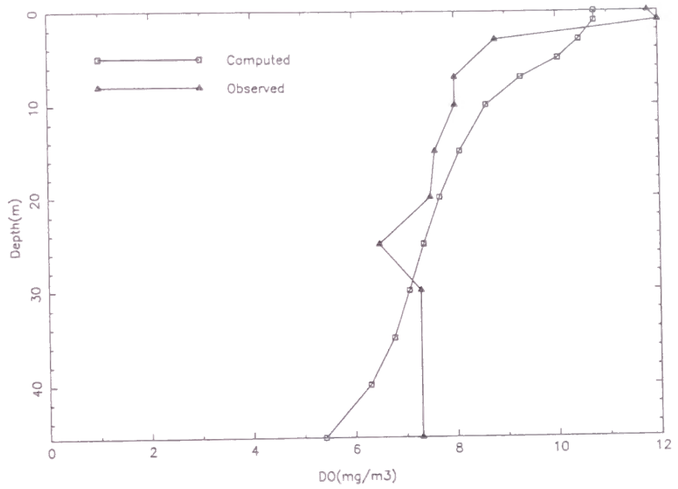

Figure 6.12: Comparison between computed and observed DO (July 25)

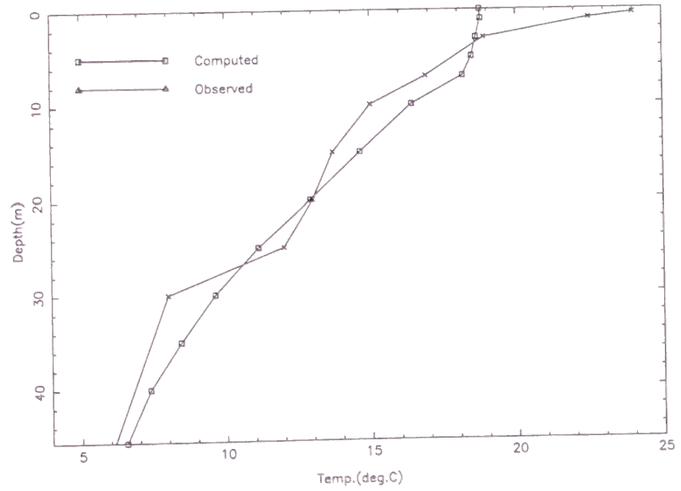

Figure 6.13: Comparison between computed and observed water temperature (July 25)

6.3.2 Oso Reservoir

In order to know the long term behavior of the model, computation is executed for the Oso Reservoir in irrigation period, i.e., from April to September. For the Oso Reservoir (Fig.6.14), quite adequate water quality data of inflow and climate are available in compensation for the lack of data inside the reservoir. The key data are listed in Tables 6.7,6.8 and 6.9.

Table 6.7: Monthly atmospheric temperature (Oso Reservoir,1988)

Month	Apr	May	Jun	Jul	Aug	Sep
Ave.	13.5	18.8	21.5	25.4	26.6	21.8
Max.	18.9	25.1	27.2	28.5	32.3	28.3
Min.	8.1	12.4	15.8	20.8	20.8	15.2

Table 6.8: Monthly frequency of clear and cloudy (rainy) days (Oso Reservoir)

Month	Apr	May	Jun	Jul	Aug	Sep
Clear	23	22	17	22	25	22
Cloudy	7	9	13	9	6	8

Fig.6.15 shows the time-variations of P, Z and N at the outlet of the reservoir. The time-variation of DO and COD at the same place are illustrated in Fig.6.16. As shown in Fig.6.15 and 6.16, the model gives stable solutions which quite agree with the expected ones in a long term computation.

Monthly variations of the vertical distributions of flow, temperature and water quality constituents, obtained from the computations, are illustrated in Appendix A.

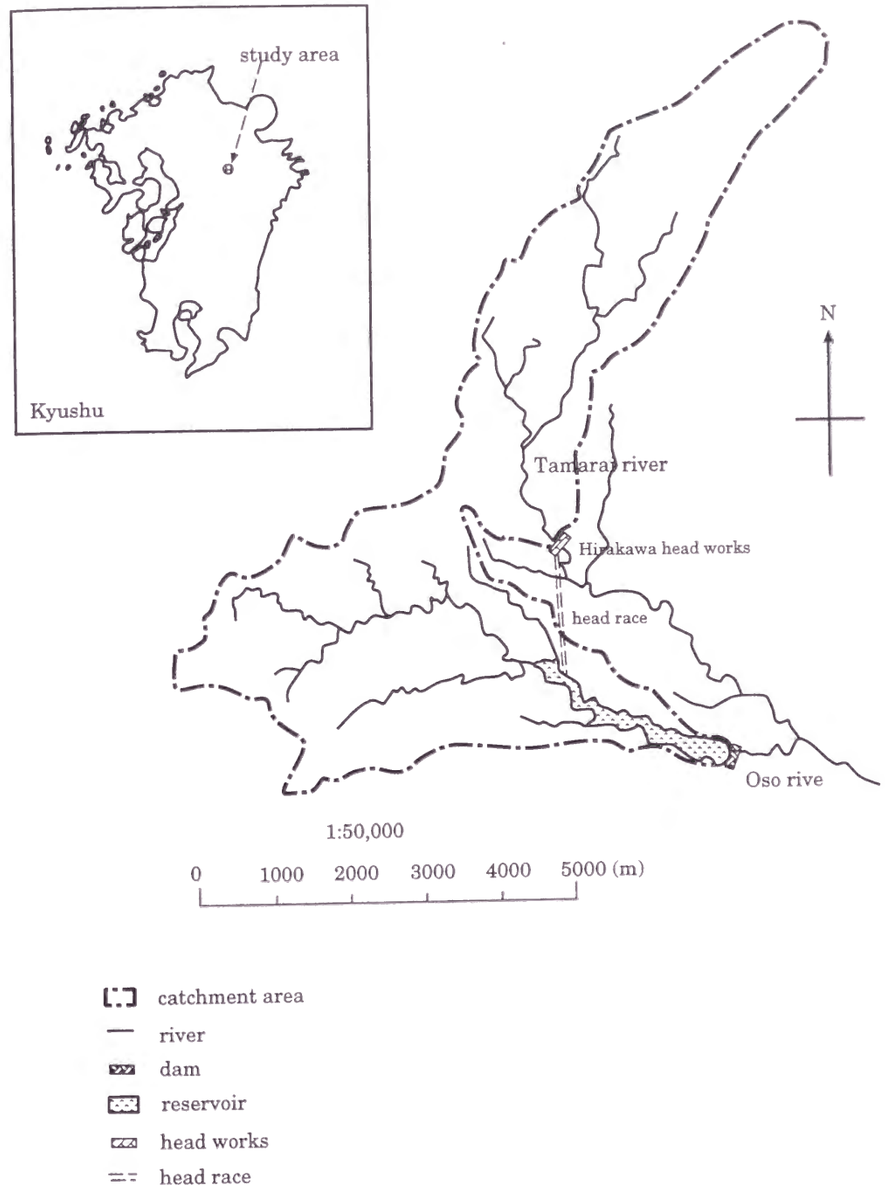

Figure 6.14: Topography of Oso Reservoir

Table 6.9: Monthly averaged discharge and water quality (Oso Reservoir)

Month	Feb	Mar	Apr	May
discharge$[m^3/s]$	0.019	0.018	0.680	0.108
$\theta[^\circ C]$	4.3	4.8	15.6	18.9
COD$[mg/\ell]$	1.4	1.1	1.3	1.2
PO_4-P$[mg/l]$	0.016	0.008	0.010	0.016
NH_4-N$[mg/l]$	0.02	0.04	0.02	0.02

Month	Jun	Jul	Aug	Sep
discharge$[m^3/s]$	3.053	1.910	1.742	0.943
$\theta[^\circ C]$	14.8	18.4	19.7	17.1
COD$[mg/\ell]$	1.0	1.0	1.0	0.8
PO_4-P$[mg/l]$	0.012	0.012	0.009	0.011
NH_4-N$[mg/l]$	0.02	0.02	0.02	0.02

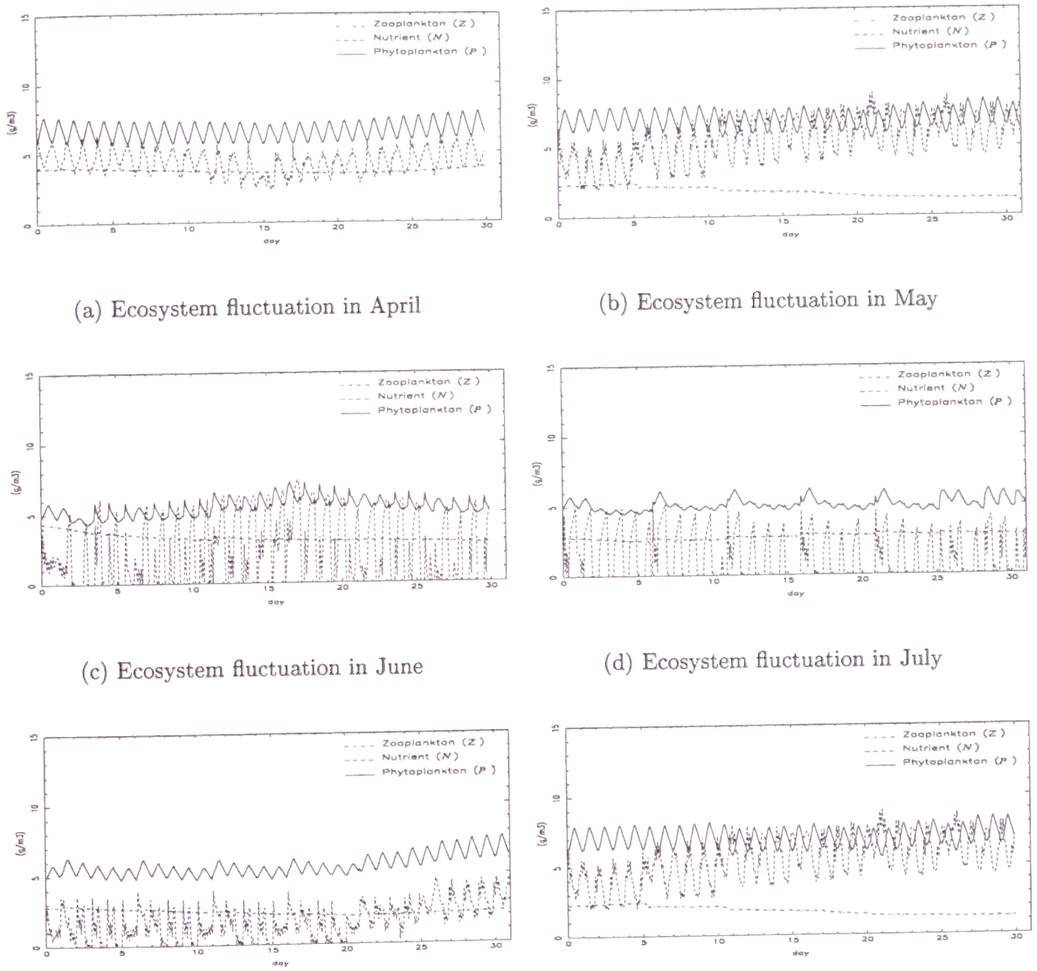

(a) Ecosystem fluctuation in April

(b) Ecosystem fluctuation in May

(c) Ecosystem fluctuation in June

(d) Ecosystem fluctuation in July

(e) Ecosystem fluctuation in August

(f) Ecosystem fluctuation in September

Figure 6.15: Ecosystem fluctuation at the outlet of the reservoir

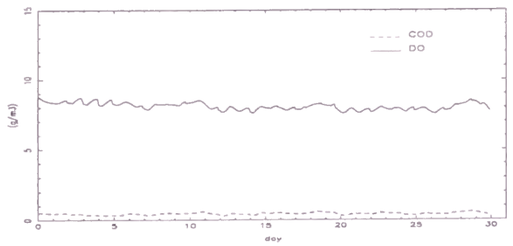

(a) DO and COD fluctuations in April

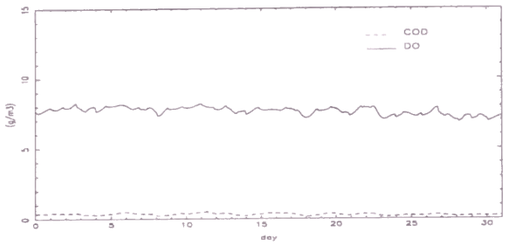

(b) DO and COD fluctuations in May

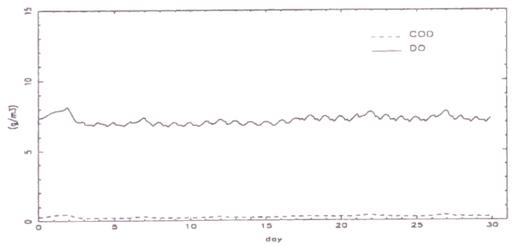

(c) DO and COD fluctuations in June

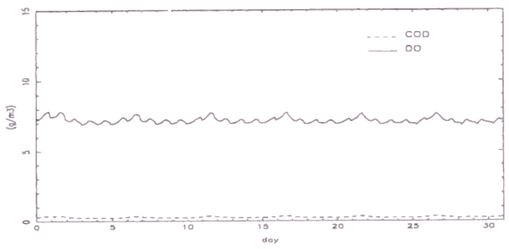

(d) DO and COD fluctuations in July

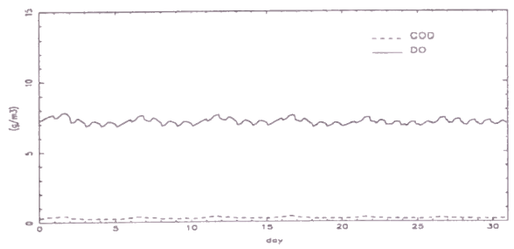

(e) DO and COD fluctuations in August

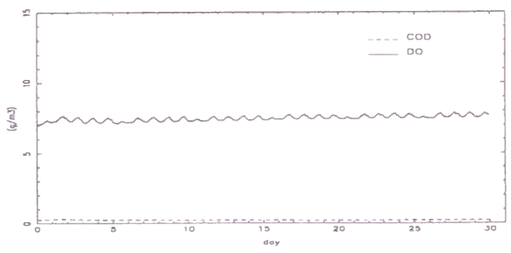

(f) DO and COD fluctuations in September

Figure 6.16: DO and COD fluctuations at the outlet of the reservoir

6.4 Conclusions

The side-view model of DO which consists of FT, PP and DO sub-models has been presented for the analysis in a reservoir. The concluding remarks are summarized as;

(a) The results of DO in the demonstrative computations agree with the observed data quite well. Though we do not have enough data of nutrients and planktons, the model might give quite appropriate results for such variables in the sub-models.

(b) The vertical distributions of θ and DO are highly correlative despite the difference of their boundary conditions. From this fact, their vertical eddy diffusivities can be assumed the same. Therefore, they can be expressed by the function of Brunt-Väisälä frequency.

(c) Though in this model the consumption of DO at the bed was assumed to be constant, it is required to include the appropriate sub-model since its influence on the DO distribution is quite significant.

(d) Linkage of the three basic sub-models must be modified so that more rigorous interactions among the water quality constituents considered can be reproduced, i.e., not one-way but mutual dependencies of the sub-models can be implemented.

The DO model presented herein could be considered as an efficient tool for water quality analysis in a reservoir. However, the successful results in all cases cannot be guaranteed, because of the existence of many site-depend conditions and parameters. And it cannot forecast the unusual plankton blooming, because it is inherently unstable phenomenon. To make the model versatile and reliable, more modification efforts are required.

Chapter 7

SUMMATION

7.1 Summary and Conclusions

Chapters 3 to 6, which are the key chapters of this thesis, are summarized as follows.

Chapter 3: Modelling is based on the equations of water motion and heat transport which are densimetrically coupled via the equation of state. The heat transport equation expressed in term of water temperature includes the internal absorption of short wave radiation. Since these equations lack the expression of vertical free convection by which a surface layer of limited depth is to be isothermal, a reasonable technique is employed to make the model reproduce the effect of such a convection without destroying the mechanism of the forced convection that can be expressed by the equations. Spatial integration for building 3-D numerical model is implemented by consistently using the Galerkin approximation for all space coordinates with the basis functions: 2-D linear and Chebyshev polynomial functions in the horizontal and vertical domains, respectively. Time is stepwise marched with a combined use of the Kawachi and the forward time schemes of the explicit type. The capability of the model is tested by simulating two different thermally stratified flows in a hypothetical reservoir and a real irrigation tank, and comparing the latter simulation results to the observed data available. The results show that in computational practice the model is capable of satisfactorily reproducing the 3-D structures of thermal stratification.

Chapter 4: A numerical procedure for solving the time-dependent, incompressible

Navier-Stokes equations and the heat and salinity transport equations, coupled through the density-state equation, is presented. The method is based on a set of finite element formulation and time-marching procedure. The finite element formulations consist of two steps, i.e., the first step for the depthwise distributions of the primitive variables of interest using Chebyshev polynomials, and the second step for the horizontal distributions of the coefficients of the polynomials using a two-dimensional triangular basis set. The time-marching procedure is executed with the Kawachi and FT explicit schemes combined with the velocity correction technique. The fully three-dimensional reproduction of the convective currents, salinity, and heat transport is accomplished with the aid of Petrov Galerkin integrations with the well-defined triangular basis set in the horizontal domain. As a demonstrative model operation, vertical circulations with a caballing effect and inverse gravitational circulations with a topographic heat accumulation effect are analyzed in hypothetical bodies of water. Reproducing the solutions expected, the model could be a useful tool in the 3-D analyses of density-driven flows.

Chapter 5: A side-view finite element model is developed to simulate vertically 2-D thermal stratification in man-made reservoirs. Using flat-shaped rectangular, trapezoidal, and triangular elements which consist of vertical and horizontal 1-D elements, the model can avert numerical inaccuracy caused by large aspect ratios and can consider the depth dependent field variables as vertically continuous. Treatment of the velocities near the inclined slip bed is modified to satisfy the continuity condition, and treatment of confluences is newly introduced to meet the complex geometrical conditions. Vertical eddy diffusivities are estimated by the newly proposed parameterization using Brunt-Väisälä frequency. The capability of the model is investigated through a few demonstrative computations for hypothetical and real reservoirs, comparing the computed results with the theoretical or observed data available. As a result, the present model proves to be a practical tool for hydro-thermal analyses of man-made reservoirs.

Chapter 6: A side-view finite element model is developed to simulate the variation of dissolved oxygen (DO) in a reservoir. Taking the relationships among flow, water temperature, nutrients, plankton, and DO into consideration, the model is built with three sub-models, viz, 1) Flow and Temperature (FT) sub-model, 2) Phytoplankton

(PP) sub-model, and 3) DO sub-model. The results from the FT and PP sub-models are directly reflected on the final DO sub-model through advection, diffusion, and source terms. Based on the fact that the vertical distributions of water temperature and DO are highly correlative, the model uses the vertical diffusivity expressed in terms of Brunt-Väisälä frequency by which strong effects of thermal stratification on the distributions of the field variables can be reproduced. A verification of the model is carried out in comparison with the measured data in the Osakabe Reservoir and the long term model behavior is tested through the computation in the Oso Reservoir. The results show that the model is capable of satisfactorily reproducing the DO distribution in a vertical plane, and thus, can be an alternative tool for forecasting the DO in a reservoir.

Numerical modelling of hydraulic and environmental problems is the subject matter of this thesis. The present study focuses on four subjects. The hydraulic and geometric characteristic common to the four subjects is that the body of water is shallow, i.e, the magnitude of the horizontal length is much greater than the vertical one. This characteristic induces computational inaccuracy in finite element computations, when the domain of interest is discretized using usual triangular, quadrilateral and/or tetrahedron elements. A cause of this inaccuracy appears in formation of the global matrix. There is a great difference of the digit among the values of the matrix elements, which is mainly due to the thin shape of elements. When the global matrix is solved, small digit values are often ignored or disappear in computational procedures and give inaccurate results. This is one of the important reasons why building of a hydraulic and environmental model for shallow waters is yet difficult. Therefore, development of advanced numerical models that endure such a serious characteristic is strongly required, which is the origin of this study.

The models presented in this thesis are built using a peculiar manner in their discretizations, viz., different basis sets are used separately in depthwise and horizontal directions. This manner may make the codes of the models a little more complex, but the inaccuracy due to the thinness of the elements can be evaded theoretically. As a result, the models surely possess such accuracy and show stable computations in the actual application to the four subjects. The manner introduced into this study creates a

stir in the numerical approaches to the hydraulic and environmental problems of shallow waters.

Coupled hydrodynamics and mass transport models are being used to study complex eutrophication problems in various bodies of waters. The occurrence of nutrient fed algal blooms is an important environmental issue and the understanding and control of these events increase the need for coupled hydrodynamics and water quality models. Now nothing can replace the position of the numerical models in making comparative risk assessments of alternative environmental management scenarios. In environmental hydraulic studies, numerical models are in many ways much more attractive than empirical hydraulic models. However, the future of our natural environment and the ecosystem can be altered drastically by a slight difference in the conditions. It should be noted that the computational results and predictions, including those in this thesis, show just one of many situations that can take place. Therefore, the appropriate collection of observed and experimental data is indispensable for modelling procedures. Unsuitable parameters yield inaccurate results, even if they appear to be appropriate.

The more intensively various hydro-environmental problems are studied, the greater the importance of coupled hydrodynamics and water quality models become. The models are expected to evolve into more realistic models, adopting newly obtained mechanisms that actually occur in nature.

Finally, it is concluded that the models developed in this study can be attractive alternatives to the conventional numerical models and be a foundation for future development of the hydraulic and environmental modelling.

7.2 Follow-up Studies

Some problems are still left to be discussed in follow-up studies. They are summarized below.

(a) In order to obtain appropriate results on water quality and eutrophication models, the simplification of the mechanism of water quality and ecosystems is important. Unnecessarily complex models will not work without impractically accurate parameterization. However, the degree of complexity is still of great interest. It should be discussed more intensively and the models presently developed should be verified precisely again.

(b) Through research, the validity of parameterization for vertical diffusivities using Brunt-Väisälä frequency can be proved. However, due to the lack of observed data, its appropriate function could not be chosen. This should be determined in follow-up studies.

(c) The waters dealt with in this thesis have free surfaces. The water level in a reservoir may vary seriously, depending on the water demands. However, the present models assume only small fluctuations of the surface, restricting their applicability to such a reservoir. The models should be improved to cope with this problem using a re-meshing procedure.

(d) A better grasp of the situation in the bodies of water, a deeper elucidation of the mechanism of the phenomena and more precise forecast of the future state are utterly imperative to make the hydro-environmental models truly useful. As another forward step, it is a sheer need that for reasonable preservation of the waters the methodologies for their control and management are developed with inclusion of the hydrodynamical and ecological models presented in this thesis. In addition, use of the tools such as artificial intelligence [26] in the field of environmental hydraulics may impact on the realm of modelling and controlling of the waters.

References

[1] Auer, M. T. and S. W. Effler ; "Variablity in Photosynthesis: Impact on DO Model", *Proc. ASCE*, Vol. 115 (EE5), pp. 944–963, 1989

[2] Auer, M. T. and S. W. Effler ; "Calculation of Daily Average Photosynthesis", *Proc. ASCE*, Vol. 116 (EE2), pp. 412–418, 1990

[3] Ban, M. ; *"Studies on Stratified Estuarine Hydraulics for Water Resource Development"*, Doctoral thesis, Kyoto University, 1989

[4] Ban, M., T. Kawachi and I. Minami ; "Two-Dimensional Side View Model for Currents in Stratified, Shallow Waters by the Finite Element Method", *Trans. JSIDRE*, 142, pp. 19–26, 1989

[5] Banks, R. B. and F. F. Herrera ; "Effect of Wind and Rain on Surface Reaeration", *Proc. ASCE*, Vol. 103 (EE3), pp. 489–504, 1977

[6] Bowden, K. F. ; "Horizontal Mixing in the Sea Due to a Shearing Current", *J. Fluid Mech.*, Vol. 21, pp. 83–95, 1965

[7] Chen, C. W. and G. T. Orlab ; "Ecologic Simulation of Aquatic Environments ", *Systems Analysis and Simulation in Ecology, III*, pp. 475–588, Academic Press, NY, 1975

[8] Cheng, R. T., T. M. Powell and T. M. Dillon ; "Numerical Modles of Wind-driven circulation in Lakes", *Appl. Math. Modelling*, Vol. 1, pp. 141–159, 1976

[9] Cooley, R. L. ; "New Procedure for Numerical Solution of Variably Saturated Flow Problems", *Water Resources Research*, Vol. 19 (5), pp. 1271–1285, 1983

[10] Davies, A. M. and A. Owen ; "Three Dimensional Numerical Sea Model using the Galerkin Method with a Polynomial Basis Set", *Appl. Math. Modelling*, Vol. 1, pp. 421–428, 1979

[11] Deardorff, J. W. ; "A Numerical Study of Three-Dimensional Turbulent Channel Flows at Large Reynolds Numbers", *J. Fluid Mech.*, Vol. 41 (part 2), pp. 453–480, 1970

[12] Di Tro, D. M., D. J. O'Conner and R. V. Thomann ; "A Dynamic Model of the Phytoplankton Population in Sacrament-San Joaquin Delta", *Advance in Chemistry*, (Series No.16), pp. 131–180, 1971

[13] Donea, J., S. Giuliani, H. Laval and L. Quartapelle ; "Finite Element Solution of the Unsteady Navier-Stokes Equations by a Fractional Step Method", *Comp. Meth. Appl. Mech. Eng.*, Vol. 30, pp. 53–73, 1982

[14] Echart, C. ; "Prosperties of Water, Part II, The Equation of State of Water and Sea Water at Low Temperature and Pressures", *Amer. J. Sci.*, Vol. 256, pp. 225–240, 1958

[15] Franks, P. J. S., J. S. Wroblewski and G. R. Flierl ; "Behavior of a simple plankton model with fool-level acclimation by herbivores", *Marine Biology*, Vol. 91, pp. 121–129, 1986

[16] Fujihara, M. ; *"Modelling Flow and Water Quality in Aquaculture Ground"*, Doctoral thesis, Kyoto University, 1997

[17] Fujihara, M., T. Kawachi and G. Oohashi ; "Physical-biological Coupled Modelling for Artificially Generated Upwelling", *Trans. JSIDRE*, 189, pp. 69–79, 1997

[18] Fujihara, M., S. Kubo and M. Yamamoto ; "A Numerical Model on Estimating Reasonable Inflow Rate in a Nursery Aquaculture Pond", *Fishering Engineering*, Vol. 30 (2), pp. 69–79, 1993

[19] Goda, K. and S. Ebise ; "Eutrophication in a Dam Reservoir and its Simulation", *Proc. JSCE*, Vol. 263, pp. 49–61, 1977 (in Japanese)

[20] Harashima, A. and Y. Oonishi ; "The Coriolis Effect Against Frontogenesis in Steady Buoyancy-driven Circulation", *J. Oceanogr. Soc. Jpn.*, Vol. 37, pp. 49–59, 1981

[21] Harleman, D. R. F. ; "Recent Development in Water Quality Modelling and Management", *"Hydraulic and Environmental Modelling: Coastal Waters"*, edited by R. A. Falconer, S. N. Chandler-Wilde, and S .Q. Liu, Vol. 1, pp. 15–28, Bradford, UK, Ashgate Publ.Co., 1992

[22] Harleman, D. R. F. and K. D. Stolzenbach ; "Fluid Mechanics of Heat Disposal from Power Generation", *Ann. Review Fluid Mech.*, Vol. 4, pp. 7–32, 1972

[23] Hiramatsu, K. ; "Three Dimensional Finite Element Analysis of Thermally Stratified Flows", Master's thesis, Kyoto University, 1993

[24] Hiramatsu, K., T. Kawachi, E. Ichion and Y. Nada ; "A Modified Side-View Model for Thermal Analysis in Man-Made Reservoirs", *Trans. JSIDRE* (in press)

[25] Hiramatsu, K., T. Kawachi, H. Kim and Y. Yoshitake ; "Polynomial Finite Element Solution of 3-D Density Driven Currents using the Velocity Correction Method", *Trans. JSIDRE*, 185, pp. 747–754, 1996

[26] Hiramatsu, K., T. Kawachi, H. Kurimoto, F. MD. Abul and M. Fukatsu ; "Numerical Estimation of Water Polluting Points using Neural Networks", *"Hydrodynamicsaulic: Theory and Applications"*, edited by A. T. Chwang, J. H. W. Lee, and D. Y. C. Leung, Vol. 2, pp. 1069–1074, Hong Kong, A.A.Balkema Publ.Co., 1996

[27] Hiramatsu, K., T. Kawachi and Y. Nada ; "Side-View Modelling of Dissolved Oxygen in Thermally Stratified Reservoirs", *Trans. JSIDRE* (in press)

[28] Hiramatsu, K., T. Kawachi, Y. Nada and H. Kim ; "Side-view Modelling for Water Quality Forecats in a Man-made Reservoir", *"Hydrodynamics: Theory and Applications"*, edited by H. Kim, S. H. Lee, and S. J. Lee, Vol. 1, pp. 587–592, Seoul, Uiam Publ.Co., 1998

[29] Holley, E. R., D. R. F. Harleman and H. B. Fischer ; "Dispersion in Homogeneous Estuary Flow", *Proc. ASCE*, Vol. 96 (HY8), pp. 1691–1709, 1970

[30] Hondzo, M., C. R. Ellis and H. G. Stefan ; "Vertical Diffusion in Small Stratified Lake: Data and Error Analysis", *Proc. ASCE*, Vol. 117 (HY10), pp. 1352–1369, 1991

[31] Hondzo, M. and H. G. Stefan ; "Lake Water Temperature Simulation Model", *Proc. ASCE*, Vol. 119 (HY11), pp. 1251–1273, 1993

[32] Hua, H. ; "Accurate Method for Calculation of Saturation DO", *Proc. ASCE*, Vol. 115 (EE5), pp. 988–990, 1990

[33] Huber, W. C., D. R. F.Harleman and P. J. Ryan ; "Temperature Prediction in Stratified Reservoirs", *Proc. ASCE*, Vol. 98 (HY4), pp. 645–666, 1972

[34] Huyakorn, P. S. ; "Solution of Steady-State, Convective Transport Equation using an Upwind Finite Element Scheme", *Appl. Math. Modelling*, Vol. 1, pp. 187–195, 1977

[35] Huyakorn, P. S., P. F. Andersen, J. W. Mercer and H. O. White Jr. ; "Salt water intrusion in Aquifers: Development and Testing of a Three-Dimensional Finite Element Model", *Water Resources Research*, Vol. 23 (2), pp. 293–312, 1987

[36] Ippen, A. I. and D. R. F. Harleman ; "Steady-state Characteristics of Subsurface Flow", *Gravity Wave Symposium Nat. Bur. of Stands. Circulation*, 521, pp. 79–93, 1951

[37] Iwasa, Y. and N. Matsuo ; "Mathematical Model for Analysis and Prediction of Hydraulic Behaviors in Reservoir Dynamics in View of Thermal Aspect", *Proc. JSCE*, Vol. 308, pp. 59–68, 1981

[38] Iwasa, Y., N. Matsuo and Y. Asao ; "Numerical Analysis of Stored Waters in Reservoir Hydraulics and Its Engineering Applications", *Trans. DPRI, Kyoto University*, Vol. 22 (B-2), pp. 341–354, 1979

[39] J., Perrels. P. A. and M. Karelse ; "A Two-Dimensional Laterally Averaged Model for Salt Intrusion in Esturies", *Transport Models for Inland and Coastal Waters*, pp. 483–534. Academic Press Inc., 1981

[40] Jørgensen, S. E. ; "A Eutrophication Model for a Lake", *Ecological Modelling*, Vol. 2, pp. 147–165, 1976

[41] JSCE ; *"Hydraulic Formulas"*, JSCE, 1985 (in Japanese)

[42] Karpid, S. R. and G. D. Raithby ; "Laterally Averaged Hydrodynamics Model for Reservoir Predictions", *Proc. ASCE*, Vol. 116 (HY6), pp. 783–793, 1990

[43] Katayama, T. ; "An Optimization Model of River Wter Quality Management", Master's thesis, Kyoto University, 1995

[44] Kawachi, T. ; "Three-Dimensional Finite Element Model of Density-Stratified Flow Using Depth-Dependent Polynomial Basis Functions", *Trans. JSIDRE*, 156, pp. 93–100, 1991

[45] Kawachi, T, M Ban and K. Hiramatsu ; "3-D Finite Element Simulation of Salt-Water Intrusion in an Esturarine Barrage", *"Hydraulic and Environmental Modelling: Estuarine and River Waters"*, edited by R. A. Falconer, K. Shiono, and G. S. Matthew, Vol. 2, pp. 201–212, Bradford, UK, Ashgate Publ.Co., 1992

[46] Kawachi, T., K. Hiramatsu, T. Hasegawa and M. Makita ; "Three Dimensional Finite Element Modelling of Thermal Stratification in Shallow Waters", *Trans. JSIDRE*, 168, pp. 87–95, 1993

[47] Kawachi, T., K. Hiramatsu and Y. Nada ; "Forecasting Analysis of Water Quality in a Man-made Reservoir", Technical Report, submited to JACREP, 1998 (In Japanese)

[48] Kawachi, T., M. Yangyuoru, K. Hiramatsu, K. Unami and T. Hasegawa ; "A Finite Element Model of Steady Regulated Flow in Open Channel Networks", *Trans. JSIDRE*, 173, pp. 59–69, 1994

[49] Kawahara, M. and K. Ohmiya ; "Finite Element Analysis of Density Flow Using the Velocity Correction Method", *Int. J. Num. Meth. Fluid*, Vol. 5, pp. 981–993, 1985

[50] Kishi, M. ; "Numerical model for mariculture reflecting upon oxygen consumption by bottom mud", *Bull. Coastal Oceanography*, Vol. 32 (1), pp. 43–53, 1994

[51] Kishi, M. J. and K. Nakata ; "Simulation of Ecosystems in Internal Bay and its Problem", *Marine Science*, Vol. 10 (10), pp. 796–806, 1978

[52] Kishi, M. J., M. Uchiyama and Y. Iwata ; "Numerical Simulation model for Quantitative Management of Aquaculture", *Ecological Modelling*, Vol. 72, pp. 21–40, 1994

[53] Koutitas, C. and B. O'Connor ; "Modelling Three-Dimensional Wind-induced Flows", *Proc. ASCE*, Vol. 106 (HY11), pp. 1843–1865, 1980

[54] Koutitas, C. and B. O'Connor ; "Finite Element Fractional Steps Solution of the 3-D Coastal Circulation Model", *Adv. Water Res.*, Vol. 5, pp. 167–170, 1982

[55] Kumagai, M., H. Maeda and Y. Oonishi ; "Vertical Circulation and Formation of Anoxic Layer", *Jpn. J. Limnol.*, Vol. 47 (1), pp. 27–35, 1986 (in Japanese)

[56] Lee, J. H. W., R. S. S. Wu and Y. K. Cheung ; "Forecasting of Dissolved Oxygen in Marine Fish Culture Zone", *Proc. ASCE*, Vol. 117 (EE6), pp. 816–833, 1991

[57] Lee, J. H. W., R. S. S. Wu, Y. K. Cheung and P. P. S. Wong ; "Dissolved Oxygen Variations in Marine Fish Culture Zone", *Proc. ASCE*, Vol. 117 (EE6), pp. 799–815, 1991

[58] Leendertse, J. J and S. K. Liu ; "A Three-dimensional Turbulent Energy Model for Nonhomogeneous Estuaries and Coastal Sea Systems", *Hydrodynamics of Estuaries and Fjords*, pp. 387–405, Elsevier Sci. Pub. Co., 1978

[59] Leonard, A. ; "Energy Cascade in Large-Eddy Simulation of Turbulent Fluid Flows", *Adv. Geophy.*, Vol. 18A, pp. 237–248, 1974

[60] Losordo, T. M. and R. H. Piedrahita ; "Modelling Temperature Variation and Thermal Stratification in Shallow Aquaculture Ponds", *Ecological Modelling*, Vol. 54, pp. 189–226, 1991

[61] Mackay, D. and A. T. K. Yeun ; "Mass Transfer Coefficient Correlation for Volatilization of Organic Solutes from Water", *Envirn. Sci. Tech.*, Vol. 17 (4), pp. 211–217, 1983

[62] Makita, M. ; "Finite Element Analysis of Spatially Distributed Water Quality in an Estuarine Network System", Master's thesis, Kyoto University, 1993

[63] Mamayev, O. I. ; "The Influence of Stratification on Vertical Turbulent Mixing in the sea", *Bull. Acad. Sci. USSR*, pp. 494–497, 1958, Geophys.Ser., translated by Salkind,V.A.

[64] Martin, S. C. ; "Application of Two Dimensional Water Quality Model", *Proc. ASCE*, Vol. 114 (EE2), pp. 317–336, 1988

[65] Martin, S. C., S. W. Effer, J. V. DePinto, F. B. Trama, P. W. Rodgers, J. S. Dobi and M. C. Wodka ; "Dissolved Oxygen Model for a Dynamic Reservoir", *Proc. ASCE*, Vol. 111 (EE5), pp. 647–664, 1985

[66] Matsui, T. ; "Measurements and Parameterization of the Vertical Eddy Diffusivity", *Coastal Oceanography*, Vol. 31 (1), pp. 67–80, 1993 (in Japanese)

[67] Matsuo, N. ; *"Hydraulic Studies on Prediction of Parameterization for Water Temperature, Turbidity and Eutrophication in Reservoirs"*, Doctoral thesis, Kyoto University, 1982 (in Japanese)

[68] Mizukami, A. and M. Tsuchiya ; "A Finite Element Method for the Three Dimensional Non-Steady Nvier-Stokes Equations", *Int. J. Num. Meth. Fluid*, Vol. 4, pp. 349–357, 1984

[69] Munk, W. H. and E. R. Anderson ; "Notes on A Theory of the Thermocline", *J. Marine Research*, Vol. VII (3), pp. 276–294, 1948

[70] Nyholm, N. ; "A Simulation Model for Phytoplankton Growth and Nutrient Cycling in Eutrophic, Shallow Lakes", *Ecological Modelling*, Vol. 4, pp. 279–310, 1978

[71] O'Conner, D. J. and D. M. Di Toro ; "Photosynthesis and Oxygen Balance in Streams", *Proc. ASCE*, Vol. 96 (SA2), pp. 547–571, 1970

[72] O'Conner, D. J. and W. E. Dobins ; "The Mechanism Reaeration in Natural Streams", *Proc. ASCE*, Vol. 82 (SA6), pp. 1115–1130, 1956

[73] Oonishi, Y. ; "Development of the Current Induced by the Topographic Heat Accumulation (I)", *J. Oceanogr. Soc. Jpn.*, Vol. 31, pp. 243–254, 1975

[74] Osborn, T. R. and C. S. Cox ; "Oceanic FIne Structure", *Geophys. Fluid Dyn.*, Vol. 3, pp. 321–345, 1972

[75] Ramaswamy, B. and T. C. Jue ; "Some Recent Trends and Developments in Finite Element Analysis for Incompressible Thermal Flows", *Int. J. Num. Meth. Engineering*, Vol. 35, pp. 671–707, 1992

[76] Sado, K. ; "Fundamental Study on Heat Balance of River Water", *Proc. JSCE*, Vol. 330, pp. 69–79, 1983 (in Japanese)

[77] Saito, T., H. Ichikawa, T. Nozawa and Y. Ito ; "Water Temperature and Heat Budget in Benten Ike Pond ", *Suion no Kenkyu (Water Temperature Study)*, Vol. 25 (1), pp. 2–14, 1981 (in Japanese)

[78] Shimura, M. and M. Kawahara ; "Two Dimensional Finite Element Flow Analysis using the Velocity Correction Method", *Proc. JSCE*, Vol. 338 (I-10), pp. 51–59, 1988

[79] Smagorinsky, J. ; "General Circulation Experiments with the Primitive Equations I.The Basis Experiments", *Monthly Weather Review*, Vol. 91 (3), pp. 99–164, 1963

[80] Smagorinsky, J., S. M. Manabe and J. L. Holloway ; "Numerical Results from a Nine-Level General Circulation Model of the Atmosphere", *Monthly Weather Review*, Vol. 93 (12), pp. 727–768, 1965

[81] Streeter, H. W. and E. B. Phelp ; "Studies of the Pollution and Natural Purificationof the Ohio River, Part III: Factors Concerned in the Phenomena of oxidation and Reareation", *Public Health Bulletin*, 146, 1925

[82] Thomann, R. V. and J. A. Mueller ; *"Principles of Surface Water Quality Modeling and Control"*, Harper & Row, NY, 1987

[83] Todd, D. A. ; "Stream Dissolved Oxygen Analysis and Control", *Proc. ASCE*, Vol. 111 (EE3), pp. 336–352, 1985

[84] Walsh, J. J. ; "A Spatial Simulation Model of the Peru Upwelling Ecosystem", *Deep-Sea Research*, Vol. 22, pp. 201–236, 1975

[85] Walters, R. A. ; "A Time- and Depth-Dependent Model for Physical Chemical and Biological Cycles in Temperature Lakes", *Ecological Modelling*, 8, pp. 79–96, 1980

[86] Wang, J. D., A. F. Blumberg, H. L. Butler and P. Hamilton ; "Transport Prediction in Partially Stratified Tidal Water", *Proc. ASCE*, Vol. 116 (HY3), pp. 380–396, 1990

[87] Welander, P. ; "Theoretical Forms for the Vertical Exchange Coefficients in Stratified Fluid with Application to Lakes and Seas", *Acta Regiae Scietatis Scientiarum et Litterarum Gothoburgensis*, Geophysica 1, pp. 1–26, 1968

[88] Yanagi, T. and A. Isobe ; "Generation Mechanism of Thermohaline Front in Shelf Sea", *"Oceanic and Anthropogenic Controls of Life in the Pacific Ocean"*, edited by V. I. Ilyichev *et al.*, pp. 11–13. Kluwer Academic Publ., 1992

[89] Young, D. L. and G. H. Lin ; "Modeling of Thermally Stratified Lakes with Free Surface", *24th Congress of IAHR*, Vol. D, pp. 137–144, 1989

Appendix A

The results pertaining to water quality analyses discussed in Chapter 6 are illustrated in this Appendix.

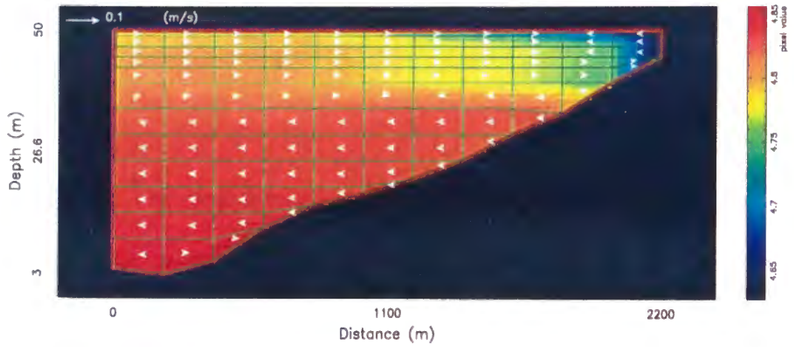

Temperature distribution in Oso reservoir

Figure A.1: Hydro-thermal distributions (March 10)

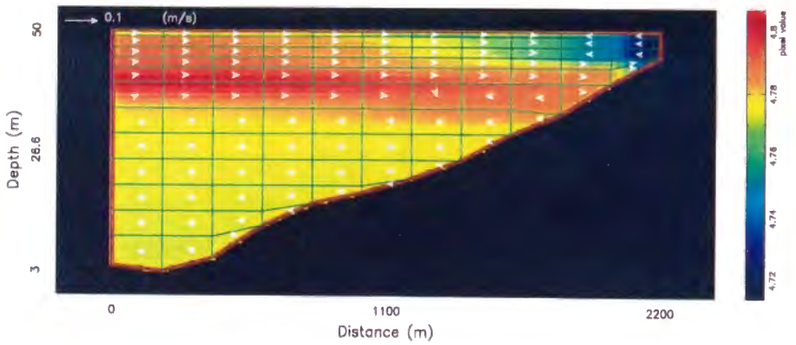

Temperature distribution in Oso reservoir

Figure A.2: Hydro-thermal distributions (March 20)

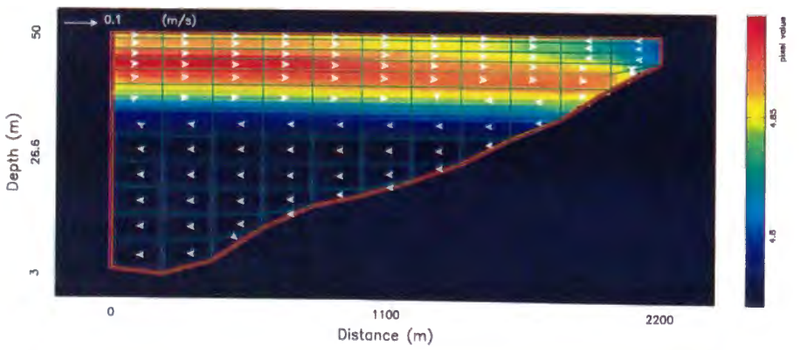

Temperature distribution in Oso reservoir

Figure A.3: Hydro-thermal distributions (March 30)

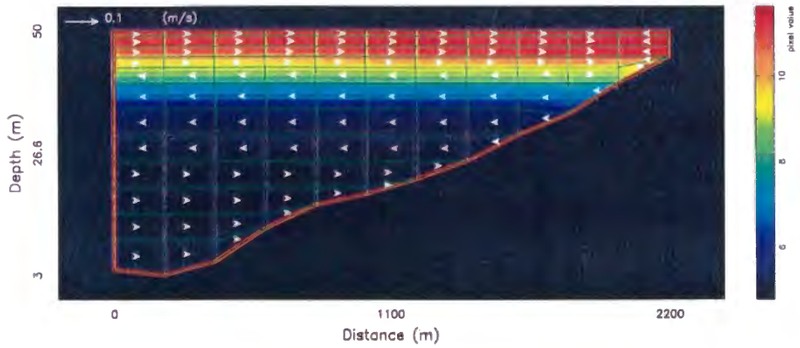

Temperature distribution in Oso reservoir

Figure A.4: Hydro-thermal distributions (April 10)

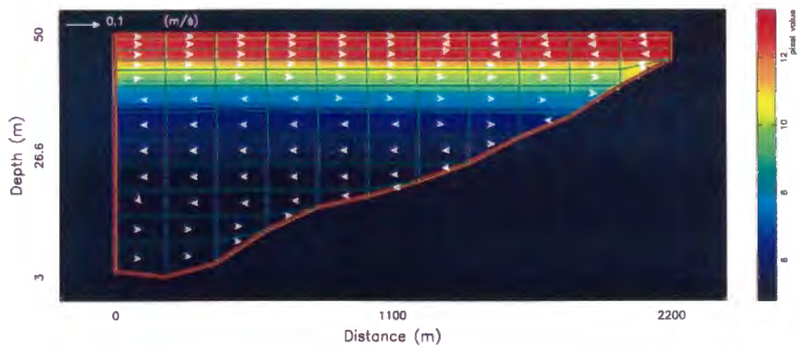

Temperature distribution in Oso reservoir

Figure A.5: Hydro-thermal distributions (April 20)

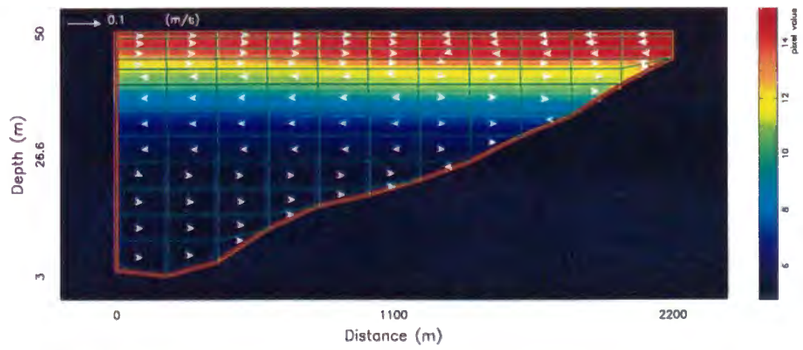

Temperature distribution in Oso reservoir

Figure A.6: Hydro-thermal distributions (April 30)

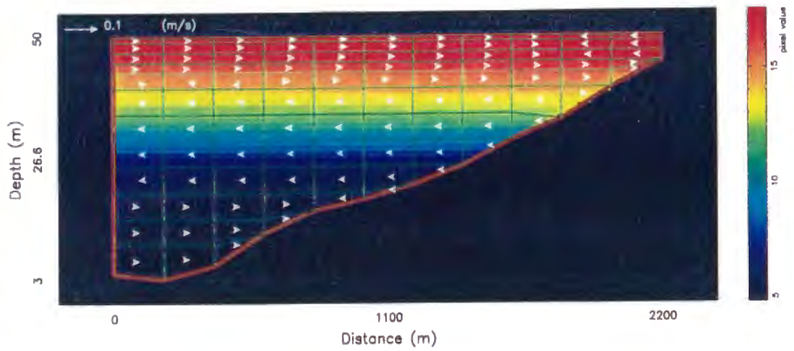

Temperature distribution in Oso reservoir

Figure A.7: Hydro-thermal distributions (May 10)

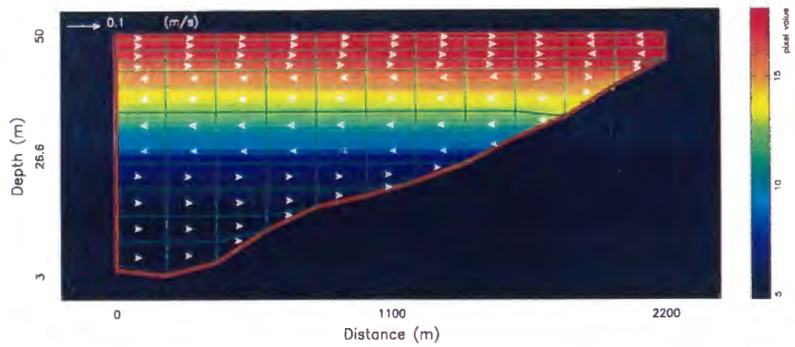

Temperature distribution in Oso reservoir

Figure A.8: Hydro-thermal distributions (May 20)

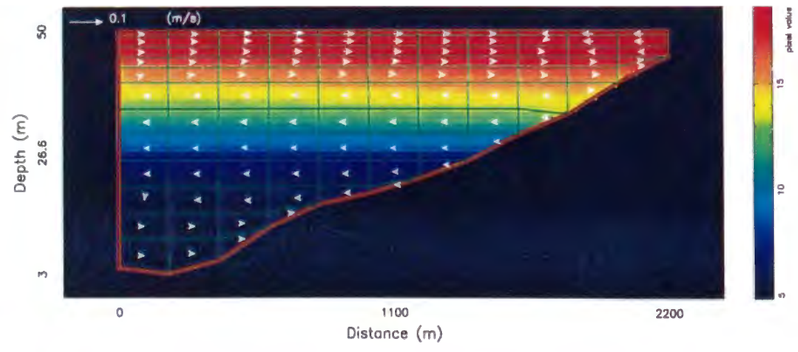

Temperature distribution in Oso reservoir

Figure A.9: Hydro-thermal distributions (May 30)

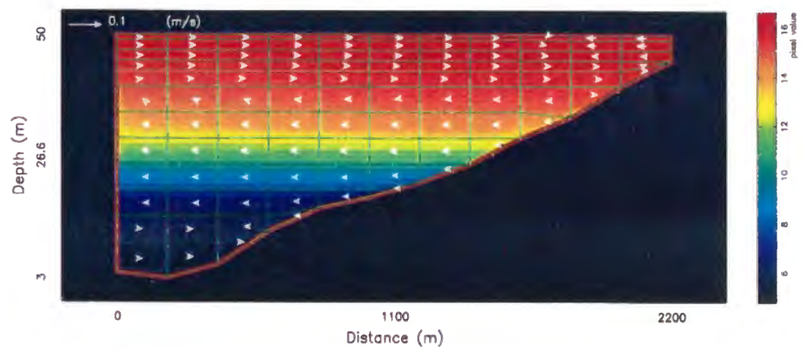

Temperature distribution in Oso reservoir

Figure A.10: Hydro-thermal distributions (June 10)

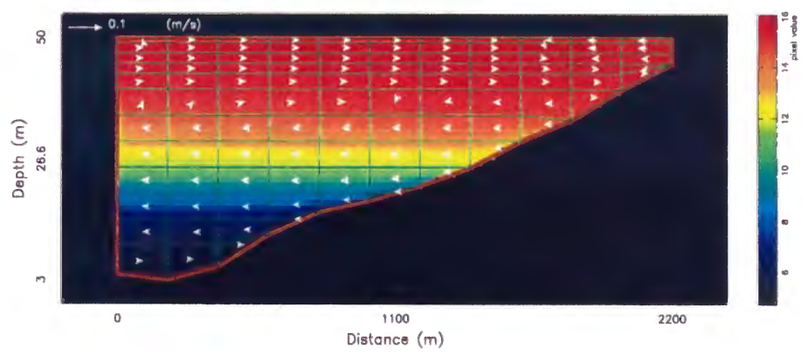

Temperature distribution in Oso reservoir

Figure A.11: Hydro-thermal distributions (June 20)

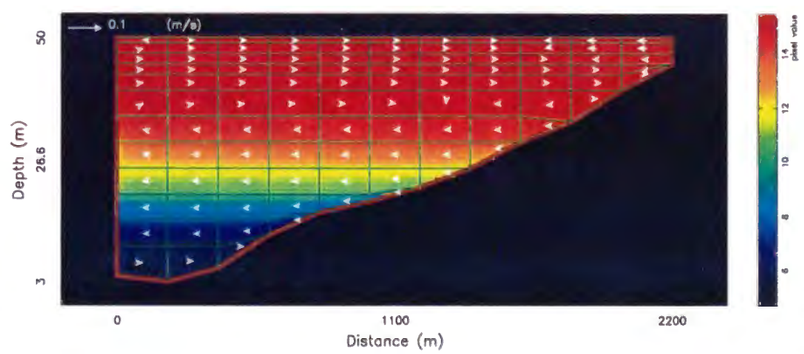

Temperature distribution in Oso reservoir

Figure A.12: Hydro-thermal distributions (June 30)

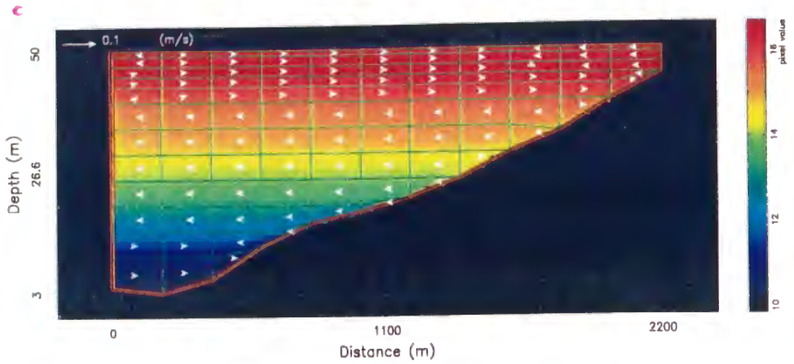

Temperature distribution in Oso reservoir

Figure A.13: Hydro-thermal distributions (July 10)

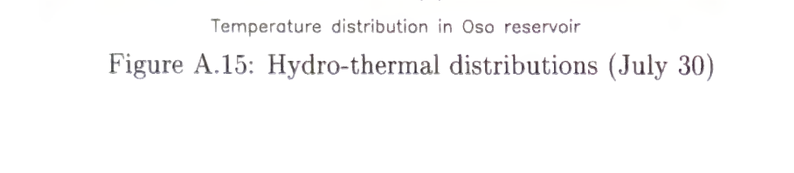

Temperature distribution in Oso reservoir

Figure A.14: Hydro-thermal distributions (July 20)

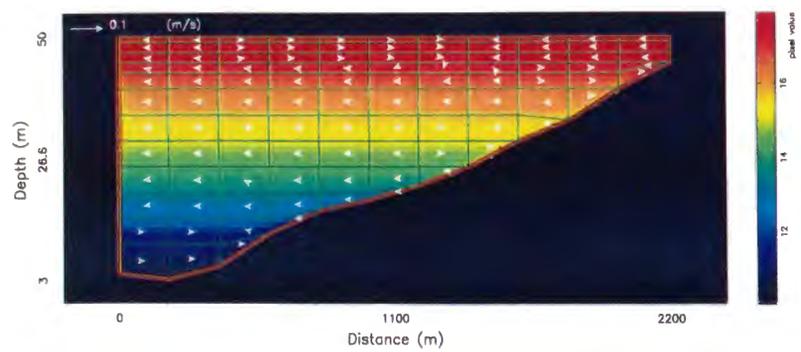

Temperature distribution in Oso reservoir

Figure A.15: Hydro-thermal distributions (July 30)

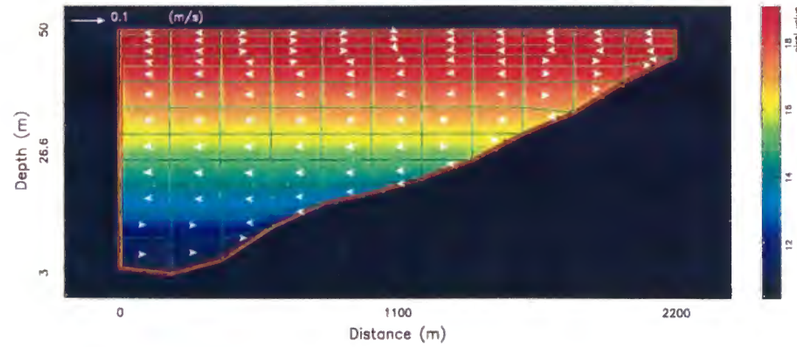

Temperature distribution in Oso reservoir

Figure A.16: Hydro-thermal distributions (August 10)

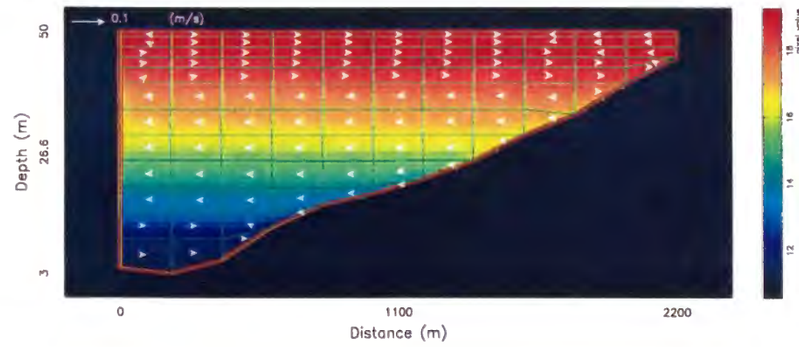

Temperature distribution in Oso reservoir

Figure A.17: Hydro-thermal distributions (August 20)

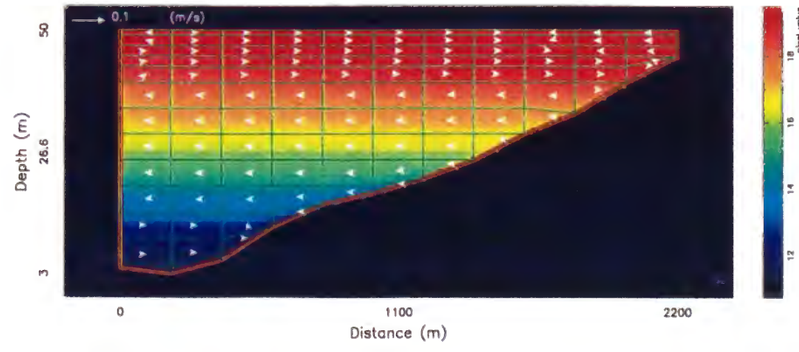

Temperature distribution in Oso reservoir

Figure A.18: Hydro-thermal distributions (August 30)

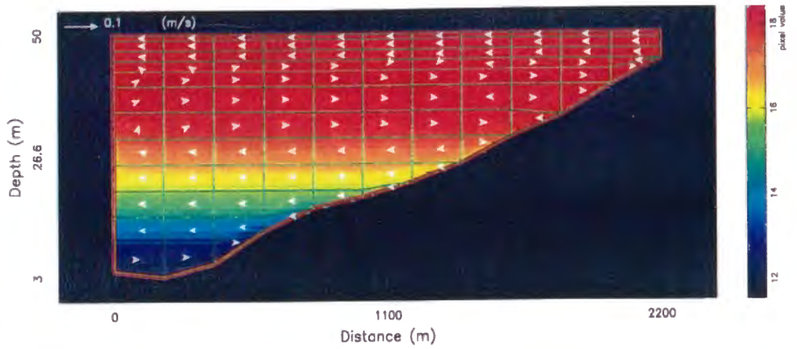

Temperature distribution in Oso reservoir

Figure A.19: Hydro-thermal distributions (September 10)

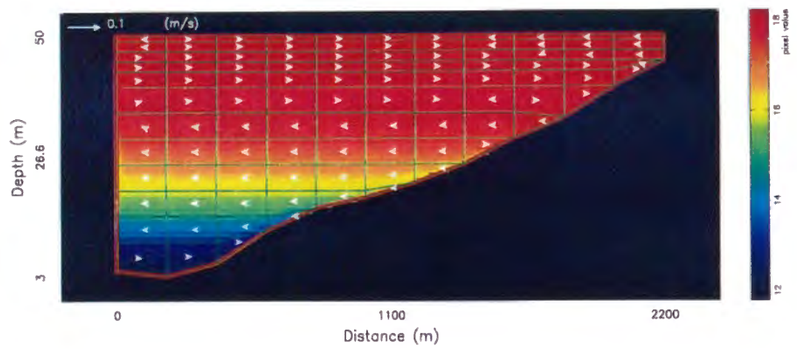

Temperature distribution in Oso reservoir

Figure A.20: Hydro-thermal distributions (September 20)

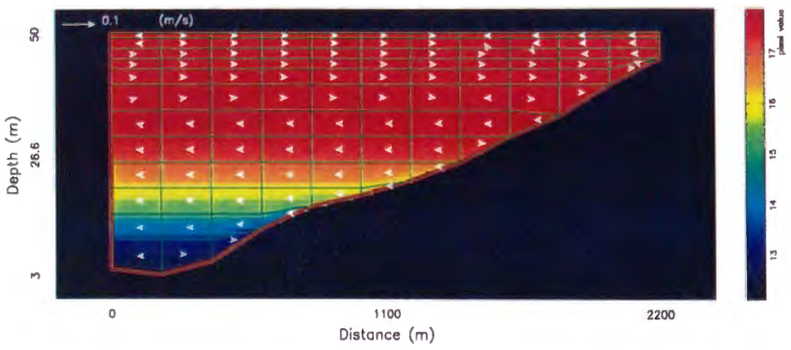

Temperature distribution in Oso reservoir

Figure A.21: Hydro-thermal distributions (September 30)

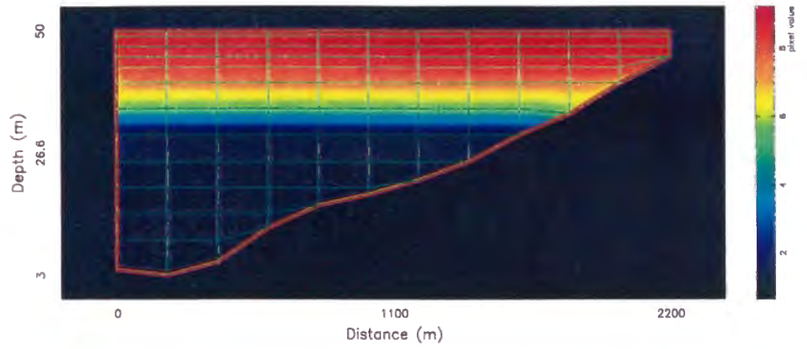

Phytoplankton distribution in Oso reservoir

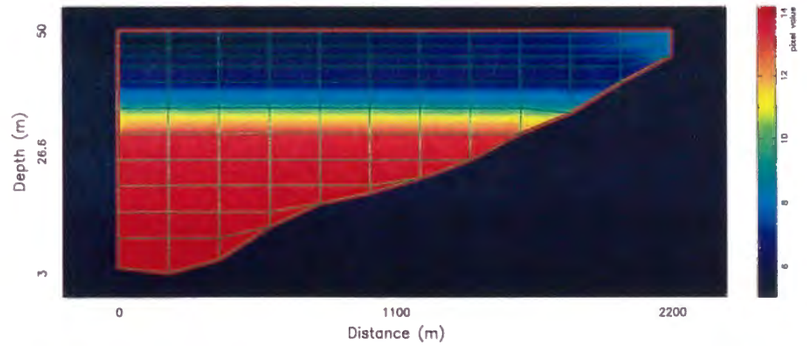

Nutrient distribution in Oso reservoir

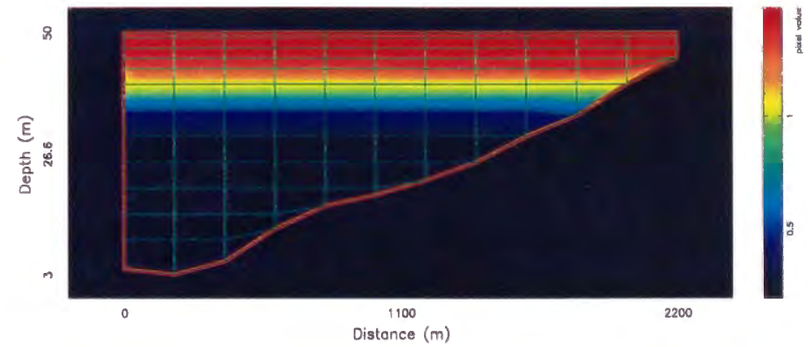

Zooplankton distribution in Oso reservoir

Figure A.22: Planktons ecosystem (March)

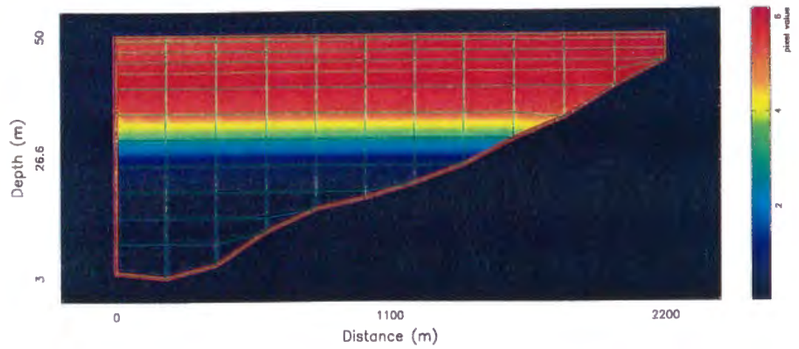

Phytoplankton distribution in Oso reservoir

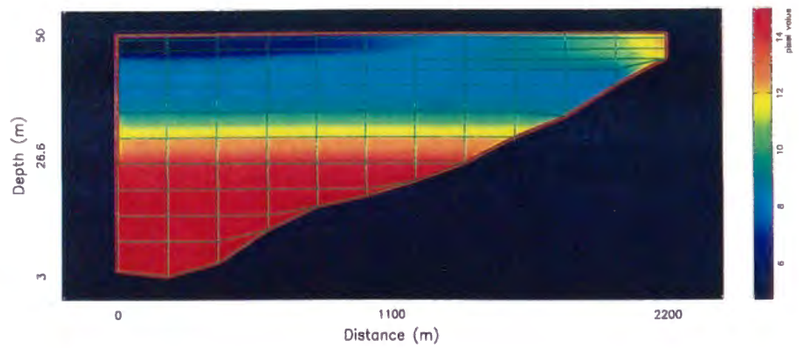

Nutrient distribution in Oso reservoir

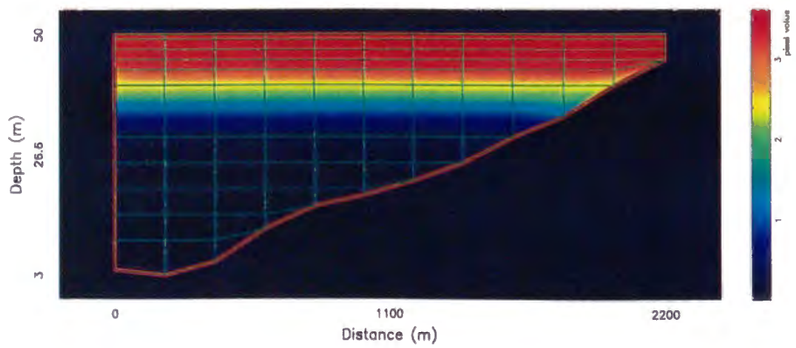

Zooplankton distribution in Oso reservoir

Figure A.23: Planktons ecosystem (April)

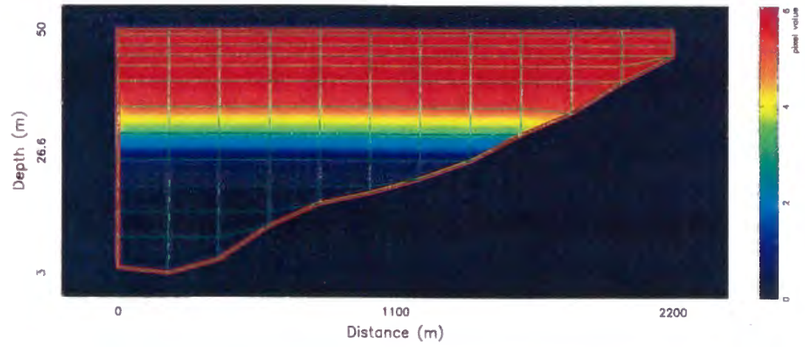

Phytoplankton distribution in Oso reservoir

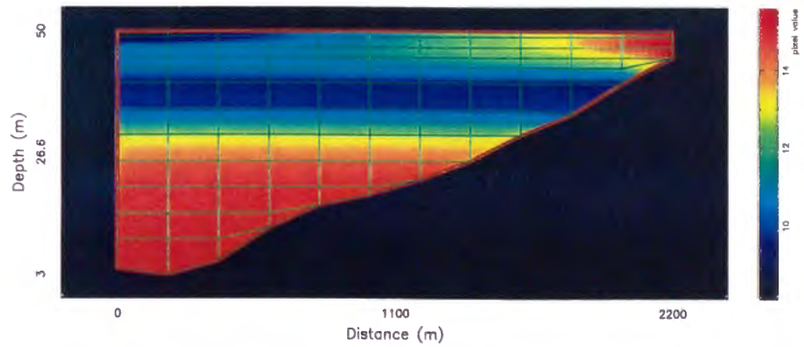

Nutrient distribution in Oso reservoir

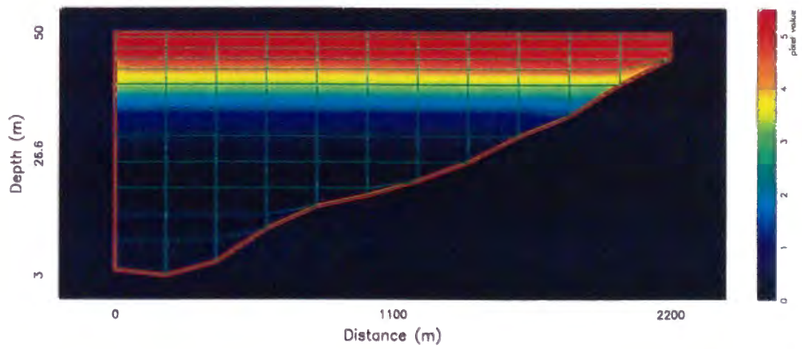

Zooplankton distribution in Oso reservoir

Figure A.24: Planktons ecosystem (May)

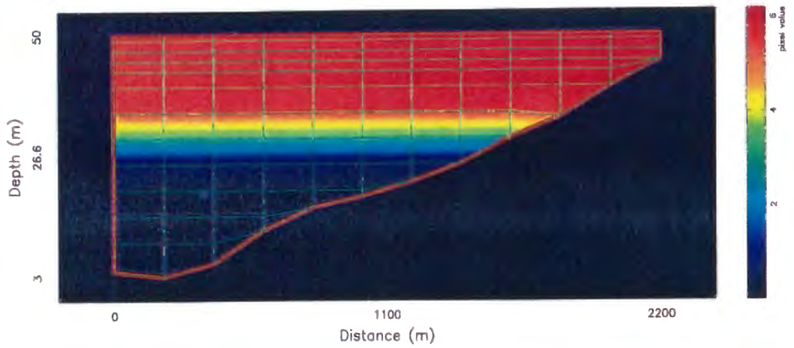

Phytoplankton distribution in Oso reservoir

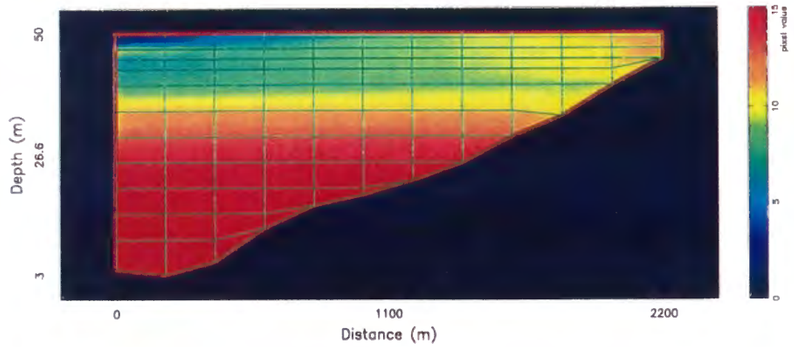

Nutrient distribution in Oso reservoir

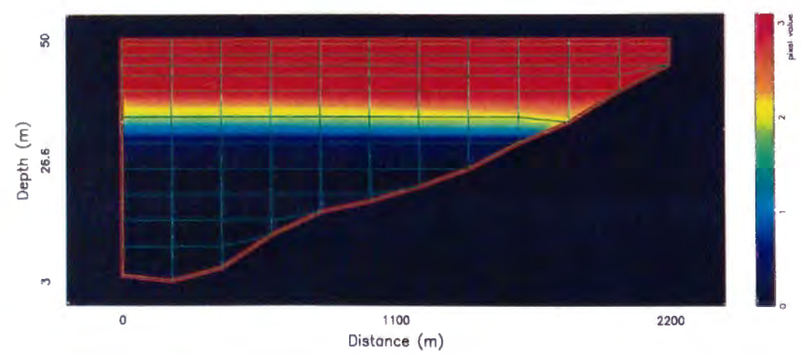

Zooplankton distribution in Oso reservoir

Figure A.25: Planktons ecosystem (June)

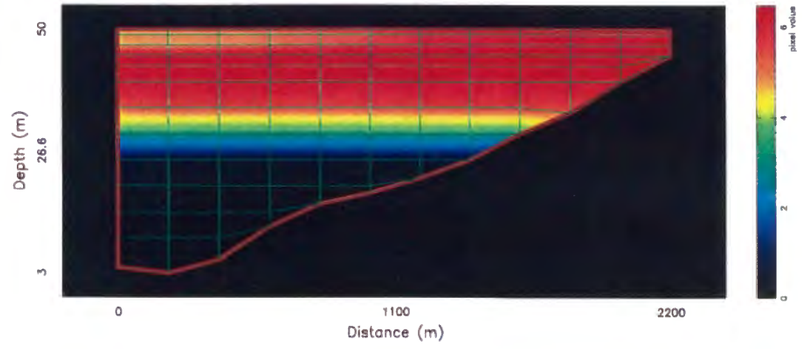

Phytoplankton distribution in Oso reservoir

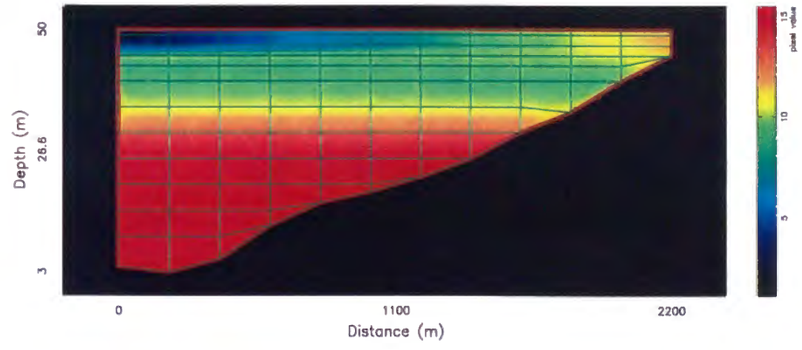

Nutrient distribution in Oso reservoir

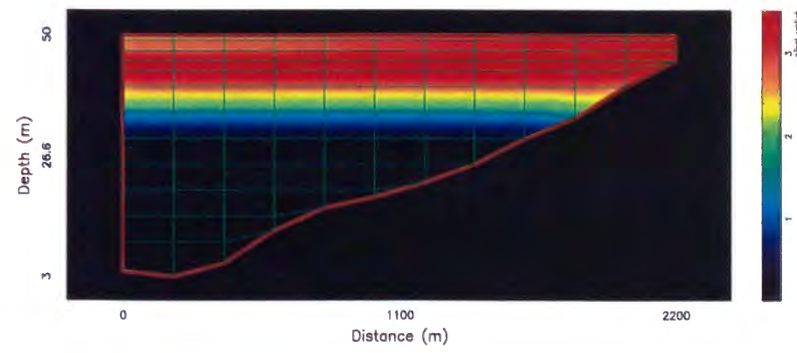

Zooplankton distribution in Oso reservoir

Figure A.26: Planktons ecosystem (July)

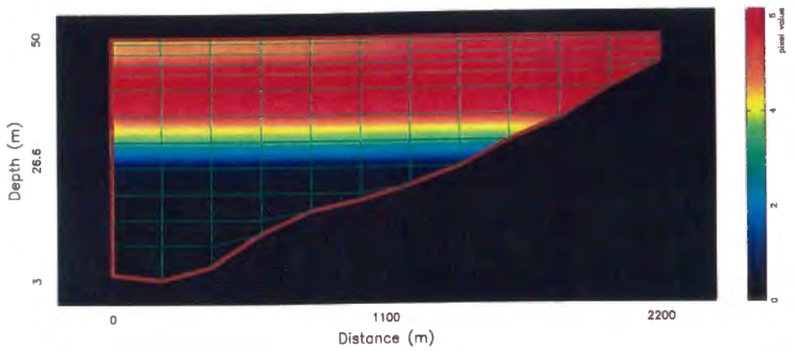

Phytoplankton distribution in Oso reservoir

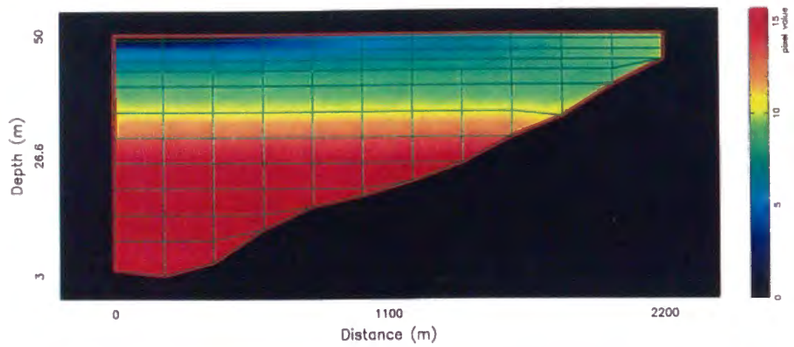

Nutrient distribution in Oso reservoir

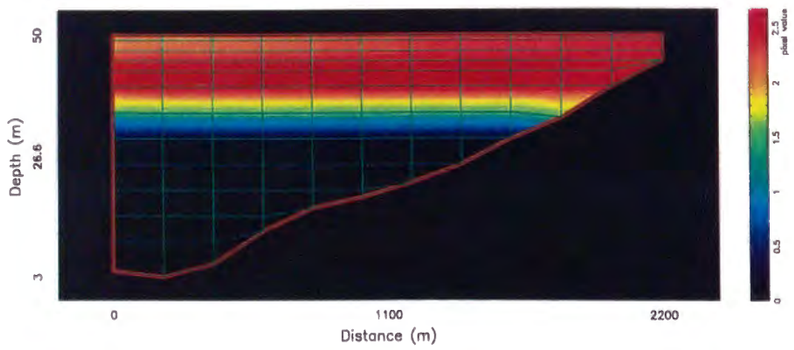

Zooplankton distribution in Oso reservoir

Figure A.27: Planktons ecosystem (August)

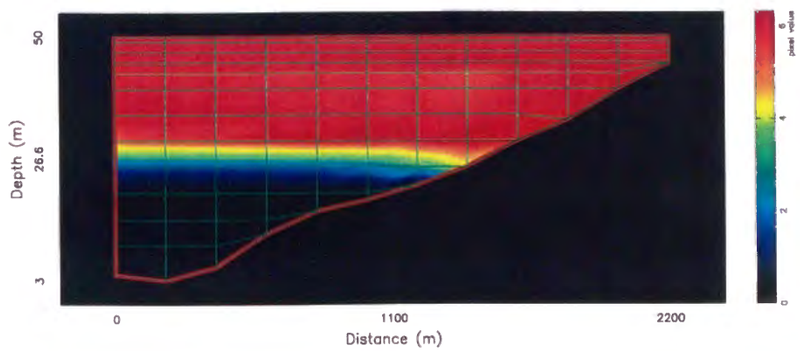

Phytoplankton distribution in Oso reservoir

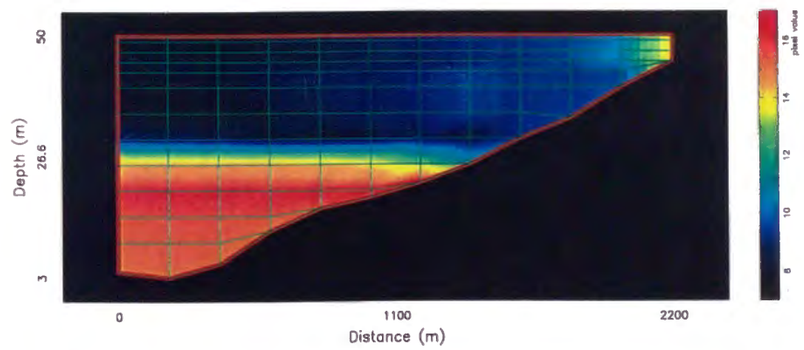

Nutrient distribution in Oso reservoir

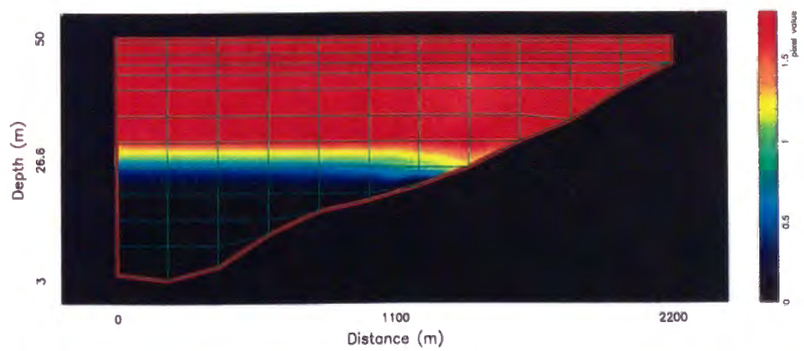

Zooplankton distribution in Oso reservoir

Figure A.28: Planktons ecosystem (September)

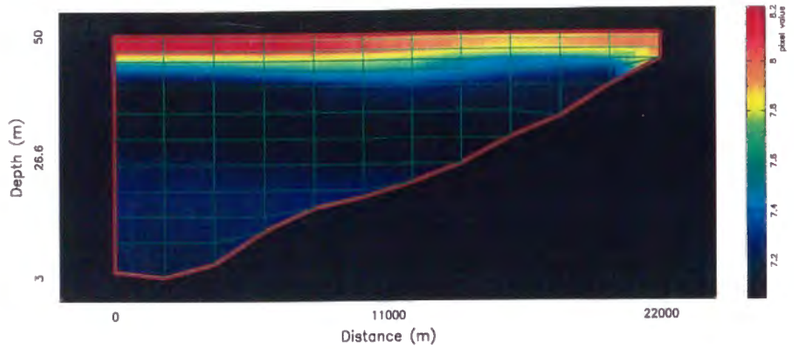

Figure A.29: DO distribution (April 10)

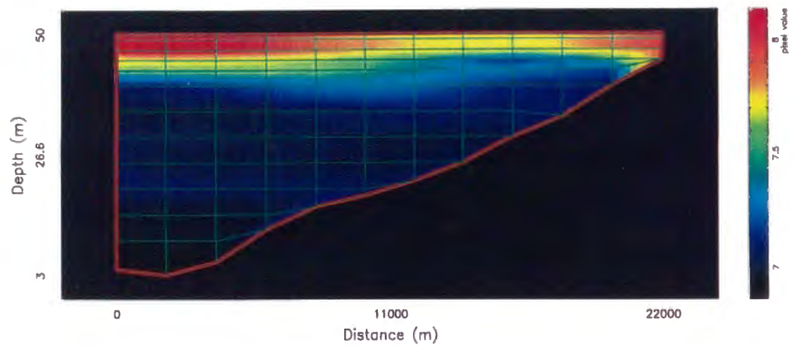

Figure A.30: DO distribution (April 20)

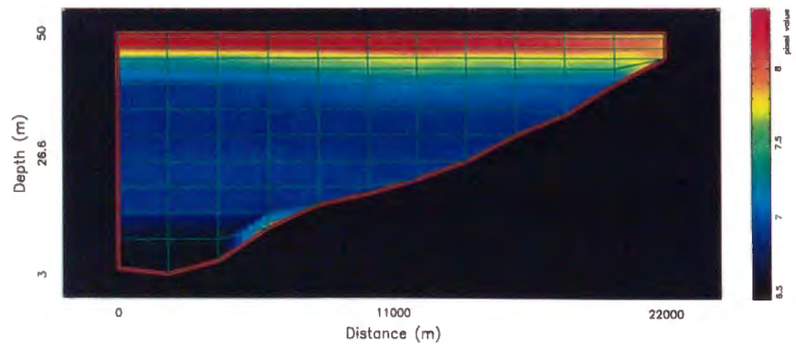

Figure A.31: DO distribution (April 30)

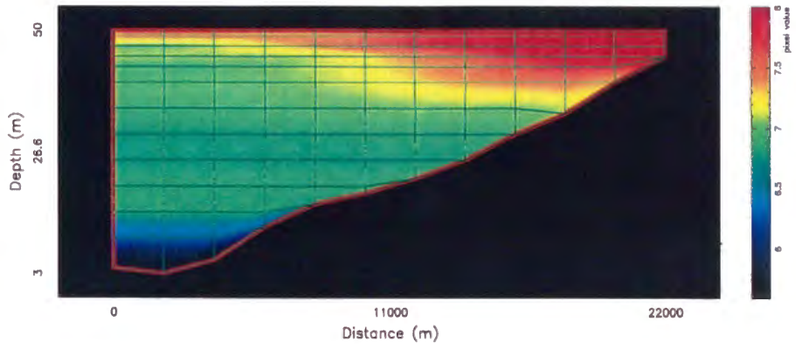

Figure A.32: DO distribution (May 10)

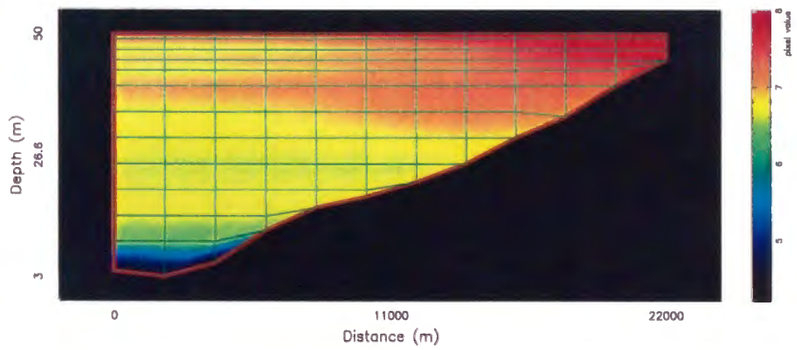

Figure A.33: DO distribution (May 20)

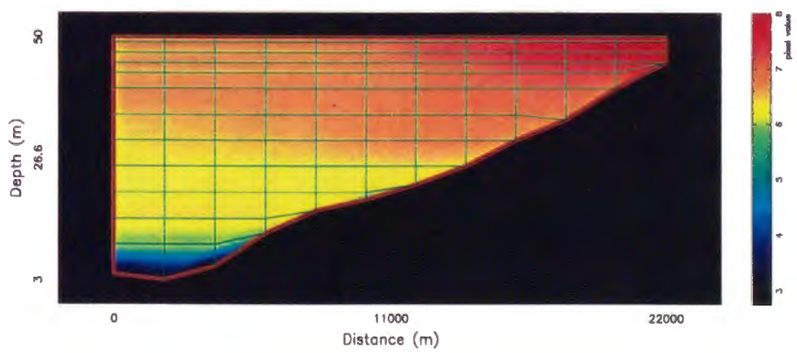

Figure A.34: DO distribution (May 30)

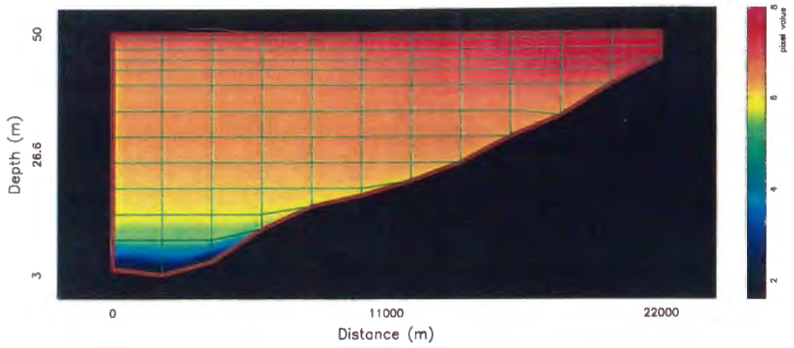

Dissolved Oxygen in Oso reservoir

Figure A.35: DO distribution (June 10)

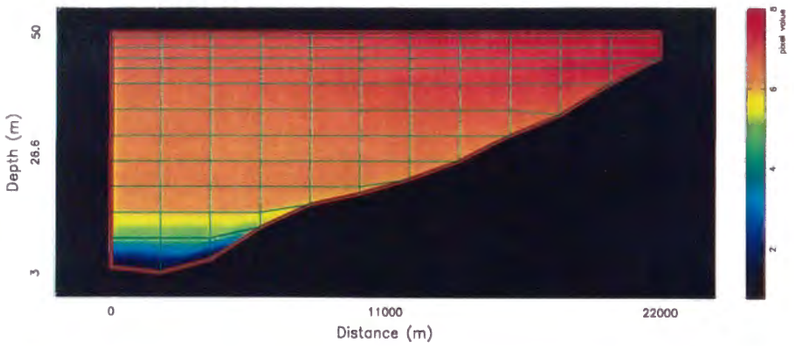

Dissolved Oxygen in Oso reservoir

Figure A.36: DO distribution (June 20)

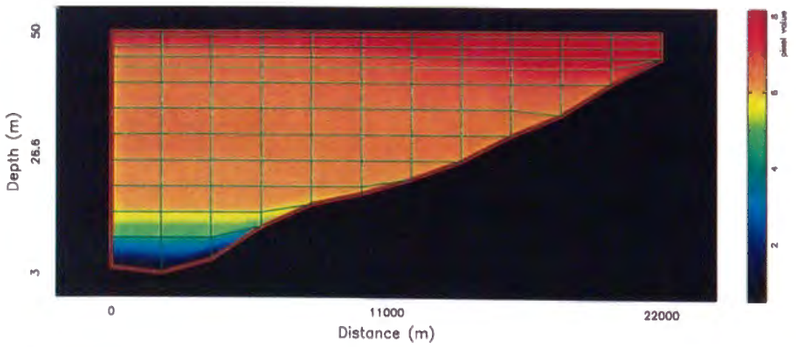

Dissolved Oxygen in Oso reservoir

Figure A.37: DO distribution (June 30)

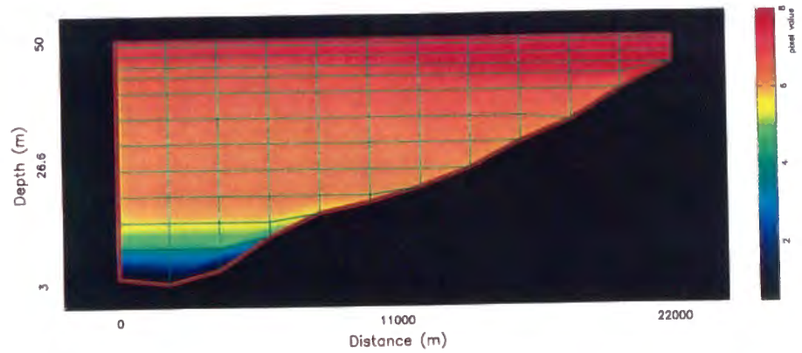

Dissolved Oxygen in Oso reservoir

Figure A.38: DO distribution (July 10)

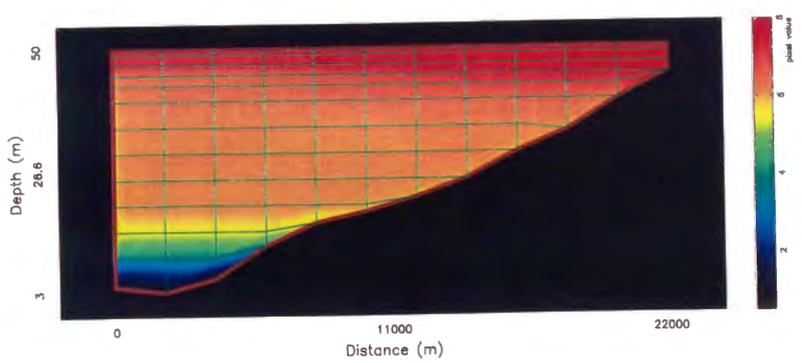

Dissolved Oxygen in Oso reservoir

Figure A.39: DO distribution (July 20)

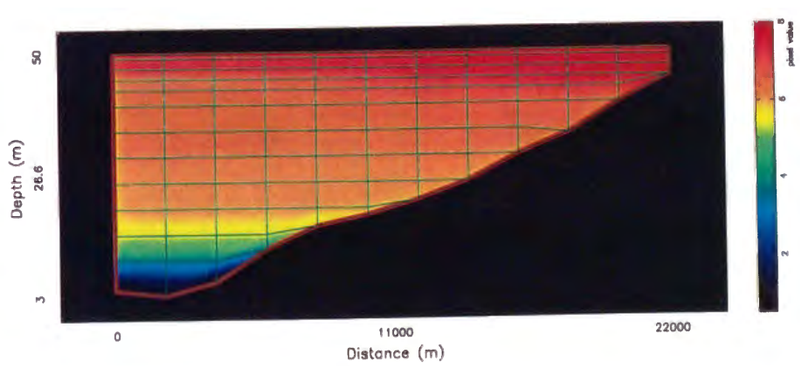

Dissolved Oxygen in Oso reservoir

Figure A.40: DO distribution (July 30)

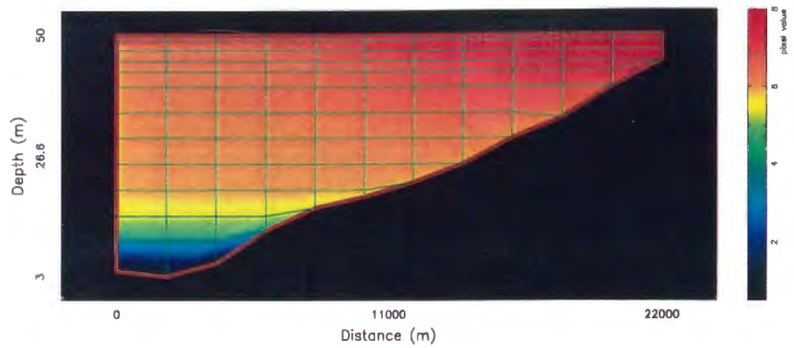

Dissolved Oxygen in Oso reservoir

Figure A.41: DO distribution (August 10)

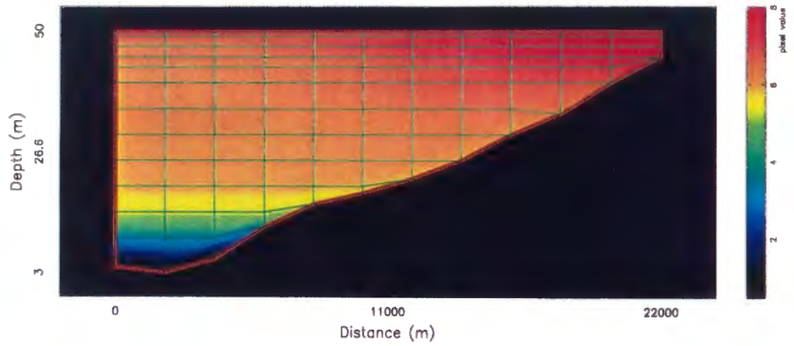

Dissolved Oxygen in Oso reservoir

Figure A.42: DO distribution (August 20)

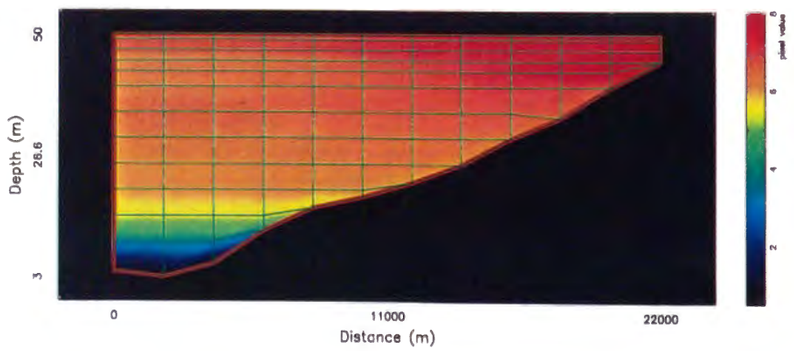

Dissolved Oxygen in Oso reservoir

Figure A.43: DO distribution (August 30)

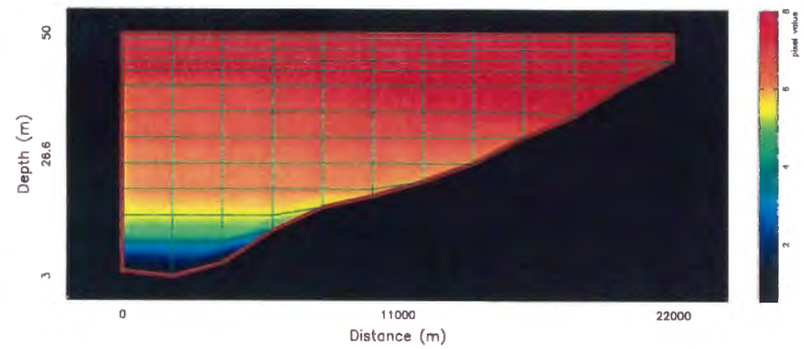

Dissolved Oxygen in Oso reservoir

Figure A.44: DO distribution (September 10)

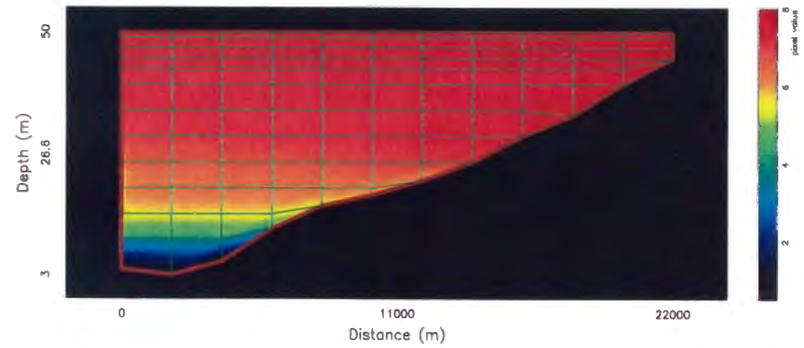

Dissolved Oxygen in Oso reservoir

Figure A.45: DO distribution (September 20)

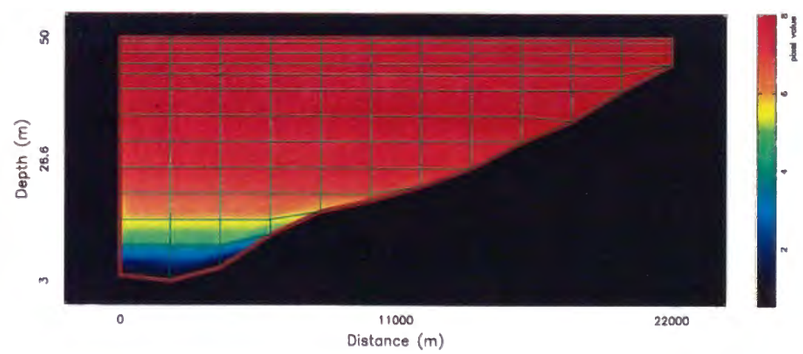

Dissolved Oxygen in Oso reservoir

Figure A.46: DO distribution (September 30)

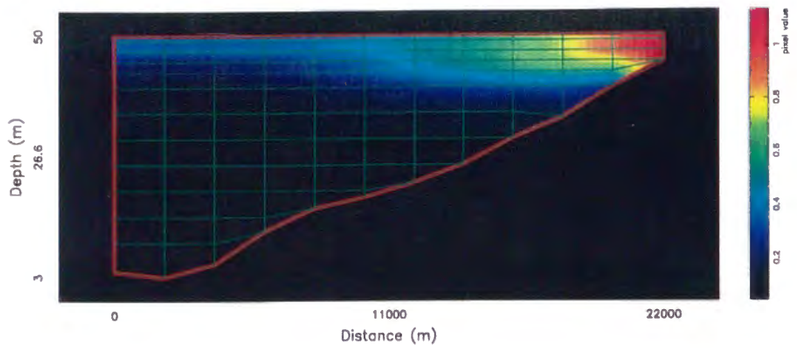

COD in Oso reservoir

Figure A.47: COD distribution (March)

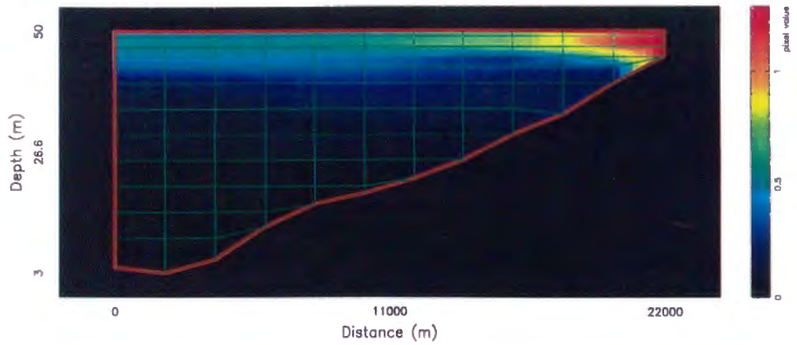

COD in Oso reservoir

Figure A.48: COD distribution (April)

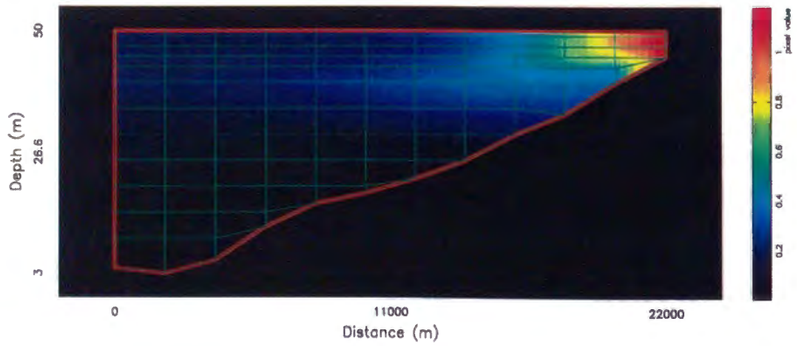

COD in Oso reservoir

Figure A.49: COD distribution (May)

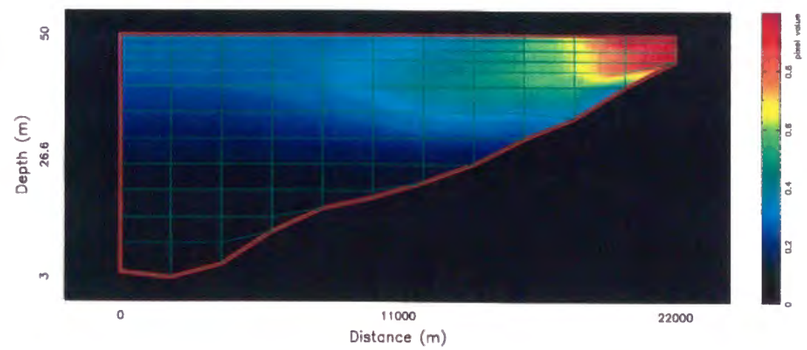

COD in Oso reservoir

Figure A.50: COD distribution (June)

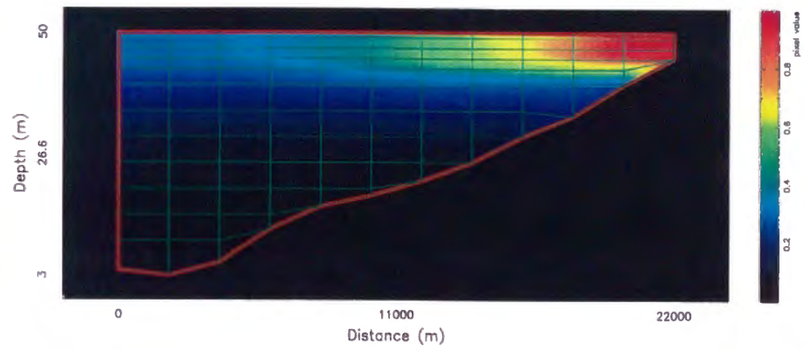

COD in Oso reservoir

Figure A.51: COD distribution (July)

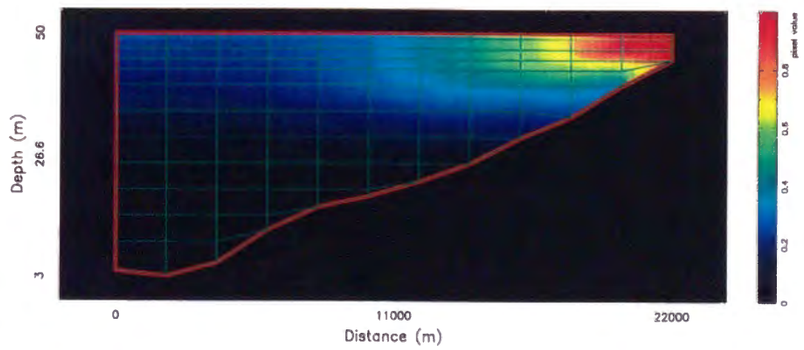

COD in Oso reservoir

Figure A.52: COD distribution (August)

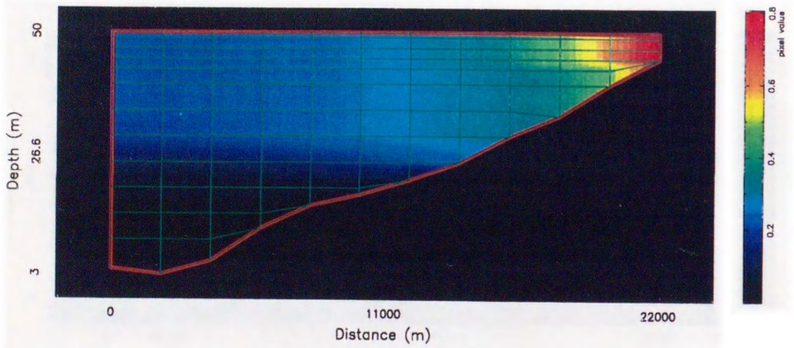

Figure A.53: COD distribution (September)